Identification of colorectal cancer cells that mediate relapse after chemotherapy by marker gene Mex3a

Adrián Álvarez-Varela[1,2], Laura Novellasdemunt[1,2], Francisco M. Barriga[1], Xavier Hernando-Momblona[1,2], Adrià Cañellas[1,2], Sara Cano-Crespo[1], Marta - Sevillano[1,2], Carme Cortina[1,2], Diana Stork[1], Clara Morral[1], Gemma Turon[1], Laura Jiménez-Gracia[3], Ginevra Caratù[3], Holger Heyn[3,4], Daniele VF Tauriello[1], Lidia Mateo[1], Sabine Tejpar[5], Elena Sancho[1,2], Camille Stephan-Otto Attolini[1], Eduard Batlle[1,2,6]

1. Institute for Research in Biomedicine (IRB Barcelona). The Barcelona Institute of Science and Technology. Baldiri i Reixac 10, 08028 Barcelona, Spain.
2. Centro de Investigación Biomédica en Red de Cáncer (CIBERONC), Barcelona, Spain.
3. CNAG-CRG, Centre for Genomic Regulation, Barcelona Institute of Science and Technology, Barcelona, Spain.
4. Universitat Pompeu Fabra, Barcelona, Spain.
5. Molecular Digestive Oncology, Department of Oncology, Katholieke Universiteit Leuven, Leuven, Belgium.
6. ICREA, Pg. Lluís Companys 23, 08010 Barcelona, Spain.

Corresponding author: eduard.batlle@irbbarcelona.org

The standard of care for advanced colorectal cancer (CRC) includes treatment with chemotherapeutic drugs that target the cell proliferation machinery[1]. In CRC patients with overt metastases, chemotherapy initially halts tumor growth but, almost inevitably, disease progresses after some cycles of treatment. Adjuvant chemotherapy is also administered to eliminate minimal residual disease, yet it only diminishes the risk of relapse by 10-25%[2]. Previous studies have shown that patient-derived organoids predict responses to chemotherapy[3–6]. Therefore, we used them as models to investigate the mechanisms behind the limited benefit of these treatments. Whereas CRC organoids expand from highly proliferative Lgr5+ tumor cells, we discovered that lack of optimal stem cell growth conditions specifies a latent Lgr5+ cell population. These cells expressed the gene Mex3a, were largely insensitive to chemotherapy and regenerated the organoid culture after treatment. In mouse models of metastatic latency, Mex3a+ cells contributed marginally to metastatic outgrowth. However, after chemotherapy treatment, Mex3a+ cells produced large cell clones that regenerated metastatic disease. Using lineage-tracing analysis combined with single cell profiling, we showed that drug-tolerant persister Mex3a+ cells downregulate the WNT/Lgr5+ stem cell program immediately after chemotherapy and adopt a transient regenerative state

reminiscent of that of fetal intestinal progenitors[7,8] and revival gut stem cells[9]. In contrast, Mex3a-deficient tumor cells differentiate towards a goblet cell-like phenotype and are unable to resist chemotherapy. Our findings reveal that adaptation of cancer stem cells to suboptimal niche environments protects them from drug treatment and identify a candidate cell of origin of relapse after chemotherapy in CRC.

MAIN

Suboptimal stem cell niche induces a latent Mex3a+ state

The organoid culture medium mimics the colonic stem cell niche[10–13]. Supplementation with WNT promotes the expression of the stem cell program, EGF provides mitogenic signals, and inhibitors of TGF-β and BMP signaling are necessary to counteract cytostasis and differentiation[10–13]. The most common genetic alterations during CRC progression occur in genes that control the key signaling pathways that allow colon stem cell expansion. Mutations in Apc, Kras, and Smad4 or Tgfbr2 render tumor stem cells independent of the crypt niche and facilitate growth in foreign environments[14]. Supporting this view, we and others showed that colon organoids engineered with four driver mutations (Apc, Kras, P53 and Tgfbr2 or Smad4; AKPT/AKPS) can be cultured in the absence of stem cell factors and, upon inoculation in mice, they generate metastatic outgrowths in the liver and lungs with high efficiency[15–18]. However, the vast majority of human primary CRCs and metastases only carry mutations in two or three driver pathways[10,19,20]. Indeed, the establishment of patient-derived organoid (PDO) biobanks showed that a large proportion of CRCs arising in patients exhibit partial dependency on niche signals and require supplementation with complete stem cell medium for expansion[10,19]. We studied this phenomenon in mouse tumor organoids (MTOs) engineered with defined genetic alterations in driver pathways[21]. Supplementation with recombinant TGF-β arrested the growth of AKP (Apc -/-; Kras G12D/+ ; P53 -/-) MTOs cultures (Fig. 1a). Likewise, MTOs bearing wild-type KRAS alleles, i.e. APS (Apc -/- ; P53 -/-; Smad4-/-) or APT (Apc -/- ; P53 -/- ; Tgfbr2 -/-), did not expand in the absence of EGF (Fig. 1b and Extended data Fig. 1a). We however found that MTOs remained viable for more than a week under these suboptimal culture conditions. AKP MTOs resumed expansion after removal of TGF-β (Fig. 1a) whereas supplementation of EGF after 10 days restored growth rates of APS (Fig. 1b) or APT organoids (Extended data Fig. 1a). While performing these experiments, we discovered that the suboptimal niche factor combination (no EGF for APS or APT and TGF-β supplementation for AKP) conferred broad chemotherapy resistance to triple

mutant MTOs. Cell viability assays demonstrated a large increase in IC50s for 5FU, oxaliplatin and SN38 (the active metabolite of irinotecan) - the three chemotherapeutic drugs most commonly used to treat CRC patients - in arrested versus exponentially growing triple mutant MTOs (Fig. 1c-d, Extended data Fig. 1b and Extended data Fig. 2a-c). MTOs with single loss of function mutations in Apc (A) or with Apc combined with p53 (AP) mutations also acquired chemotherapy resistance under suboptimal niche factor conditions (Extended data Fig. 2a-b). In contrast, quadruple mutant AKPS or AKPT MTOs kept proliferating in no_EGF/+TGF-β medium and remained sensitive to chemotherapy (Extended data Fig. 2a-c). The drug-tolerant persister phenotype was reversible as shown by experiments where APS MTOs underwent two consecutive cycles of culturing under suboptimal stem cell conditions and then were re-challenged with chemotherapy (Extended data Fig. 2d).

These observations suggest that CRC cells exposed to a suboptimal niche environment acquire a latent phenotype and gain intrinsic resistance to chemotherapy. To gain insights into this phenomenon, we performed RNA sequencing followed by gene set enrichment analysis (GSEA)[22] (Fig. 1e,f, Extended Data Fig. 1c and Supplementary Table 1). TGF-β signaling in AKP MTOs induced the expression of the signature genes of revival stem cells[9] and fetal progenitors[8] (Fig. 1e), in agreement with previous studies[23]. TGF-β also induced upregulation of pathways and genes related to epithelial-to-mesenchymal transition (Fig. 1e). Lack of EGFR signaling in APS and APT MTOs increased the levels of a subset of secretory and Paneth cell specific genes as previously reported for human CRCs[24] (Fig. 1f , Extended Data Fig. 1c). Although growth arrest triggered by lack of the mitogen EGF or by activation of TGF-β signaling involved substantially different mechanisms and downstream gene programs, we identified some shared features. The latent phenotype in both MTO genotypes was characterized by silencing of proliferation gene programs and general downregulation of metabolic pathways including glycolysis, oxidative phosphorylation and fatty acid metabolism (Fig. 1.e-f, Extended Data Fig. 1c and Supplementary Table 1). Extracellular matrix remodeling and sensing genes were also upregulated in both AKP and APS MTOs (Fig 1.e,f). It called our attention that the Mex3a+ cell signature[25] was amongst the gene sets enriched in common between latent AKP and APS or APT MTO cultures (Fig. 1e,f and Extended Data Fig. 1c). Furthermore, Mex3a mRNA was upregulated in all three triple mutant CRC genotypes (Fig. 1g,h and Extended Data Fig. 1d). Using AKP and APS MTOs engineered with a tdTomato reporter cassette inserted in the endogenous Mex3a locus, we confirmed that MTO cells gain Mex3a

expression under suboptimal stem cell niche culture conditions (Fig. 1i). Quadruple mutant AKPS MTOs contained fewer Mex3a+ cells that triple mutant MTOs when cultured in either complete stem cell medium (Extended Data Fig. 2e) or no_EGF/+TGF-β conditions (Extended Data Fig. 2f).

Mex3a marks latent Lgr5+ cells in human CRC

We next investigated chemoresistance in CRC patient-derived organoids (PDOs). 5 out the 11 PDOs analyzed acquired broad resistance to chemotherapy under suboptimal growth factor conditions, (Extended Data Fig. 3a-c). A prime example was PDO7, which became resistant to 5-FU, SN38 and Oxaliplatin when cultured in suboptimal medium (Extended Data Fig. 3b,c). As in the case of MTOs, PDO7 engineered with a Tomato reporter knock-in cassette in the Mex3a locus showed increased proportions of Mex3a+ cells in no_EGF/+TGF-β medium (Extended Data Fig. 4a-c). We also engineered PDO7 with Ki67-RFP and LGR5-GFP knock-in cassettes[26] and found upregulation of MEX3A mRNA in LGR5-GFP-hi/Ki67-low cells purified by FACS from xenografts (Extended Data Fig. 4d-g). To broaden the relevance of these findings, we studied the relationship between MEX3A, LGR5 and cell proliferation in human CRC using a patient sample cohort analyzed by single-cell RNA sequencing (see ref [27] and methods). Analysis of pooled epithelial tumor cells corresponding to 37 CRC samples revealed two subsets of LGR5-high cells defined by either high or low expression of the Ki67 proliferation signature (Fig. 1j-l). The LGR5-hi/KI67-lo cell population was specifically marked by MEX3A mRNA (Fig. 1j-l). Analysis of individual samples in this cohort confirmed that two-thirds contained a LGR5-hi/MEX3A-hi cell population characterized by low expression of proliferation genes (Extended Data Fig. 5a-b). According to the expression levels of cell cycle signature genes, 50% of LGR5-hi/MEX3A-hi cells were predicted to reside in G0 and 38% in G1 phase of the cell cycle. In contrast, most LGR5-hi/MEX3A-low cells were in G2/M and S phases (Fig. 1m and Extended Data Fig. 5c). Furthermore, a gene expression signature containing the top 100 differentially expressed genes in LGR5-hi/MEX3A-hi versus LGR5-hi/MEX3A-low cells predicted with elevated significance increased risk of disease relapse in a large CRC patient transcriptomic cohort (n=816 AJCC stage I-III patients) even after adjusting for clinical variables (age, gender, site, MSI status and stage; HR= 1.50, P=0.007; Extended Data Fig. 6e,f) whereas LGR5-hi/MEX3A-lo cells associated with good prognosis (HR= 0.66, P=0.006; Extended Data Fig. 6g,h). From all these results, we tentatively conclude that MEX3A marks a subset

of latent LGR5+ cells that associates with chemoresistance in both mouse and human CRC.

Clonal dynamics of Lgr5+ and Mex3a+ cells in Apc mutant tumors

Mex3a gene encodes a RNA-binding protein expressed by a restricted subset of Lgr5+ intestinal stem cells (ISCs) in healthy crypts[25]. Lgr5-hi/Mex3a-hi cells are multipotent ISCs that exhibit a low proliferative rate[25]. To investigate the relationship between Mex3a and Lgr5 during intestinal carcinogenesis, we generated $Apc^{fl/fl}$ mice bearing both Mex3a-tdTOMATO[25] and Lgr5-EGFP-creERT2[28] alleles (Fig. 2a-c). We induced recombination of the Apc locus in Lgr5+ cells and analyzed Lgr5-GFP+ cell populations. Consistent with our previous study[25], only few (~10%) Lgr5+ cells in healthy colonic mucosa expressed Mex3a-Tomato reporter (Fig 2b-c and Extended Data Fig. 7a). In colon adenomas, however, around 50% of Lgr5+ cells were marked by Mex3a-Tomato (Fig 2b-c and Extended Data Fig. 7b). The Lgr5+/Mex3a+ cell population exhibited lower proliferation rates than Lgr5+/Mex3a- cells shown by EdU incorporation (Fig. 2d). Gene expression profiling confirmed global downregulation of proliferation and metabolism-related gene sets in Mex3a+/Lgr5+ adenoma cells (Fig. 2e). This analysis also revealed increased TGF-β signaling and downregulation of EGFR/KRAS signature genes amongst the top significant enriched gene sets suggesting a role for these pathways in the specification of the Lgr5+/Mex3a+ population in adenomas (Fig. 2e and Supplementary Table 2). Indeed, Apc mutant adenoma-derived organoids cultured in the absence of EGF or supplemented with TGF-β exhibited a large increase in the number of Mex3a-Tomato+/Lgr5-GFP+cells (Extended Data Fig. 7c,d) and, as we previously showed, resisted chemotherapy (Extended Data Fig. 2b). We also assessed the organoid forming capacity of Mex3a+ and Lgr5+ populations (Extended Data Fig. 7e-g), a property that correlates with cancer stem cell potential. Mex3a+/Lgr5+ tumor cells isolated from adenomas formed organoids more efficiently than Mex3a-/Lgr5+ cells (Extended Data Fig. 7e) albeit organoids generated by these two populations exhibited similar growth rates (Extended Data Fig. 7f). Of note, organoids that originated from the two populations contained Mex3a+ and Lgr5+ cells in similar proportions (Extended Data Fig. 7g). Moreover, Mex3a-/Lgr5+ adenoma cells cultured in suboptimal niche factor conditions (-EGF or + TGF-β) acquired a latent Mex3a+/Lgr5+ state (Extended data Figure 7h,i). Overall, these findings denote that the Mex3a program is not hardwired and demonstrate extensive plasticity between the active Mex3a- and latent Mex3a+ cancer stem cell states depending upon optimal and suboptimal niche environments.

We next introduced Mex3a-creERT2 allele in APCMin/+; Rosa26-TOMATO mice. 24-48h after induction with tamoxifen, we observed a Tomato-labeled cell population in both healthy epithelium and adenomas (Fig. 2f). In normal crypts, Mex3a-creERT2-mediated recombination was restricted to 1-2 cells per crypt located preferentially around position +4 (Fig. 2f), which is consistent with our previous study[25]. In contrast, the frequency of recombined cells was largely increased in adenomas (Fig. 2f and Extended Data Fig. 7j). At early time-points after tamoxifen administration (16 hours), tomato+ adenoma cells retained increased levels of Mex3a mRNA (Extended Data Fig. 7ik) and showed lower BrdU incorporation than Tomato- cells (Fig. 2g). We next performed clonal analysis in ApcMin/+ adenomas using Mex3a-creERT2 and Lgr5-creERT2 alleles. In these experiments, we inoculated a low tamoxifen dose so that the progeny of individual cells could be tracked over time. Quantification of Tomato labelling on tissue sections at the initial time-point (2 days) indicated that we marked similar numbers of Mex3a+ and Lgr5+ cells (1.05% +/- 0.01 versus 0.53% +/- 0.01 of the adenoma area respectively). Although the quantification of clone number and size in 2D precluded conclusions about the absolute contribution of Mex3a+ and Lgr5+ cells to tumor growth, a comparative analysis revealed important differences in the dynamics of the two populations (Fig. 2h-j and Extended Data Figure 7l). Consistent with previous studies[29,30], Lgr5+ colonic adenoma cells generated large clonal patches (Fig. 2i-j). However, we also observed a substantial fraction of small size Lgr5+ cell-derived clones even after 15 days (Fig. 2j and Extended Data Figure 7l). In contrast, Mex3a+ cells contributed substantially lower amount of progeny over time compared to Lgr5+ cells (Fig. 2h), a difference that is also reflected in the frequency of small clones (<10 cells) generated by the two populations (Fig. 2i-j and Extended Data Figure 7l). Taken together, these data reveal the existence of a slow proliferative Lgr5+ cell population in adenomas characterized by high Mex3a expression levels.

Mex3a restrains secretory differentiation of latent Lgr5+ cells

Mex3a null mice die around birth, which precludes analyses of Mex3a function in the adult epithelium[31]. To overcome this limitation, we generated mice bearing Mex3a-floxed alleles and crossed them with villin-creERT2 strain that enables efficient recombination in the entire intestinal epithelium. Mex3a deficiency in the adult intestinal epithelium did not cause an overt phenotype neither morphological alterations or obvious changes in the specification of the main intestinal cell lineages implying that the function of Mex3a is dispensable for intestinal homeostasis (Extended Data Fig. 8). We also obtained mice with a Mex3a-floxed allele combined with a

Mex3a-Tomato knock-in allele. In the latter, the tomato cassette disrupts the Mex3a open reading frame, which results in a null allele (Fig. 2k). This configuration enabled tracking cells that switched on Mex3a promoter in a background of Mex3a loss of function (Fig. 2k). Adenomas arising in Villin-creERT2; $Apc^{fl/+}$; $Mex3a^{fl/TOM}$ mice lacked Mex3a expression (Extended Data Fig. 9a), downregulated signature genes of Mex3a+ adenoma cells (Fig. 2l and Extended Data Fig. 9b) and showed upregulation of secretory cell specific genes (Fig. 2m). GSEA confirmed enrichment of signature genes of goblet and Paneth cells in Mex3a-Tom+/KO cells (Extended Data Fig. 9b). Accordingly, Mex3a-deficient cells isolated from adenoma organoids exhibited increased UEA-1 lectin surface staining, a marker of glycans commonly used to identify secretory cells in the gut (Extended Data Fig. 9c,d). Therefore, Mex3a not only marks slow proliferative Lgr5+ stem cell-like tumor cells but it is also necessary to sustain their undifferentiated state. Villin-creERT2; $Apc^{fl/+}$; $Mex3a^{fl/TOM}$ exhibited reduced tumor burden in the gastrointestinal tract compared to control villin-creERT2; $Apc^{fl/+}$; $Mex3a^{+/TOM}$ mice and 5-FU treatment extended very significantly their survival (Fig. 2n and Extended Data Fig. 9e).

Drug-tolerant Mex3a+ persister cells regenerate CRC after therapy

To explore the contribution of Mex3a+ cells to chemotherapy resistance in advanced CRC we derived ApcMin/+; Mex3a-creERT2; Rosa26-TOMATO colon adenoma organoids and, by means of CRISPR/Cas9 editing, introduced loss-of-function mutations in P53 (P) combined with either oncogenic mutations in Kras (G12D; K) or loss of function Smad4 (S) alleles (Fig. 3a and Extended Data Fig. 10a). These APS and AKP MTOs enabled the study of Mex3a+ cells in advanced CRC through lineage tracing analysis. A tomato-labeled population emerged in triple mutant MTOs after 4-OH-Tamoxifen addition (Fig. 3b and Extended Data Fig. 10b,c). After 16 hours, the number of Tomato+ cells in APS and AKP MTOs cultured in complete stem cell media was around 10% (Fig. 3b and Extended Data Fig. 10b), which is consistent with our previous observations using Mex3a-Tomato knock-in MTOs (Fig. 1i). AKP and APS MTO cultures switched to suboptimal niche factor conditions after OH-Tamoxifen treatment conserved similar proportions of Tomato-labelled cells implying that both pre-existing Mex3a+ and Mex3a- cells adapted similarly to this growth limiting conditions (Extended data Figure 10d). We also found that the proportion of the Mex3a tomato-labeled progeny in control cultures did not change substantially over time (Fig. 3c,d). However, levels of Mex3a measured by RT-qPCR declined over time in the Tomato+ progeny whereas expression of the proliferation marker AurkB increased

suggesting that Mex3a+ cells give rise to proliferating Mex3a- daughter cells (Extended data Figure 10e).

Treatment with chemotherapy (FOLFIRI or FOLFOX regimes) caused extensive cell death and organoid shrinkage (Fig. 3c, Extended Data Fig. 10f and Extended Data videos 1 and 2). After 20 days, most organoids appeared necrotic (arrows in Fig. 3c). Yet, we observed the presence of some MTOs of small size, which according to their morphology under a bright field microscope remained viable. Invariably, these MTOs contained increased proportions of Tomato+ cells (Fig. 3c,d, Extended Data Fig. 10f and Extended Data videos 1 and 2). Approximately 20 days after treatment cessation, some organoids resumed growth. In the resulting cultures, the majority of viable cells were tomato+ (60-80% by flow cytometry; Fig. 3d) implying that they originated from chemotherapy-persister Mex3a+ cells. A and AP MTOs also regenerated from Mex3a+ cells after chemotherapy treatment (Extended Data Fig. 10g-k). As a control for lineage tracing experiments, we used a retroviral vector to introduce a creERT2 cassette downstream of the CMV promoter which drives constitutive expression irrespectively of the cell type. We tritiated the tamoxifen dose necessary to recombine approximately the same number of cells than with the Mex3a-creERT2 cassette (5-10%) and tracked the fate of labelled cells after treatment. These experiments revealed that, as opposed to Mex3a+ cells, the progeny of a randomly recombined subset of tumor cells by the CMV-creERT2 driver declined over time after chemotherapy (Extended Data Fig. 11). This result further highlights the unique properties of the pre-existing Mex3a+ cell population to resist a lethal chemotherapy dose and regenerate the MTO culture after treatment. It also rules out the possibility that any tumor cell within a CRC is able to adopt a drug-tolerant persister cell state as recently suggested by a study that used a lentiviral barcoding approach[32].

We have previously shown that intrasplenic inoculation of quadruple mutant (AKPT) MTOs in c57BL/6 mice produces rapidly growing liver metastases that kill the host in only 3-4 weeks[21]. Triple mutant MTOs (APS and AKP) also colonized the liver efficiently yet they generated micrometastases that proliferated slower (Extended Data Fig. 12). Only after a prolonged latency time, triple mutant metastases entered an exponential growth phase shown by *in vivo* bioluminescence analysis (Extended Data Fig. 12). In the case of APS MTOs, the period between inoculation and the onset of rapid growth spanned 60-80 days (Fig. 3e and Extended Data Fig. 12). We leveraged this model of metastatic latency to investigate the contribution of Mex3a+ cells to

chemotherapy resistance and disease relapse. By giving a single injection of tamoxifen 88 days after APS MTO inoculation, we marked ~4% of all tumor cells in micrometastases (Fig. 3f-g). These Mex3a+ cells contributed to a reduced amount of progeny in untreated mice as shown by the quantification of Tomato+ cells in tumors during exponential growth phase (day 46 post-tamoxifen induction) and at experimental end time-points (day 117 post-tamoxifen induction) (Fig. 3f-g). A continuous FOLFIRI regime during 46 days aimed at eliminating micrometastases caused a reduction of bioluminescence (Fig. 3e). However, 50% of mice relapsed and eventually succumbed to overt liver metastatic disease. Tracking of Mex3a+ cells that were recombined just before chemotherapy treatment demonstrated striking clonal amplification of their progeny at experimental endpoints (Fig. 3f-l and Extended data Fig. 13) to the extent that some metastases were completely formed by Tomato+ cells (Extended Data Fig. 13a). At experimental endpoints, Tomato+ clones contained both Mex3a+ and Mex3a- cells shown by in situ hybridization (Fig. 3f and Extended Data Fig. 13d). It was also evident the presence of residual Tomato+ cell clusters, which resisted therapy but did not expand further (Extended Data Fig. 13b). Therefore, Mex3a+ cells present in micrometastases resist chemotherapy and, after treatment cessation, undergo a large expansion that regenerates the disease.

To analyze the role of Mex3a+ cells in human CRC, we devised an *in vivo* cell ablation strategy. Using CRISPR/Cas9, we introduce an inducible suicide cassette composed of a FKBP_caspase 9 fusion (iCaspase9) plus a Tomato reporter[33,34] into the MEX3A locus of PDO7 (MEX3A_iCT; Fig. 3j-m and see also Extended Data Fig. 4a,b) and, subsequently, inoculated this genome-edited PDO into immunodeficient mice (Fig. 3j-m). In these experiments, treatment of mice with AP20187 (Dimerizer or DIM), a compound that induces dimerization of the FKBP_Caspase-9 fusion, reduced by half the 10% Mex3a-Tomato brightest cell population present in xenografts (Fig. 3k). The limited cell killing activity of the FKBP_caspase 9 knock-in cassette is probably due to low expression levels of the Mex3a locus. Reduced numbers of MEX3A-hi cells did not affect xenograft growth rates implying that this population is dispensable in unperturbed tumors (Fig. 3l). A 10 days FOLFIRI regime halted tumor growth yet, 2 weeks after treatment ended, all xenografts resumed their expansion (Fig. 3l). Despite suboptimal MEX3A+ cell ablation efficiency in these experiments, the combination of dimerizer plus FOLFIRI prolonged substantially the therapeutic effects of the treatment (Fig. 3l-m).

Mex3a+ cells give rise to fetal/revival stem cell-like cells upon chemotherapy

We next sought to understand how Mex3a+ cells adapt to chemotherapy. To this end, we combined single cell RNA sequencing and lineage tracing analysis as described in Fig 4a,b. We identified discrete subsets of Mex3a-expressing cells in untreated AKP MTOs (arrow Fig. 4c). 4 days after FOLFIRI treatment, we sorted viable Tomato+ cells that survived the treatment and sequenced their transcriptomes. At this early time point, the residual drug-tolerant persister cell population silenced Mex3a expression (Fig. 4c). The global Lgr5+ ISC gene program, including bona-fide ISC marker genes such as Lgr5 and Smoc2, was also downregulated (Fig. 4d and Extended Data Fig. 14a). Instead, there was a remarkable upregulation of the transcriptional program of revival stem cells (Fig. 4e and Extended Data Fig 14b). Revival stem cells are specified by activation of the transcriptional regulator YAP and mediate the regeneration of the intestinal epithelium after radiation[9]. They share features with the fetal-like developmental program expressed in the crypts after injury[7,8,35,36]. Indeed, we found increased levels of multiple markers of fetal intestinal progenitors and YAP target genes in the chemotherapy resistant residual population such as Anxa1, Ctgf (Ccn2), or Basp (Extended Data Fig. 14b). Ly6a (Sca-1), a fetal progenitor marker induced by IFN-γ in injured crypts[8] was however constitutively expressed in AKP MTOs at high levels (not shown). We validated changes in the expression of marker genes for these populations by RT-qPCR (Extended Data Fig 15). The Mex3a-to-revival/fetal conversion was consistent in both AKP (Fig. 4a-h, Extended Data Fig. 14) and APS MTOs (Extended Data Fig. 16) implying a common mechanism of adaption after chemotherapy irrespectively of the genotype. Tomato+ cells present 30-50 days after FOLFIRI treatment in fully regenerated MTO cultures downregulated the revival/fetal stem cell program, regained expression of WNT target genes and contained again a small proportion of Mex3a+ cells (Fig. 4a-h, Extended Data Fig. 14 and Extended data Fig. 15). In an independent experiment, we tested whether these newly formed Mex3a+ cells retained a drug-persister phenotype (Fig. 4i-k). Indeed, after a second round of FOLFIRI, 60-80% of MTOs cells originated from Mex3a+ cells demonstrating reversibility of the drug-tolerant persister cell phenotype (Fig. 4i-k). Finally, in these experiments we sorted and sequenced equivalent numbers of Tomato+ and Tomato- cells, which enable the analysis of the minority of cells that originated from the non-Mex3a+ cell population after chemotherapy. We found that the cell states present in tomato-negative cells completely overlap with that of tomato-positive cells in both AKP (Fig. 4l and Extended Data Fig. 17) and APS MTOs (Extended Data Fig. 16). Thus, either non-Mex3a+ drug-tolerant cells adopt the same transcriptional states than

Mex3a+ cells during treatment or, more likely, tomato- cells reflect failure of the knock-in creERT2 cassette to recombine a proportion of Mex3a+ cells.

Mex3a-deficient CRC cells are sensitive to chemotherapy

To obtain definitive evidence of the role of Mex3a+ cells during relapse after chemotherapy, we generated Mex3a knockout AKP MTOs using CRISPR/Cas9 (Fig. 5a). Lack of Mex3a did not affect growth kinetics in complete stem cell conditions yet these MTOs were unable to survive in no_EGF/+TGF-β medium (Fig. 5b,c). Mex3a-deficient MTOs also showed striking susceptibility to chemotherapy and were unable to regenerate the culture after FOLFIRI treatment (Fig. 5b,c). Two independent Mex3a knockout AKP MTOs showed similar behaviors in these conditions (Fig. 5b,c). To assess chemotherapy sensitivity in vivo, we inoculated wild-type and Mex3a KO1 AKP MTOs into the liver of c57BL/6 mice (Fig. 5d). We measured liver bioluminescence and initiated a chemotherapy regime at the onset of exponential growth phase. Echoing our findings in adenomas, Mex3a KO metastases were enriched in secretory-like cells shown by UEA-1 lectin staining (Fig. 5e). FOLFIRI treatment delayed growth of wild-type AKP tumors but all mice eventually succumbed to metastatic disease (Fig. 5d). In contrast, all mice bearing Mex3a-deficient metastases developed robust responses to chemotherapy (Fig. 5d); three showed no signs of relapse over the follow-up period (two months) and in two other mice metastatic disease relapsed with delayed kinetics (Fig. 5d).

Prompted by these results, we applied scRNAseq to investigate the fate of Mex3a-deficient cells during FOLFIRI treatment. We characterized the response of two independent WT and Mex3a knock-out AKP MTOs at 2- and 5-days post-treatment (Data for KO1 in Fig. 5g-k and Extended Data Fig. 18 and for KO2 in Extended Data Fig. 19). Mex3a KO1 and KO2 MTOs clustered together in the UMAP but occupied a distinct space than their WT counterparts implying the existence of different cell states in the two genotypes (Fig. 5g and Extended Data Fig. 18a and 19a). Consistent with our previous findings, wild type AKP CRC cells adopted a regenerative revival/fetal-like stem cell state after chemotherapy shown by global upregulation of gene signatures and well-known marker genes for these populations (Fig. 5i, Extended Data Fig. 18b,c and Extended Data Fig. 19c,d). A cell subset also showed elevated expression of YAP targets genes (Extended Data Fig. 18d,e and Extended Data Fig. 19e,f). The upregulation of revival/fetal-like markers genes started 2 days after chemotherapy and was particularly evident 5 days post-treatment. As we

demonstrated previously through lineage tracing analysis (Fig. 4a-j), this population originated from chemoresistant Mex3a+ cells. Indeed, a string of Mex3a+ cells linked untreated and treated wild-type cell clusters in the UMAP (arrow in Fig. 5h). In contrast, the residual Mex3a-deficient population that we recovered 2 days after chemotherapy in Mex3a KO MTOs showed residual expression of the regenerative/fetal-like program and instead upregulated the Lgr5+ ISC gene signature and key ISC maker genes such as Lgr5 and Smoc2 (Fig. 5i,j and Extended Data Fig. 18b-g and Extended Data Fig. 19c-h). Many of these Lgr5+ cells adopted a goblet-like cell phenotype demonstrated by elevated expression of Atoh1 and Spdef1, two master transcription factors of this lineage, and of effector genes Muc2 and Tff3 (Fig. 5k, Extended Data Fig. 18h,i and Extended Data Fig. 19i-j). We also noticed that the proliferation signature remained elevated after chemotherapy in Mex3a-deficient MTOs compared to their wild-type counterparts (Extended Data Fig. 18j,k). All these findings were consistent in both Mex3a-deficient AKP MTOs. At 5 days of post-treatment, we could not isolate sufficient cells from Mex3a KO1 MTOs but residual KO2 cells expressed high levels of apoptosis-related genes at this timepoint (Extended Data Fig. 19j-k).

DISCUSSION

Our data supports that not all functionally important cells contribute to CRC growth[34,37,38] ; in unchallenged tumors, some cells expand continuously whereas others are held in reserve. Slow-cycling drug-tolerant cells have been observed in multiple tumor types[39,40], including CRC[37,41,42]. However, cellular diversity represented a major challenge to define the precise identity and features of this cell population[39,40]. We identify a latent chemotherapy-tolerant cell state that results from suboptimal adaptation of LGR5+ stem cell-like cells to their niche. This population emerges in CRCs bearing an incomplete set of driver mutations such as those carrying wild-type EGFR or TGF-β signaling pathways. We speculate that other constraints such as a limited nutrient availability may also induce MEX3A+ latent cells. Nevertheless, the majority of CRCs are characterized by genetic alterations in only two or three driver pathways[10,19,20]. Our own analysis of a large CRC patient cohort corroborated that dual and triple mutant pathways are the most common genotypes in full-blown primary CRCs and metastases (Extended Data Fig. 20). Furthermore, recent studies support the early dissemination of these tumors[43]. Therefore, the MEX3A+ cell population described herein may contribute to therapy failure in a substantial proportion of patients and may be of particular relevance for disseminated tumor cells during the metastatic latency period.

The MEX3A cell state is not hardwired as shown by the observation that MEX3A+ cells isolated from tumors give rise to organoids when cultured in optimal stem cell conditions. Lineage tracing also demonstrates that MEX3A+ cells can re-activate and generate progeny in intact tumors. Our data fit in well with a model whereby LGR5+ cells adopt active (MEX3A-) and latent (MEX3A+) states depending on occupancy of optimal or suboptimal niches respectively. Upon chemotherapy, drug-tolerant persister MEX3A+ cells are transcriptionally reprogrammed; they switch-off genes that characterize LGR5+ ISCs and adopt a state reminiscent of that of fetal epithelium and of revival stem cells. In healthy epithelium, a rare cell subset named revival stem cells are capable of resisting radiotherapy and regenerating the damaged mucosa [9]. A fetal reversion has been described in the intestinal mucosa upon injury linked to cell survival and tissue regeneration[7,8,35,36]. Both transcriptional programs depend on the activity of the transcription factor YAP[7–9,35,36]. We show that fetal, revival and YAP expression programs are transiently co-opted by chemoresistant Mex3a+ CRC cells. It is tempting to speculate that adaptive mechanisms of resistance such as adaptive mutability[44] or epigenetic remodeling[39,40] are facilitated by the acquisition of this primitive state. In agreement with the reversible nature of the drug-tolerant persister cell phenotype observed in other tumor types[45,46], these programs are switched-off upon regeneration, and the drug-tolerant persister MEX3A+ cell population is reconstituted. Whereas the targets of the RNA-binding protein MEX3A+ remain to be determined, our data indicates that its function regulates the transition towards the fetal/revival stem cell state. MEX3A-deficient cells upregulate a secretory program and are unable to survive the treatment. Overall, our findings reveal how pre-existing cell heterogeneity imposed by adaption to different stem cell niches shape chemotherapy responses in CRCs and may help develop strategies to improve the outcome of current treatments by targeting the MEX3A+ drug-persister cell population.

ACKNOWLEDGEMENTS

We thank all members of the laboratory for support and discussions. We are grateful for the outstanding assistance by the IRB Barcelona core facilities for histopathology, functional genomics, mouse mutant, and advanced digital microscopy as well as the flow cytometry, animal facilities of the UB/PCB, and the CRG genomic unit. We thank Antonio Berenguer for expert support on statistics. CM and AA-V have held La Caixa predoctoral fellowships, AC and LJ-G an FPU fellowship from Spanish Ministry of education. HH is a Miguel Servet (CP14/00229) researcher funded by the Spanish Institute of Health Carlos III (ISCIII) and the Agencia Estatal de Investigación (AEI) and FEDER (SAF2017-89109-P). LN holds a Beatiu de Pinos fellowship from Generalitat de Catalunya. This work has been supported by ERC advanced grant 884623 (residualCRC), Spanish Ministry of Science PID2020-119917RB-I00, and 2017-SGR-698 (Generalitat de Catalunya). IRB Barcelona is the recipient of a Severo Ochoa Award of Excellence from MINECO. The single cell profiling of CRC samples was supported by the Belgian Federation against Cancer grant nos. 2018-127 and 2016-133 and by a grant from Fondation Roi-Baudouin. S.T. is supported by a Senior Clinical Investigator award of the Research Foundation—Flanders.

AUTHOR CONTRIBUTIONS

EB and AA-V conceived the study, coordinated experiments and wrote the manuscript. EB supervised the study. AA-V designed and performed key experiments including in vitro and in vivo lineage tracing, generated Mex3a-CreErt2 knock in mouse model. LN generated and characterized Mex3a KO MTOs. FB generated Tomato-creERT2 mice, and Mex3a-Floxed mice. AC performed experiments of latency in triple mutant MTOs *in vitro* and *in vivo*. SC performed experiments of chemotherapy resistance in MTOs. HH provided support with scRNAseq experiments. XH-M performed all mice work. AA-V, CM, DS, CC, SC, and GT generated CRISPR-engineered organoids. CS-OA and LM analyzed scRNAseq data and performed statistical analysis. MS performed IHC. ES provided strategic support and helped with figures and manuscript writing. DT generated MTOs. ST granted access to single cell RNA sequencing data.

AUTHOR INFORMATION

The authors declare no competing financial interests. Correspondence and requests for materials should be addressed to eduard.batlle@irbbarcelona.org.

METHODS

MTOs. We described the establishment of MTOs from primary tumors arising in GEMMs with combined distinct genetic alterations[21]. In brief, triple mutant AKP MTOs were established from CRCs arising in Lgr5-creERT2; Apc$^{fl/fl}$; Kras$^{LSL-G12D}$; Trp53$^{fl/fl}$ mice; ATP MTOs from Lgr5-creERT2; Apc$^{fl/fl}$; Tgfbr2$^{fl/fl}$; Trp53$^{fl/fl}$ mice and AKPT in Apc$^{fl/fl}$; Kras$^{LSL-G12D}$; Trp53$^{fl/fl}$; Tgfbr2$^{fl/fl}$ mice. APK+ Smad4 were generated by introducing a mutation in the SMAD4 locus in APK MTOs using CRISPR/Cas9 as previously described [21]. MTOs were cultured as detailed in[21]. Cultures were checked bimonthly for mycoplasma contamination.

MTO latency and chemotherapy resistance. Complete stem cell medium corresponds to standard medium used for CRC organoid cultures[21]. It is supplemented with 10 mM HEPES, Glutamax, B-27 without retinoid acid (all Life Technologies), 50 ng/ml recombinant human EGF (Peprotech), 100 ng/ml recombinant human NOGGIN and 1 µM galunisertib (LY2157299) in advanced DMEM/F12. For no EGF conditions, we used the same medium without supplementing EGF. In +TGFβ conditions, TGFBR1 inhibitor galunisertib was removed from the medium and 5 ng/ml of active TGFβ1 (Peprotech, 100-21-B) were added. To test chemotherapy resistance, MTOs were cultured in complete stem cell medium or in medium lacking EGF and supplemented TGFβ1 (5 ng/ml) for three days. Organoids were then dissociated with trypsin, and single cells were re-suspended in BME (3533-010-02, Bio-Techne) (around 100 cells per µl). 15 µl drops containing organoid cells were seeded on 96-well flat bottom plates (153596, Cultek). 5FU (sigma, F6627), SN38 (MedChem, HY-13704) and oxaliplatin (MedChem, HY-17371) were added in a range of concentrations as in ref [3] in both stem cell medium or in absence of EGF +TGFβ1 medium. Cell viability was assayed in triplicates using CellTiter-Glo® (G9682, Promega) after 4 days of drug incubation according to manufacturer's instructions. Luminescence signal was quantified in a GloMax® 96 Microplate Luminometer (Promega). Dose - response curves were fitted and corresponding IC50 values were estimated using a four-parameter log-logistic model[47] as implemented in the drc R package[48].

Ethics and animal maintenance. All experiments with mouse models were approved by the Animal Care and Use Committee of Barcelona Science Park (CEEA-PCB) and the Catalan government. Mice were maintained in a specific-pathogen-free (SPF)

facility with a 12-h light–dark cycle and given ad libitum access to standard diet and water.

Genetically modified mice. Lgr5-EGFP-IRES-creERT2 (B6.129P2-Lgr5tm1(cre/ERT2)Cle/J; stock 008875), Reporter strain Rosa26-Stop-TdTomato (B6.Cg-Gt(ROSA)26Sortm14 (CAG-tdTomato)Hze/J , Stock No: 007914) and ApcMin/+ mice were obtained from The Jackson Laboratory. The intestinal epithelium specific Cre (VillinCreERT2)[49] was provided by S. Robine. Conditional $Apc^{fl/fl}$ was provided by Christine Perret[50]. Mex3a-tdTomato reporter mouse was previously generated in the lab[25].

Generation of Mex3a-CreERT2 knock-in mice. We previously described the generation of Mex3a-tdTomato-creERT2 mice[25]. Although Tomato is expressed in these mice, the efficiency of recombination is very low[25] possibly due to poor expression of the bi-cistronic knock-in cassette. To overcome this drawback, we generated a new knock-in mouse strain carrying the creERT2 cassette without the tdTomato reporter. In brief, a cassette bearing a Cre-ERT2/WPRE/bGH polyA was inserted in frame with the Mex3a start codon in exon 1. See Extended Methods for details.

Adenoma formation in mice. $Apc^{fl/fl}$ $Lgr5^{eGFPCreERT2}$ recombination was induced by a single 8 mg/kg intraperitoneal injection of tamoxifen (Sigma, T5648) followed by treatment with 2% DSS in drinking water for five consecutive days to enhance the number of colonic adenomas. APC fl/+; Villin-CreERT2 recombination was induced with 4 consecutive injections of Tamoxifen (80 mg/kg), followed by 2% DSS treatment for 5 days. The general condition of animals was monitored using animal fitness, weight controls and tests to detect blood in stools throughout the experiment. When deteriorating clinical alterations were observed, the animals were culled.

Mex3a and Lgr5 tracing in $APC^{min/+}$ adenomas. APC^{min} animals developed spontaneous intestinal polyps by 8 to 12 weeks of age. To ensure single cell clone recombination in adenomas, we performed these experiments administrating diluted Tamoxifen (sigma) at 8 mg/kg in $Mex3a^{CreErt2/+}$; $Rosa26\text{-}^{Stop\text{-}TdTomato/\ TdTomato}$, and at 1.6 mg/kg in $Lgr5^{CreErt2/+}$; $Rosa26\text{-}^{Stop\text{-}TdTomato/\ TdTomato}$. Animals were sacrificed 2, 7 or 15 days after Tamoxifen induction, and fixated as previously described [51].

Clonal quantification for in vivo lineage tracing. Once all samples were collected, we performed immunohistochemical staining of 3 mm histological sections as described above using the primary antibody against tdTomato (rabbit, Rockland, 600-401-379). Images for clone quantification were acquired using a NanoZoomer-2.0 (Hamamatsu). For clonal quantification, images were processed using ImageJ by a custom-made macro. In brief, Tomato positive objects were detected and thresholds were calculated automatically. The algorithm grouped objects that resided in close proximity (< 12 μm) so that they were considered as unique clones. Clonal area was relativized to the total area (μm2) of the tumor section. For figure 2h and 3g, total tomato size (regardless of the number of clones) was calculated per adenoma area, to identify the overall contribution of tom+ clones to adenoma growth. In figure 2j, 3(h,i) and Extended data figure 7l, the area per clone is plotted, to show differences in the size of individual clones.

For figure 3g,h and I, Tomato area was relativized to total epithelial area. Epithelium was detected using ImageJ macro including size of nuclei and cells as parameters to create a mask in which area of Tomato positive pixels was identified. To calculate number of cells, we estimated the size of single cells in histological sections and interpolated the number of cells per each clone and per section.

BrDU and EdU detection in Lgr5$^{GFP/+}$;Mex3a$^{tdTomato/+}$ adenomas. 40 mg/kg EdU (click chemistry tools 1149-100) was administered 16h prior sacrificing. A minimum of 50.000 Mex3a+ and Mex3a- in Lgr5GFP+ cells were isolated by FACs sorting. EdU was detected using Click-iT™ EdU Alexa Fluor™ 647 Flow Cytometry Assay Kit (C10419). BrdU (125 mg/kg, Medchemtronica, HY-15910) was detected in paraffin sections by immunohistochemistry using anti-BrdU antibody (abcam, Ref.: ab6326), and was quantified using Qupath v0.2.0. or a custom made ImageJ macro.

Mouse adenoma organoid cultures. Adenomas from Villin-CreERT2; APC$^{fl/+}$ mice ; Mex3a-$^{tdTomato/+}$ were dissected and washed in PBS. Dissected material was roughly chopped with razor blades, followed by enzymatic digestion with 200 U/ml collagenase IV HBSS for 30 min at 37 °C. Tissue fragments were subsequently plated in a drop of cold basement-membrane extract (BME) medium (Cultrex BME Type 2, Amsbio): 40 µl in a 24h prewarmed (37 °C) well of a standard 24-well plate (Corning). After 5 min, Complete Stem Cell medium was added. In initial passages, MTO medium was supplemented with the antimicrobial reagent Normocin (InvivoGen).

Introduction of driver mutations in organoids using CRISPR. Guides were designed and cloned into px330-U6-Chimeric BB-CBh-hSpCas9 (Addgene: #42230), which was modified by introducing a SV40 promoter–IRFP expression cassette downstream of hSpCas9. Guide sequences: Smad4: #1, AGACAGGCATCGTTACTTGT; mo_trp53#16: AGTGAAGCCCTCCGAGTGTC, mo_kras g4: GACTGAGTATAAACTTGTGG. For donor plasmid construction, 750bp of 5´ and 3´ MmKRAS G12D homology arm (HA) flanking the knock-in insertion cassettes were synthetized by gene synthesis (Thermo Fisher) and cloned into pShuttle or pDONOR vectors. Organoids were nucleofected as explained in [21] and [26]. For Smad4 knockout mutants, three days after nucleofection, growth medium was exchanged for selection medium (+ TGFβ1 10 ng/ml and removal of Galunisertib). For p53 KO, organoids were selected using nutlin3 (MedChem, HY-50696) at 20 μM. For Kras G12D mutations, organoids were selected by seeding without EGF, and supplemented with Gefinitib (1 μM, Santa Cruz Biotechnology).

Lineage tracing in MTOs. Mex3a-CreERT2 MTOs were seeded as single cells in BME drops with fully supplemented control medium. After 2 days of growth, organoids were induced for 16h with 4-OH Tamoxifen (1 μM Sigma-Aldrich/Merck, H7904). 4OH-TAM was thoughtfully washed out with PBS, and organoids were treated as indicated. FOLFOX was a mixture of 5FU (50 μg/ml, Sigma) and oxaliplatin (100 μM MedChem HY-17371). FOLFIRI was a combination of 5FU (50 μg/μl) and SN38 (100 nM, MedChem HY-13704). After 3 days of treatment, drugs were removed, followed by addition of fresh fully-supplemented control medium. Organoids in control conditions were passaged every 3-4 days as clumps using 1-2 minute treatment with trypsin. For analysis, organoids were dissociated to single cells with trypsin for 20 minutes, followed by mechanical disaggregation, and Tomato positive cells were analyzed by flow cytometry in a FACS Aria 2.0 (BD). Data was analyzed with FACSDiva software (BD) or FlowJo V10. For experiments retracing persister cells (figure 4j and k), prior to performing lineage tracing, organoids were first treated with FOLFIRI/FOLFOX for 3 days, and allowed to recover for 30 days.

CMV-CreERT2 tracing. Adenoma organoids derived from the reporter strain Rosa26-Stop-TdTomato were mutated for Smad4 and p53 (APS organoids). Labeling of random cells was achieved by infecting with a retrovirus encoding a pRetroQ-CreERT2 construct. Virus were produced using packaging constructs in HEK293T cells in DMEM

10% FBS medium, and filtered. Trypsinized organoids (single cells) were suspended in ultra-low attachment plates (Corning) in SC medium and treated with three successive rounds of infection (adding virus- containing medium 50% v/v) in the presence of 8 µg/ml polybrene. After a week, MTOs were seeded back in BME drops and selected with 0.5-1 µg/ml puromycin (InvivoGen). pRetroQ-Cre-ERT2 was a gift from Richard Youle (Addgene plasmid # 59701; http://n2t.net/addgene:59701; RRID:Addgene_59701).

MTO-generated metastasis. For all injections, C57BL/6J mice were purchased from Janvier Labs at six weeks of age and injected at seven weeks. Sex was matched with the origin of the tumour. Intrasplenic vein injections were used for liver colonization by the introduction of intact small organoids into the portal circulation as previously described[21]; MTOs were cultured in standard six-well plates for four days and resuspended in cold HBSS to dissociate remaining BME. Cells were counted and suspended in HBSS for injection, using 1–7.5 × 10^5 cells in 70µl of HBSS per mouse. Tumor growth was inferred by emission of luciferase using IVIS Spectrum In Vivo Imaging System upon intraorbital injection of luciferin (50 µl of a 15 mg/ml solution).

Mex3a tracing in APS metastases. APS (Apc^{mut}, $p53^{mut}$, $Smad4^{KO}$) Mex3a-CreERT2 organoids were inoculated in the liver of C57BL/6J. A single shot of Tamoxifen (200 mg/kg) was administrated to induce recombination of Mex3a cells at clonal level. Mice were sacrificed 2, 46 or 117 days after TAM induction. 2 days after recombination, we injected intraperitoneally 3 doses per week of FOLFIRI over the period of 46days. FOLFIRI cocktail contained 5-FU (30 mg/kg), Irinotecan (73 mg/kg) and Leucovorin (90 mg/kg). Control animals were treated with vehicle following the same regimen.

Genome editing of PDO7. For the generation of Mex3a-iCaspase9-T2A-tdTomato in PDO7 we followed the same strategy as reported in[34]. In brief, guides were designed as explained above (hsMex3a_g1: CCCGTGCCCCATGCCTCCG), and donor Hs Mex3a homology arms (HA) flanking the knock-in insertion cassettes were synthetized by gene synthesis (Thermo Fisher) and cloned into pShuttle or pDONOR vectors.

***In vivo* ablation in PDO7 xenografts**. For subcutaneous injections, PDO7 was cultured in standard six-well plates for 4 to 5 days and recovered in cold HBSS as undissociated organoids. To determine the cell number, a 10% fraction was trypsinized and counted using TC20 automated cell counter (Bio-Rad). Organoids were

suspended in 100 µl HBSS with 50% BME and 1.5 × 10^5 cells per flank were injected in Beige (CB17.Cg-PrkdcscidLystbg-J/Crl) female mice. Growth was scored by palpation and volume was measured with a caliper (multiplying three orthogonal diameters and dividing by two) twice per week. In accordance with our IACUC protocol, mice with tumors over 300 mm3 in volume were euthanized. For inducible ablation experiments we treated animals with 5mg/kg of dimerizer (AP20187, Medchem express, HY-13992) when tumors reached an average size of 40 mm^3. Dimerizer was administrated intraperitoneally for three consecutive days prior to chemotherapy and then maintained throughout the experiment on a daily basis until the end of FOLFIRI treatment. Animals received 5 doses of FOLFIRI (5-FU (30 mg/kg), Irinotecan (73 mg/kg) and Leucovorin (90 mg/kg)) over a period of 10 days. 13 xenographs were analyzed for NT, FOLFIRI and DIM+FOLFIRI conditions (5 mice per group), and 13 xenographs for the DIM condition (4 mice).

Human single-cell RNA-seq data analysis. We analyzed a previously described CRC patient cohort [27] that includes 25 samples from Medical Samsung Center (Seoul. South Korea) and 6 from Katholieke Universiteit Leuven (Belgium) (GSE132465, GSE132257 and GSE144735). We included 11 additional CRC patient samples from KU Leuven. This study was approved by the institutional review board of Commissie Medische Ethiek UZ KU Leuven/Onderzoek. The study was carried out in accordance with ethical guidelines and all patients provided written informed consent. The study participants were patients diagnosed with CRC who underwent surgery without previous treatment. After resection, samples from the tumor and nonmalignant colon tissues were collected and immediately transferred for tissue preparation and processing in the 10X Chromium platform as described in reference[27]. We only analyzed data from epithelial tumor cells. Count matrices for these additional 11 CRC samples were deposited in ArrayExpress under accession number E-MTAB-993. Signatures for LGR5 cells and KI67 are detailed in Supplementary Table 3. A detailed description of methodology utilized for the scRNAseq analysis is detailed in Extended Methods section.

Mouse single-cell RNA-seq tracing data analysis. Recombination of Mex3a cells in AKP and APS organoids carrying a Mex3a KI Cre-ERT2 locus was achieved by 16h pulse of 4OH-Tamoxifen after two days of growth. Following 4OH-Tamoxifen removal, FOLFIRI was added to the media. After 3 days of treatment, drugs were removed, followed by addition of fresh fully-supplemented control medium. Fluorescence-activated cell sorting was used to purify live cells (DAPI Negative) right after 16 hours

of Tamoxifen (before FOLFIRI), 4 days (after FOLFIRI treatment) and 30 days after the addition of FOLFIRI (Recovery timepoint). For the last two timepoints, cells were presorted based on their tracing reporter (tdTomato) expression. Count matrices were deposited in ArrayExpress under accession number E-MTAB-11145. A detailed description of methodology utilized for the scRNAseq analysis is detailed in Extended Methods section.

Induction of Mex3a KO adenomas. We aimed to generate a floxed Mex3a gene to induce organ specific Mex3a KO. In brief, loxP sites were placed at either side of the coding region of exon 2. See Extended Methods for details. We then established a mouse colony bearing $Mex3a^{fl/fl}$ alleles combined with Villin-CreERT2 and $APC^{fl/+}$. Recombination and adenoma formation was induced by 4 consecutive shots of Tamoxifen followed by DSS treatment as explained above. Recombination was checked by qPCR.

Generation of Mex3aKO AKP organoids. We used CRISPR-Cas9 technology to insert a puromycin resistance cassette that disrupted the first exon of the Mex3a gene. The donor plasmid construction was synthetized by gene synthesis (ThermoFisher), and consisted of a 2890 bp DNA fragment containing 935 bp of 5' Mex3a homology arm (HA), 1022 bp of SV40 promoter and puromycin cassette followed by 933 bp of 3' Mex3a homology arm. Small guide RNAs (GGAGAACTAGGATGTTTCGG) were designed <10 bp around the desired site of knock-in insertion using the https://portals.broadinstitute.org/gpp/public/analysis-tools/sgrna-design web tool and were cloned into a pX330-hSpCas9 plasmid as previously described [26]. To generate Mex3a knock-out organoids, 2 x 10^6 of single cell suspensions of trypsinized mouse cells were nucleofected with 7 µg of donor plasmid and 2 µg of px330-Cas9 corresponding plasmids using Lonza nucleofector kit V (VVCA-1003) and program A-32 in an Amaxa-II nucleofector following manufacturer instructions.
Culture medium was exchanged with medium containing puromycin (0.5-1 µg/ml) 3 days after nucleofection. For clonal expansion, puromycin-resistant organoids were seeded one cell per well in a 96 well plate and expanded. Knock-out was verified by western blot.

Mex3a KO single-cell RNA-seq experiments.
Two Mex3a WT clones (parental and a derived clone) and two Mex3a KO clones AKP mouse organoids were treated with FOLFIRI. Three different timepoints were used for this experiment, before treatment, and 2 or 5 days after start of the FOLFIRI treatment.

Organoids from each timepoint were trypsinized and live cells (DAPI negative) were used for the analysis. The Count matrices were deposited in ArrayExpress under accession number E-MTAB-11146. A detailed description of methodology utilized for the scRNAseq analysis is detailed in Extended Methods section.

Statistical analyses. To test statistical significance between samples from two different groups two-tailed Student's t tests were used. When comparing samples from the same animal paired t tests were applied. When normality of data could not be ensured paired or unpaired Wilcoxon tests were used [52]. For figures 1(g, h) S1d, S7i and S15a (g, h), raw qPCR values were normalized against the housekeeping gene Tbp for each sample individually. qPCR data on human samples (S4b, e,f and g) were normalized to human PPIA for each sample individually. A linear model was fit to the resulting values with condition, experiment and MTO/PDO as covariates. All contrasts in this publication were performed using the *glht* function of the multcomp R package[53] with no p-value adjustment. Values to generate plots were corrected by experimental batch by subtracting the corresponding coefficient estimated by the linear model. Values were further centered around the original mean. For adenoma tracing experiments, comparisons related to % of tdTomato over time in Lgr5 and Mex3a (Fig 2j) were estimated through a mixed effects linear model. The model was fitted to the means of percentages computed by tumor and mouse successively. All mixed effects models throughout the publication were fitted using the *lmer* function from the lme4 R package[54] with no p-values adjustment. A boxcox transformation was applied with lambda = 0.25, chosen with the function boxcox of the MASS R package[55]. For comparison of clonal size (Fig. 2k), a mixed effects linear model was applied to the cells per clone after a boxcox transformation with lambda=0.25. Mouse and tumor were included as nested random effects. For testing differences in BrdU across genotypes (Ext. Data Fig. 12c), a mixed effects linear model was fitted to percentages after a boxcox transformation with lambda=0 (logarithmic). The genotype was included as a fixed term and the mouse as a random effect. For in vitro and in vivo tracing of AKP and APS organoids upon different treatments (Fig. 3 d,g, Fig. 5j,k, Ext. Data Fig. 10e,g and Ext. Data Fig. 11a), a mixed effects linear model was applied to the percentage of Tomato positive cells after normalizing to the corresponding values at time 0 and a boxcox transformation with lambda=0.25. The biological replicate was included as a random effect in the model. For comparisons between conditions in Mex3a ablation experiment in xenograft model, a mixed effects linear model was applied to the tumor volume after applying a logarithmic transformation. Treatment and time were combined in one fixed term and the replicate was included as random effect. For survival analysis

in Fig 2n, a Wilcoxon test was used to compare differences in the mean time to event. All group data are represented by the mean and errors bars are the standard error of the mean (s.e.m.) and statistical tests and plots were generated with GraphPad Prism unless indicated.

Sample sizing and collection. All samples and animals were assigned randomly to experimental conditions, as well as sample collection. Automated blind quantifications and blind data analysis were done whenever possible. Images from a minimum of three mice were quantified in each experiment and each condition.

Data availability

Expression arrays and RNA-seq data are available at Gene Expression Omnibus (GEO). The accession number for the expression arrays reported in this paper are GEO: GSE163171 (Mex3a pos Lgr5+ vs. Mex3a Neg Lgr5+ adenoma cells); GSE187650 (Tomato+ cells in $Mex3a^{tom/+}$ and $Mex3a^{Tom/flox}$). For RNA-seq data: GSE163035 (AKP and APT niche factor experiments) and GSE187512 (APS under no EGF conditions). Count matrices for single cell RNAseq experiments were deposited in ArrayExpress under accession number E-MTAB-993 (human data set), E-MTAB-11145 (AKP and APS tracing experiments) and E-MTAB-11146 (AKP Mex3a KO experiment).

REFERENCES

1. Van Cutsem, E., Cervantes, A., Nordlinger, B., Arnold, D. & The ESMO Guidelines Working Group. Metastatic colorectal cancer: ESMO clinical practice guidelines for diagnosis, treatment and follow-up. *Ann. Oncol.* **25**, iii1–iii9 (2014).
2. Argilés, G. *et al.* Localised colon cancer: ESMO Clinical Practice Guidelines for diagnosis, treatment and follow-up†. *Ann. Oncol.* **31**, 1291–1305 (2020).
3. Ooft, S. N. *et al.* Patient-derived organoids can predict response to chemotherapy in metastatic colorectal cancer patients. *Sci. Transl. Med.* **11**, (2019).
4. Vlachogiannis, G. *et al.* Patient-derived organoids model treatment response of metastatic gastrointestinal cancers. *Science (80-.).* **359**, 920–926 (2018).
5. Ganesh, K. *et al.* A rectal cancer organoid platform to study individual responses to chemoradiation. *Nat. Med.* **25**, 1607–1614 (2019).
6. Yao, Y. *et al.* Patient-Derived Organoids Predict Chemoradiation Responses of Locally Advanced Rectal Cancer. *Cell Stem Cell* **26**, 17-26.e6 (2020).
7. RC, M. *et al.* Identification of Lgr5-independent spheroid-generating progenitors of the mouse fetal intestinal epithelium. *Cell Rep.* **5**, 421–432 (2013).
8. Nusse, Y. M. *et al.* Parasitic helminths induce fetal-like reversion in the intestinal stem cell niche. *Nature* **559**, 109–113 (2018).
9. Ayyaz, A. *et al.* Single-cell transcriptomes of the regenerating intestine reveal a revival stem cell. *Nature* **569**, 121–125 (2019).
10. Fujii, M. *et al.* A Colorectal Tumor Organoid Library Demonstrates Progressive Loss of Niche Factor Requirements during Tumorigenesis. *Cell Stem Cell* **18**, 827–838 (2016).
11. Sato, T. *et al.* Single Lgr5 stem cells build crypt-villus structures in vitro without a mesenchymal niche. *Nature* **459**, 262–265 (2009).
12. Jung, P. *et al.* Isolation and in vitro expansion of human colonic stem cells. *Nat. Med.* 1225–1227 (2011). doi:10.1038/nm.2470
13. Sato, T. *et al.* Long-term expansion of epithelial organoids from human colon, adenoma, adenocarcinoma, and Barrett's epithelium. *Gastroenterology* **141**, 1762–72 (2011).
14. Batlle, E. & Clevers, H. Cancer stem cells revisited. *Nat. Med.* **23**, 1124–1134 (2017).
15. Matano, M. *et al.* Modeling colorectal cancer using CRISPR-Cas9–mediated engineering of human intestinal organoids. *Nat. Med.* **21**, 256–62 (2015).
16. Tauriello, F. *et al.* TGF β drives immune evasion in genetically. *Nat. Publ. Gr.* **554**, 538–543 (2018).
17. Fumagalli, A. *et al.* Genetic dissection of colorectal cancer progression by orthotopic transplantation of engineered cancer organoids. *Proc. Natl. Acad. Sci.* **114**, E2357–E2364 (2017).
18. O'Rourke, K. P. *et al.* Transplantation of engineered organoids enables rapid generation of metastatic mouse models of colorectal cancer. *Nat. Biotechnol.* **35**, 577–582 (2017).
19. van de Wetering, M. *et al.* Prospective Derivation of a Living Organoid Biobank of Colorectal Cancer Patients. *Cell* **161**, 933–945 (2015).
20. Muzny, D. M. *et al.* Comprehensive molecular characterization of human colon and rectal cancer. *Nature* **487**, 330–337 (2012).
21. Tauriello, D. V. F. *et al.* TGFβ drives immune evasion in genetically reconstituted colon cancer metastasis. *Nature* **554**, 538–543 (2018).
22. Subramanian, A. *et al.* Gene set enrichment analysis: a knowledge-based approach for interpreting genome-wide expression profiles. *Proc Natl Acad Sci U S A* **102**, 15545–15550 (2005).

23. Han, T. *et al.* Lineage Reversion Drives WNT Independence in Intestinal Cancer. *Cancer Discov.* **10**, 1590–1609 (2020).
24. Lupo, B. *et al.* Colorectal cancer residual disease at maximal response to EGFR blockade displays a druggable Paneth cell–like phenotype. *Sci. Transl. Med.* **12**, (2020).
25. Barriga, F. M. *et al.* Mex3a Marks a Slowly Dividing Subpopulation of Lgr5+ Intestinal Stem Cells. *Cell Stem Cell* **20**, 801-816.e7 (2017).
26. Cortina, C. *et al.* A genome editing approach to study cancer stem cells in human tumors. *EMBO Mol. Med.* **9**, 869–879 (2017).
27. Lee, H.-O. *et al.* Lineage-dependent gene expression programs influence the immune landscape of colorectal cancer. *Nat. Genet.* **52**, 594–603 (2020).
28. Barker, N. *et al.* Identification of stem cells in small intestine and colon by marker gene Lgr5. *Nature* **449**, 1003-10U1 (2007).
29. Schepers, A. G. *et al.* Lineage Tracing Reveals Lgr5+ Stem Cell Activity in Mouse Intestinal Adenomas. *Science (80-.).* **337**, 730–735 (2012).
30. Kozar, S. *et al.* Continuous Clonal Labeling Reveals Small Numbers of Functional Stem Cells in Intestinal Crypts and Adenomas. *Cell Stem Cell* **13**, 626–633 (2013).
31. B, P. *et al.* MEX3A regulates Lgr5 + stem cell maintenance in the developing intestinal epithelium. *EMBO Rep.* **21**, (2020).
32. Rehman, S. K. *et al.* Colorectal Cancer Cells Enter a Diapause-like DTP State to Survive Chemotherapy. *Cell* **184**, 226-242.e21 (2021).
33. Shimokawa, M. *et al.* Visualization and targeting of LGR5 + human colon cancer stem cells. *Nature* **545**, 187–192 (2017).
34. Morral, C. *et al.* Zonation of Ribosomal DNA Transcription Defines a Stem Cell Hierarchy in Colorectal Cancer. *Cell Stem Cell* **26**, 845-861.e12 (2020).
35. Qu, M. *et al.* Establishment of intestinal organoid cultures modeling injury-associated epithelial regeneration. *Cell Res. 2021 313* **31**, 259–271 (2021).
36. S, Y. *et al.* YAP/TAZ-Dependent Reprogramming of Colonic Epithelium Links ECM Remodeling to Tissue Regeneration. *Cell Stem Cell* **22**, 35-49.e7 (2018).
37. Kreso, A. *et al.* Variable clonal repopulation dynamics influence chemotherapy response in colorectal cancer. *Science (80-.).* **339**, 543–548 (2013).
38. de Sousa e Melo, F. *et al.* A distinct role for Lgr5+ stem cells in primary and metastatic colon cancer. *Nature* **543**, 676–680 (2017).
39. Boumahdi, S. & de Sauvage, F. J. The great escape: tumour cell plasticity in resistance to targeted therapy. *Nat. Rev. Drug Discov.* **19**, 39–56 (2020).
40. Shen, S., Vagner, S. & Robert, C. Persistent Cancer Cells: The Deadly Survivors. *Cell* **183**, 860–874 (2020).
41. Puig, I. *et al.* TET2 controls chemoresistant slow-cycling cancer cell survival and tumor recurrence. *J. Clin. Invest.* **128**, 3887–3905 (2018).
42. Touil, Y. *et al.* Colon cancer cells escape 5FU chemotherapy-induced cell death by entering stemness and quiescence associated with the c-Yes/YAP axis. *Clin. Cancer Res.* **20**, 837–846 (2014).
43. Hu, Z. *et al.* Quantitative evidence for early metastatic seeding in colorectal cancer. *Nat. Genet.* **51**, 1113–1122 (2019).
44. Russo, M. *et al.* Adaptive mutability of colorectal cancers in response to targeted therapies. *Science (80-.).* **366**, 1473–1480 (2019).
45. Conti, G. De, Dias, M. H. & Bernards, R. Fighting Drug Resistance through the Targeting of Drug-Tolerant Persister Cells. *Cancers 2021, Vol. 13, Page 1118* **13**, 1118 (2021).
46. Marine, J.-C., Dawson, S.-J. & Dawson, M. A. Non-genetic mechanisms of therapeutic resistance in cancer. *Nat. Rev. Cancer 2020 2012* **20**, 743–756 (2020).
47. Seber, G. A. F. & Wild, C. J. *Nonlinear Regression*. (John Wiley & Sons, Inc., 1989). doi:10.1002/0471725315

48. Ritz, C., Baty, F., Streibig, J. C. & Gerhard, D. Dose-Response Analysis Using R. *PLoS One* **10**, e0146021- (2016).
49. el, M. F. *et al.* Tissue-specific and inducible Cre-mediated recombination in the gut epithelium. *Genesis.* **39**, 186–193 (2004).
50. Colnot, S. *et al.* Liver-targeted disruption of Apc in mice activates beta-catenin signaling and leads to hepatocellular carcinomas. *Proc. Natl. Acad. Sci. U. S. A.* **101**, 17216–17221 (2004).
51. Merlos-Suárez, A. *et al.* The Intestinal Stem Cell SignatureIdentifies Colorectal Cancer Stem Cells and Predicts Disease Relapse. *Cell Stem Cell* 1–14 (2011). doi:10.1016/j.stem.2011.02.020
52. Hothorn, T., Hornik, K., van de Wiel, M. A. & Zeileis, A. A Lego System for Conditional Inference. *Am. Stat.* **60**, 257–263 (2006).
53. Hothorn, T., Bretz, F. & Westfall, P. Simultaneous Inference in General Parametric Models. **50**, 346–363 (2008).
54. Bates, D., Mächler, M., Bolker, B. & Walker, S. Fitting Linear Mixed-Effects Models using lme4. (2014).
55. Venables, W. N. & Ripley, B. D. *Modern Applied Statistics with S*. (Springer New York, 2002). doi:10.1007/978-0-387-21706-2
56. Sanchez-Vega, F. *et al.* Oncogenic Signaling Pathways in The Cancer Genome Atlas. *Cell* **173**, 321-337.e10 (2018).
57. Yaeger, R. *et al.* Clinical sequencing defines the genomic landscape of metastatic colorectal cancer. *Cancer Cell* **33**, 125 (2018).

FIGURE LEGENDS

Figure 1 | Suboptimal stem cell niche specifies Mex3a+ cells and confers resistance to chemotherapy.

a, b, Quantification of organoid growth (mean area ± s.e.m. relative to day 3) of (**a**) AKP MTOs (Apc^{mut}, K-ras^{G12D}, $p53^{mut}$) in the presence of TGF-β, and (**b**)**,** APS MTOs (Apc^{mut}, $Smad4^{mut}$, $p53^{mut}$) in absence of EGF compared to complete stem cell medium (SC med.). Dashed lines indicate the day TGFβ was removed or EGF was re-added, respectively. *n*=4 independent wells per condition, linear model on log-transformed values. Scale bars: 50 μm. **c, d** Relative viability (ATP measurements) of AKP and APS MTOs grown in complete SC medium versus media lacking EGF or supplemented with active TGFβ1 upon treatment with increasing concentrations of SN38. Trend line was calculated using LOESS model, *n*=3. Mean ATP measurement ± s.e.m is shown. **e, f,** Relevant GSEAs obtained after RNA sequencing analysis of (**e**) AKP and (**f**) APS MTOs grown in SC medium versus either +TGFβ1 or no EGF medium respectively. Profiling was performed at day 7. Left panels in each case indicate Hallmarks or gene ontology biological processes (GOBPs) related to functional pathways (Function); right panels indicate GSEAs related to cell identity of different cell populations (Identity). The complete sets of GSEAs and identity signatures are included in Supplementary Tables 1 and 3. Gene sets are ordered based on their -log10 p-value, dashed line indicates p-value = 0.05. **g, h,** Mex3a mRNA expression levels in (**i**) AKP MTOs treated with TGF-β vs control SC medium (n=6 independent experiments); and in (**h**) APS MTOs grown in the absence of EGF vs control SC medium (n=8 independent experiments). Boxplots indicate adjusted values of Mex3a mRNA corrected by experimental batch. **i,** Representative flow cytometry profiles of dissociated $Mex3a^{Tom/+}$ AKP and APS organoids grown in complete SC medium (left panels) or in medium without EGF or supplemented with TGF-β1. Frequency of tomato positive cells in each case is referred to the number of viable cells. Upper panel shows the profile of control MTOs ($Mex3a^{+/+}$) used to establish the gates. **j-l,** UMAPs of pooled epithelial cancer cells corresponding to 37 CRC patient samples. Cells are colored according to levels of (**j**) KI67 signature, (**k**) MEX3A mRNA or (**l**) LGR5+ ISC signature. **m,** Distribution of Mex3a+/Lgr5+, Mex3a+/Lgr5- and Mex3a-/Lgr5- in cell cycle phases according to expression of cell cycle gene signatures (see methods for details).

Figure 2 | Mex3a marks a subpopulation of slow-proliferative Lgr5+ cells in adenomas.

a, Representative immunohistochemistry of tdTomato in Lgr5CreERT2; $APC^{fl/fl}$; $Mex3a^{Tom/+}$ mouse colon. Adenomas (Ad) are delimited by a dashed line. NM indicates normal mucosa**. b,** Representative flow cytometry plots of dissociated $Mex3a^{Tom/+}$ crypts (Upper panels) and adenomas (lower panels). Negative controls correspond to $Mex3a^{+/+}$ mice samples. Numbers indicate frequency of Mex3a+ cells within the Lgr5-GFP+ cell gate. **c,** Quantification (mean ± s.e.m.) of % Mex3a+ cells within Lgr5-GFP+ cells in crypts compared to adenomas, *n*=6 and *n*=8 mice respectively, Wilcoxon-test. **d,** Percentage of EdU incorporation (mean ± s.e.m.) in Mex3a+/Lgr5+ and Mex3a-/Lgr5+ adenoma cells. *n*=5 mice, Wilcoxon-test **e,** Gene set enrichment analysis in Mex3a+ versus Mex3a- tumor cells sorted from Lgr5-GFP+ adenoma cell population. Most relevant gene sets are shown, dashed line indicates p-value = 0.05. Bar direction was determined based on NES score. **f,** Upper panel: a Cre-ERT2/WPRE/bGHpolyA cassette was inserted in the translation start site of *Mex3a* locus. Image panels; Immunofluorescence of tdTomato in early recombined cells (24h after Tam administration), (upper) co-staining with stem cell marker Olfm4 in normal crypts, (lower) co-staining with BrdU in adenomas. Scale Bar 100μM in low magnification, 50μM in detail. **g,** Quantification of BrdU incorporation in tissue sections. *n* = 14 adenomas from 3 independent mice, Linear model. **h**, Area occupied by Tomato+ cells normalized per total adenoma area quantified from tissue sections. P values according to a linear model. *n*= 366 tumors (10 mice; day 2), 372 tumors (9 mice; day 7), 121 tumors (4 mice; day 15) for Mex3a-CreERT2 mice. 110 tumors (5 mice, day 2), 95 tumors (5 mice, day 7) and 126 tumors (5 mice; day 15) for Lgr5-CreERT2 tracing. **i,** Representative immunohistochemistry against reporter gene tdTomato at d2 and d15 after TAM administration in Lgr5-creERT2 and Mex3a Cre-ERT2. Scale bars 100μM. **j,** Size distribution of small clones generated by Lgr5-creERT2 and Mex3a Cre-ERT2 cassettes. **k,** Genotypes of mice bearing Mex3a-Tomato knock-in/+ (HET) and Mex3a-Tomato knock-in/floxed alleles (KO). **l.** Expression levels according to microarray data of Mex3a signature genes in Tomato+ cells isolated by FACS from Mex3a HET and KO adenomas (n=3 independent colonic tumors). **m,** Expression of secretory cell marker genes in Tomato+ cells isolated by FACS from Mex3a HET and KO adenomas (n=3 independent colonic tumors). **n,** Upper panel; timeline of treatments. Lower panel: Kaplan Meier survival plot of mice with the indicated genotypes and treatments (n=12 mice (HET), 10 (HET +5FU), 8 (Mex3a KO) and 7 (Mex3aKO + 5FU); Wilcoxon test).

Figure 3 | Mex3a+ cells regenerate metastasis after chemotherapy in mouse CRC models.

a, Schematic representation of CRISPR-Cas9-based generation of advanced colorectal cancer organoids from Mex3a-creERT2 mice. **b,** Representative image and flow cytometry plot of an APS organoid 16 hours after addition of Tamoxifen. Scale bar 50uM. Values indicate mean ± s.e.m. Tomato + cells, *n*=3 independent experiments. **c,** Recombination in Mex3a+ cells present in APS organoids was induced with Tamoxifen 16h before addition of chemotherapy. Organoids were treated during 3 days with FOLFOX or FOLFIRI and then allowed to recover for 30 days. Representative pictures of organoids at different time-points are shown. White arrows indicate necrotic organoids. Scale bar 100 μm for low magnification, 50 μm for detail. **d,** Flow cytometry quantification of Tomato+ cells in MTOs treated with FOLFIRI and FOLFOX. Frequency of populations referred to the number of viable cells (DAPI negative). For APS *n*=2 and n=4 independent experiments for FOLFOX and FOLFIRI respectively; for AKP *n*=7 and n=2; p value was calculated by a mixed effects linear model. **e,** Longitudinal intravital bioluminescence imaging (BLI) quantification (photons s−1, normalized to day 90) of the liver upon intrasplenic injection of Mex3a-CreERT2 APS MTOs in C57BL/6J mice. Mice were administered with a single dose of Tamoxifen 88 days after tumor cell injection, before chemotherapy treatment started. FOLFIRI treatment lasted 46 days and then metastasis formation was followed. **f,** Representative images of Mex3a-derived clones in metastasis. Scale bar = 50 μM. **g,** Percentage of Tomato+ from total tumor epithelial area in FOLFIRI treated vs. control metastases; p value was calculated using a linear mixed model. **h,** Average size and **i,** size distribution of Mex3a-derived clones in both treated and untreated conditions. *n*= 192 individual metastasis (from 3 mice), 199 (3), 141 (3) for non-treated condition at d2, d46 and d117 after TAM induction respectively; and *n*= 205 (3) and 45 (3) for FOLFIRI treated metastasis at d46 and 117 after TAM. Pearson's Chi-squared test was used to compare conditions at d117. **j.** Mex3a-inducible_caspase_9-Tomato allele engineered in PDO7. Quantification of MEX3A-hi cells (defined as the top 10% of the tdtomato population). **k.** The frequency of populations is referred to the number of viable epithelial cells. *n*=10 xenografts in NT, 9 in Dim treated condition; Paired Wilcoxon test. **l,** Contribution of MEX3A+ cells to PDO7 subcutaneous xenograft growth. Dimerizer was administrated during three consecutive days right before FOLFIRI treatment and maintained throughout. *n*=13 xenografts per condition; p value was calculated using a mixed linear model. **m,** Kaplan-Meier analysis of survival of the experiment in panel **l.** Mice were sacrificed when xenografts size reached or surpassed

300 mm^3. A Wilcoxon test was used to compare differences in the average time to event.

Figure 4 | Single cell transcriptomic analysis of Mex3a+ cells and progeny in AKP MTOs during chemotherapy. a, Experimental design. Tamoxifen was added for 16 hours before treatment to AKP organoids in order to induce recombination in Mex3a+ cells; then FOLFIRI treatment was applied for 4d, after which recovery was allowed for 30 days. Viable Tom+ and Tom- cells were isolated by FACS sorted after FOLFIRI treatment (4d) or the recovery period (30d) and subsequently analysed by scRNAseq. RNAseq of AKP before treatment were used as a reference. **b,** UMAP representation of untreated MTOs and sorted Tomato+ cells 4d after treatment and upon recovery (30d). **c,** Representation of Mex3a expression in UMAP (left) and quantification of expression levels as violin plots. Arrow indicate Mex3a-high cells. **d-h,** Average expression of the indicated genes signatures in individual cells represented in UMAPs (left panels) and violin plots levels (right panels). Only Tomato+ cells are shown upon treatment. **i.** Experimental design to assess contribution of Mex3a+ cells upon re-exposure to chemotherapy in APS and AKP MTO cultures regenerated from a first round of treatment. **j-k**, % of Tomato+ cells during APS (j) or AKP (k) organoid regeneration after chemotherapy assessed by flow cytometry. n= 6 independent measurements for APS and AKP organoids; p value was calculated by a linear model **l.** UMAP representation showing overlapping distributions of Tomato+ and Tomato- cells in AKP MTOs from the experiment shown in panel a-h.

Figure 5 | Analysis of Mex3a-deficient AKP MTOs.

a, Western-blot analysis of MEX3A and in wild-type and two independent CRISPR-generated AKP knock-out MTOs. Vinculin is used as a loading control **b.** Representative images of Mex3a wild-type and knock-out AKP MTOs upon recovery of No_EGF/+TGFβ condition or FOLFIRI treatment. Scale bar 50 um **c.** Bioluminescence quantification of AKP MTOs in the experiment shown in panel b. Upper panel MTOs always in complete SC medium, middle MTOs recovered from no_EGF/+TGFβ condition and lower panel MTOs recovered from FOLFIRI treatment; n=3 independent experiments; P value calculated using a lineal model. **d**, Wild-type or Mex3a KO1 AKP MTOs were inoculated through the spleen of c56Bl/6 mice. Mice were randomized in two arms (untreated or treatment with FOLFIRI as indicated). Graph shows liver bioluminescence over time as a surrogate of metastatic growth. Individual mice (thin lines) and average growth (thick lines) in each treatment group

are indicated. n=5 mice per treatment. A mixed effects linear model was applied to calculate p-values between WT FOLFIRI and KO1 FOLFIRI at day 39. **e.** Representative UEA-1 lectin staining of liver metastases generated by wild-type and Mex3a- KO1 MTOs. **f.** quantification of UEA-1 lectin staining in liver metastases. n = 5 mice for WT2 and 4 mice for WT1, KO1 and KO2. An average of 30 metastasic nodules were quantified per mice. Unpaired Wilcoxon test. **g.** Cell distribution in UMAPs of two independent WT (WT1 and WT2) and Mex3a KO1 AKP MTO cultures in untreated conditions and treated with FOLFIRI for 2 days or 5 days. Note that no viable cells were recovered in KO1 at 5d post-treatment, **h.** Mex3a comparing WT1+2 versus KO1 AKP MTOs in UMAPs. Arrow indicate Mex3a-high cells. **i-k,** Average expression of the indicated gene signatures in individual cells represented in UMAPs (left panels) or as violin plots (right panels). **l.** Graphical summary of the key findings of the study.

EXTENDED DATA FIGURE LEGENDS

Extended Data Figure 1 | Suboptimal stem cell niche conditions specify Mex3a+ cells and confer resistance to chemotherapy in APT colon cancer organoids.

a, Quantification of organoid growth (mean area ± s.e.m. relative to day 3) of APT MTOs (Apc^{mut}, $p53^{mut}$,$Tgfbr2^{mut}$) in absence of EGF compared to complete stem cell medium (SC med.). Dashed lines indicate the day EGF was re-added. *n*=4 independent wells per condition, linear model on log-transformed values. Scale bars: 50 μm. **b,** Viability (ATP measurements) of APT MTOs grown in complete SC medium versus medium lacking EGF upon treatment with increasing concentrations of SN38. Trend line was calculated using LOESS model, *n*=3. Mean ± s.e.m is shown. For details on IC50 calculations, see Extended Methods **c,** Relevant GSEAs obtained after RNA sequencing analysis of APT MTOs grown in SC medium versus medium with no EGF respectively. Profiling was performed at day 7. Left panels in each case indicate Hallmarks or gene ontology biological processes (GOBPs) related to functional pathways (Function); right panels indicate GSEAs related to cell identity of different cell populations (Identity). The complete sets of GSEAs and identity signatures are included in Supplementary Tables 1 and 3. Gene sets are ordered based on their p-value, dashed line indicates p-value = 0.05. **d** Mex3a mRNA expression levels in APT MTOs grown in the absence of EGF vs control SC medium (n=4 independent experiments). Boxplots indicate adjusted values of Mex3a mRNA corrected by experimental batch.

Extended Data Figure 2 | Suboptimal stem cell niche conditions arrest organoid growth and confer broad chemoresistance to colon cancer organoids.

a, Heatmap summarizing the effect on organoid growth under suboptimal niche conditions (absence of EGF or presence of TGFβ1) vs growth in SC complete medium (with EGF and no TGFβ1) in MTOs with the indicated genotypes. **b,** Heatmap summarizing the increase in SN38 IC50 values promoted by absence of EGF or presence of TGFβ1 in MTOs with different genotypes. Color scale shows normalized IC50s compared to IC50s in SC medium (with EGF and no TGFβ1). **c,** Viability (ATP quantification) of APS, AKP and AKP+S MTOs grown in complete SC medium versus medium lacking EGF and supplemented with active TGFβ1 upon treatment with increasing concentrations of 5FU, Oxaliplatin and SN38. Trend line was calculated using LOESS model, *n*=3. Mean ± s.e.m is shown. **d.** Scheme and Viability of APS organoids in increasing concentrations of SN38 in complete or medium with no EGF in latent-recovered organoids. Briefly, latency of APS organoids was induced by

removing EGF for 7 days. EGF was added back, thus promoting the growth of these latent APS organoids. Subsequently, EGF was removed, and effects of re-exposure to chemotherapy measured. LOESS model, *n*=3. Mean ± s.e.m is shown. **e.** Percentages of Mex3a positive cells in 3 different genotypes in SC medium calculated by Flow Cytometry. Percentages are calculated over the total number of organoid live cells. n = 8 (APS), 10 (AKP), 9 (AKPS) independent observations. Unpaired Wilcoxon test. **f.** Percentages of Mex3a positive cells in complete medium, in the absence of EGF or in the presence of TGFβ1 in APS, AKP and AKPS organoids calculated by Flow Cytometry. n = 3 (APS), 6(AKP) and 4 (AKPS) independent experiments. Paired Wilcoxon test.

Extended Data Figure 3 | Suboptimal stem cell niche conditions confers broad chemoresistance in a subset of patient derived organoids.

a, Heatmap summarizing the effect on organoid growth in medium supplemented with recombinant active TGFβ1 and in absence of EGF compared to full SC medium in a collection of human PDOs. **b.** Heatmap summarizing the increase in SN38, 5FU and Oxaliplatin IC50 values, promoted by absence of EGF or presence of TGFβ1 in the indicated PDOs. **c,** Viability (ATP quantification) of a collection of human patient derived organoids grown in complete SC medium versus medium lacking EGF and supplemented with active TGFβ1 upon treatment with increasing concentrations of 5FU, Oxaliplatin and SN38. See extended methods for details on calculation of IC50 values.

Extended Data Figure 4 | Mex3a labels slow proliferative Lgr5 stem cells in human PDO7.

a. CRISPR-Cas9 targeting strategy to introduce an inducible ablation and reporter cassette into the MEX3A locus in PDO7. Immunofluorescence shows Tomato and E-cadherin in PDO7 edited xenografts. Scale bar 50 μM. **b,** RT-qPCR analysis of MEX3A and Tomato in sorted epithelial (EPCAM+) Mex3a-tomato-hi vs. low cells from PDO7 xenografts. *n* = 4, Paired t-test. **c.** Representative flow cytometry profiles of dissociated $Mex3a^{Tom/+}$ PDO7 edited organoids grown in complete SC medium (left panels) or in medium without EGF and added TGF-β1. n=3, Paired Wilcoxon test. **d.** Flow cytometry plot of a dissociated subcutaneous xenograft generated by inoculation of PDO7-targeted with KI67-RFP fusion and LGR5-GFP reporter cassettes. Epithelial cells (EPCAM+) are shown. **e, f,** and **g,** Quantification of (**e**) MEX3A, (**f**) Lgr5 and (**g**) Ki67 mRNA by RT-qPCR in the indicated four PDO7 xenograft cell subpopulations. *n*=5 xenografts. Paired t-test.

Extended Data Figure 5 | Single cell RNA sequencing analysis of individual human CRC samples demonstrate MEX3A marks a subpopulation of low proliferative LGR5+ cells.

a. Distribution of epithelial CRC cells according to KI67 and LGR5 signatures levels in the pooled CRC patient cohort. Cells are colored by Mex3a mRNA levels. **b**. As in panel_a but showing the cell distribution in each individual CRC patient sample. **c.** Identification of LGR5-hi/Mex3a-hi and LGR5-hi/Mex3a-lo population in the UMAP of the pooled single cell CRC patient dataset. **d.** Each cell of the dataset was allocated to a cell cycle phase according to expression of specific gene signatures (see methods for details). Quantifications are shown in Fig. 1m.

Extended Data Figure 6 | Prediction of disease relapse in CRC patients by gene expression signatures of Mex3a+ cells.

a. Descriptive statistics of the pooled transcriptomic cohort of primary CRC patients used in survival analyses. **b-c.** Identification of Lgr5-high/Mex3a-high and Lgr5-high/Mex3a-low populations in scRNAseq dataset. Gene signatures of each population were generated by selecting the top 100 differentially expressed genes between the two populations (Supplementary Table 3 and supplementary methods). **e.** Stratification of patients according to high or low (split by median) average levels of the signature of Lgr5-high/Mex3a-high cells. P value and HR are adjusted by age, gender, mismatch repair status, and AJCC stage using a multivariate statistical model. **f.** Risk of relapse (log HR) expressed as a continuous variable of the Lgr5-high/Mex3a-high signature (Z-scored). Same covariates as in **e** were included in the statistical model. **g-h**, Analogous analyses to **e** and **f**, for the gene expression signature of the Lgr5-high/Mex3a-low population.

Extended Data Figure 7 | Characterization of Mex3a+ cells in adenomas from $Apc^{min/+}$ mice.

a, Gating strategy of Tom+ cells in both Crypt and Adenomas from Mex3-Tomato/+; $Apc^{fl/fl}$; Lgr5-GFP showing Lgr5 negative cells that result from the mosaic expression of the Lgr5-GFP reporter cassette. The only gene significantly upregulated in Lgr5+ versus Lgr5- within the Mex3a-Tom-high population was Lgr5 (Extended Table 2). **b,** RT-qPCR analysis of MEX3A in sorted Lgr5 Mex3a-tomato-positive vs. negative cells from adenomas. **c,** Quantification (mean ± s.e.m.) of percentages of Mex3a+ cells within Lgr5-GFP+ cells in organoids cultured in Stem Cell full medium, in absence of EGF or in presence of TGFβ1, *n*=5 independent experiments, Paired Wilcoxcon test.

d, Representative flow cytometry profile of dissociated Mex3a$^{Tom/+}$ adenoma organoids cultured under the indicated conditions. The frequency of populations is referred to the number of viable cells. Numbers are mean ± s.e.m. of control, no EGF and +TGFβ1, independent MTO cultures *(n*=8, 7, and 4, respectively, Paired Wilcoxon test) **e**, Organoid formation efficiency of tumor cell populations isolated from adenomas by FACS (number of organoids formed after 10 days / number of seeded cells). **f,** Mean organoid size of adenoma organoids from (e). **g,** Flow cytometry plots of adenoma sorted Mex3a_Tomato+ (in red) and Mex3a_Tomato- (in green) cells used for organoid formation in e (left panel), and plots from flow cytometry analyses of the resulting formed organoids derived from sorted Mex3a+ Lgr5+ (right panel, up) or Mex3a- Lgr5+ (right panel down). Right bar plot shows the quantification on the frequency of Mex3a_Tomato+ within LGR5 compartment in adenoma organoids arising after plating Mex3a+ or Mex3a- adenoma cells. Frequency is referred to the total number of live cells. n=3, Linear model after boxcox transformation to ensure normality was used to calculate p-values on e, f and g. **h,I,** Flow cytometry quantification (mean ± s.e.m.) of percentages of Mex3a_Tomato+ cells of adenoma organoids originated from Mex3a_Tomato-;Lgr5_GFP+ (h) or Mex3a_Tomato+;Lgr5_GFP+ (i) cells in SC media, noEGF and with TGFbeta for 7 days (mean ± s.e.m., n=4). **j,** Upper panel: a Cre-ERT2 / WPRE / bGH polyA cassette was inserted in the translation start site of *Mex3a* locus. Lower panel: immunohistochemistry against tdTomato reporter 48h after Tamoxifen injection. Colonic adenomas are delimited by a dashed line. **k,** RT-qPCR analysis of Mex3a and tdtomato mRNA in sorted Tomato+ cells 16h after Tamoxifen inoculation (mean ± s.e.m., *n*=3 mice, Paired t-test). **l,** Violin plot showing the distribution of clone sizes generated by Mex3a and Lgr5 cells over time. *n* =10 (day 2), 9 (day 7), 4 (day 15) mice for Mex3a, *n*=5 mice for Lgr5 tracing at each time-point. P-value was calculated using mixed effects linear model.

Extended Data Figure 8 | Mex3a deletion has no overt effect on intestinal biology

a, Schematic representation of the generation of an intestinal specific Mex3a KO. Briefly, animals homozygous for a LoxP-flanked Mex3a allele were crossed with a VillinCreERT2. Tamoxifen induction promoted the recombination of the LoxP sites, resulting in an intestinal Mex3a KO. See methods for details. **b** and **c,** Representative images and quantification of ChgA, Dclk1, Periodic acid-Schiff-Alcian Blue (PAS-AB), Keratin20, Olfm4 and Lysozyme. n = 3 independent mice per genotype. n.s stands for non significant. Generalized mixed effects linear model with poisson distribution used to calculate significance. Scale Bar 100 μm.

Extended Data Figure 9 | Characterization of Mex3a KO Adenomas. a, RT-qPCR analysis of MEX3A mRNA in Mex3a HET and KO adenomas. n = 3 adenomas (HET) and 4 (KO), t-test. **b,** Relevant GSEAs obtained after transcriptomic analysis of Tom/+ (HET) and Tom/flox (KO) in vivo adenomas sorted by expression of the tomato reporter gene. Selected GSEAs are ranked by their NES scores. **c.** Flow cytometry Histogram of Tomato+ cells in Tom/+ (HET) and Tom/floxed (KO) for Lectin. **d,** Quantification of Lectin staining in Tom+ cells in adenoma organoids derived from HET and KO adenomas. n=3, Unpaired Wilcoxon test. **e,** Quantification of number of adenomas per mice in treated and untreated Mex3a HET or KO animals. Mex3a +/+ or Mex3a fl/fl VillinCre APC fl/+ animals were induced with Tamoxifen following DSS treatment. 60 days after induction of adenomas, mice were sacrificed for the counting. See methods for details. n = 10 mice 5FU-KO, 7 5FU HET and 8 for KO and HET. Generalized linear model with poisson distribution.

Extended Data Figure 10 | Mex3a+ cells regenerate organoids after chemotherapy in A, AP and AKP tumors.

a, Schematic representation of CRISPR-Cas9-based generation of AKP advanced colorectal cancer organoids from Mex3a-creERT2 AP organoids. **b**, Representative image and flow cytometry plot of an AKP organoid 16 hours after addition of 4OH-Tamoxifen. Values indicate mean ± s.e.m. n=3 independent experiments. **c**, Representative images of AKP organoids 16h after addition of 4OH-Tamoxifen in complete stem cell medium or in medium supplemented with TGF-β1 for 7 days. Scale bar 50 μm. **d,** AKP and APS bearing Mex3a-creERT2 alleles were treated with Tamoxifen in complete stem cell media. After 16h, organoids were cultured in absence of EGF (APS) or presence of TGF β1 (AKP) for 4 days. Percentage of tomato+ cells was quantified by flow cytometry (mean ± s.e.m., n=3 independent wells). **e**, Tomato positive cells cultured in Stem Cell Media were recovered by flow cytometry at 1d, 5d or 10 days post recombination. mRNA abundance was measured by RT-qPCR (mean ± s.e.m., *n*=3, Paired t-test) **f,** Recombination in Mex3a+ cells present in AKP organoids was induced with Tamoxifen 16h before addition of chemotherapy. Organoids were treated during 3 days and then allowed to recover for 30 days. Representative pictures of organoids at different time-points are shown. Scale bar 50 μm. **g**, Lineage tracing of Mex3a+ cells in organoids derived from $APC^{Min/+}$ mice. Recombination was induced with Tamoxifen 16h before addition of chemotherapy. Organoids were treated during 3 days and then allowed to recover for 20 days. **h,**

Representative pictures of organoids at different time-points are shown. **i,** Flow cytometry quantification of Tomato+ cells in adenomas referred to the number of viable cells (DAPI negative) over time (n= 4). Scale bar 50 μm. Linear model was applied to calculate p-value. **j,** Schematic representation of CRISPR-Cas9-based introduction of p53 null alleles in adenomas organoids derived from $APC^{Min/+}$ mice carrying the Mex3a-creERT2 knock-in cassette. **k,** p53-/- APC-/- organoids were induced with Tamoxifen 16h before addition of chemotherapy. Proportion of Tomato cells over live cells was calculated by Flow cytometry. n=2 independent organoids, linear model.

Extended Data Figure 11 | Lineage tracing of tomato+ cells originating from randomly expressed CMV-CreERT2 driver.

a, Scheme of the experimental design. We aimed to trace a random a population of tomato+ cells in APS organoids. To this end, we introduced a CMV-CreERT2 with a retroviral vector. At low doses of Tamoxifen we achieved recombination of equivalent proportion of cells from organoids carrying Mex3a-CreERT2 and CMV-CreERT2 alleles. Recombination was induced with 4-OH TAM for 16 hours following FOLFIRI or FOLFOX treatment. The fraction of Tomato+ cells over time was quantified by Flow Cytometry. A linear model was used to estimate p-value.

Extended Data Figure 12 | Metastatic latency of triple mutant MTOs.

a, Quadruple mutant MTOs (AKPT or AKP+S) and triple mutant MTOs (AKP and APT) were labeled with a luciferase expression vector and inoculated through the spleen into in C57BL/6J mice. Liver metastatic growth was assessed by intravital bioluminescence imaging (BLI). Graph shows longitudinal BLI measurements (photons s−1), normalized to the day of injection. Points and lines represent individual mice, trend lines (bold) were generated using a LOESS model. For AKPT n=2, APS and AKP+S n=3 and AKP n=5 **b**, Representative images of BrdU immunohistochemistry in liver metastasis generated by triple and quadruple mutant MTO, quantified in **c.** BrdU was injected into animals 2 hours before sacrifice. A mixed effects linear model was fitted to percentages after a boxcox transformation. Scale Bar 250 μm.

Extended Data Figure 13 | Mex3a+ cells persist after chemotherapy and regenerate metastasis after FOLFIRI treatment.

a, Representative images of Tomato immunohistochemistry in liver sections containing metastases generated by Mex3a-CreERT2 APS (Apc^{mut}, $p53^{mut}$, $Smad4^{KO}$) MTOs at experimental endpoints (d117 after tamoxifen induction), in control and FOLFIRI-

treated mice. Scale bar 2mm. **b,** Example of a residual Tomato+ micro-metastatic lesion-derived from Mex3a-traced cells (d117 after tamoxifen induction). Scale Bar 1mm for low magnification, 100 μm for detail. **c,** Percentage of Tomato+ area occupied versus the metastasis size. Each dot is a metastasis and the colors indicate a different mouse**. d,** ISH of Mex3a and LGR5 in Mex3a-traced cells (tomato+) in metastasis regenerated after FOLFIRI treatment. Arrow indicates an area with Mex3a negative cells, and arrowhead point to Mex3a positive cells. Scale bar 50μM.

Extended Data Figure 14 | Expression of cell state marker genes during chemotherapy treatment and after recovery in AKP MTOs. Violin plots for key marker genes of **a,** Lgr5 ISCs; **b,** Fetal progenitors/revival stem cells; **c,** YAP target genes; and **d,** proliferative cells. Expression in both Tomato+ and Tomato- cells after FOLFIRI treatment and recovery are shown.

Extended Data Figure 15 | Expression of Fetal/revival cell state marker genes during chemotherapy treatment and after recovery in AKP and APS MTOs. RT-qPCR analysis of the expression of Mex3a, Lgr5 and two fetal progenitors/revival stem cell marker gens – Anxa3 and Basp1 - during FOLFIRI treatment and recovery. Error bars indicate mean ± SEM. n=4. A linear model was applied to calculate p-values.

Extended Data Figure 16 | Single cell RNA sequencing of Mex3a+ cells and their progeny in APS MTOs after chemotherapy and recovery. a, Experimental design. **b,** UMAP representation of untreated MTOs (NT) and sorted Tomato+ and Tomato- cells 4d after FOLFIRI treatment and upon recovery (30d). **c,** Mex3a expression overlaps in Tomato+ and Tomato- cells after recovery. **d-i,** Mex3a levels or average expression of the indicated gene signatures in individual cells represented in UMAPs (left panels) and violin plots (right panels). Levels in both Tomato+ and Tomato- are shown.

Extended Data Figure 17 | Single cell RNA sequencing of Mex3a+ cells and their progeny in APK MTOs after chemotherapy and recovery. a, Experimental design. **b-c**, UMAP representation of untreated MTOs (NT) and sorted Tomato+ and Tomato- cells 4d after FOLFIRI treatment and upon recovery (30d). Note the overlapping distribution of Tomato+ and Tomato- cells. **d-i,** Mex3a levels or average expression of the indicated gene signatures in individual tomato+ cells represented in UMAPs (left

panels). Violin plots (right panels) compare expression levels in Tomato+ and Tomato- cells after FOLFIRI treatment and upon recovery.

Extended Data Figure 18 | Single cell transcriptomic analysis comparing Mex3a WTs and KO1 AKP MTOs. **a.** Cell distribution represented as UMAPs of two independent WT (WT1 and WT2) versus Mex3a KO1 AKP MTOs in untreated conditions and after treatment with FOLFIRI for 2 days or 5 days. Note that no viable cells were recovered from KO1 at 5d post-treatment. Panels **b,d,f,h,j** show average expression levels of the indicated signatures in UMAPs. Panels **c,e,g,l,k** show violin plots for key marker genes of the indicated cell populations and cell states.

Extended Data Figure 19 | Single cell transcriptomic analysis comparing Mex3a WTs and KO2 AKP MTOs. **a.** Cell distribution represented as UMAPs of two independent WT (WT1 and WT2) versus Mex3a KO2 AKP MTOs in untreated conditions and after treatment with FOLFIRI for 2 days or 5 days. **b.** Representation of Mex3a expression in UMAPs comparing WT1+2 (right) versus KO2 AKP MTOs (left). Arrow points at Mex3a-high cells. Panels **c,e,g,i,k** show average expression levels of the indicated signatures in UMAPs (left) and violin plots (right). **d,f,h,j,l** show violin plots for key marker genes of the indicated populations and cell states.

Extended Data Figure 20 | Mutated driver pathways frequencies in CRC patients. The mutational status of the 4 major driver signaling pathways in CRC (WNT, RAS, TP53 and TGFß) was scored by assessing alterations in components of oncogenic pathways according to the curated list signaling pathway component lists described in Sanchez-Vega et al.[56] . We analyzed primary microsatellite stable primary CRCs and metastases of the MSK-impact dataset[57]. **a,** Barplot showing the number of CRC primary tumor samples with the indicated combination of mutated pathways (n=508). **b,** Barplot showing the number of metastasis samples with the indicated combination of mutated pathways (n=533). **c,** Frequency of primary CRC samples according to the number of mutated main driver pathways stratified by AJCC clinical staging at the time of diagnosis.

Figure 1

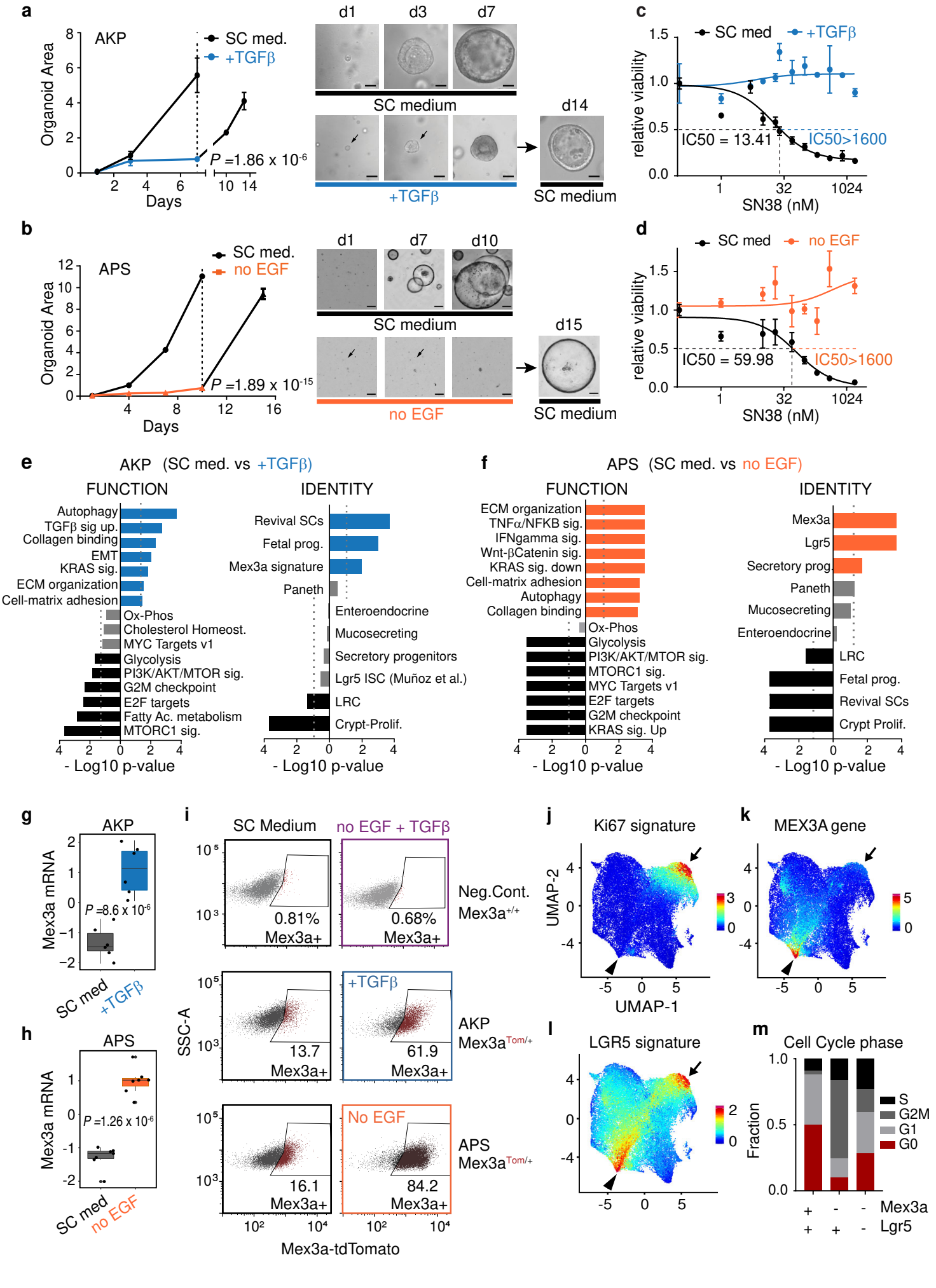
a
AKP
SC med.
+TGFβ
Organoid Area
Days
P =1.86 x 10-6
d1
d3
d7
SC medium
+TGFβ
d14
SC medium
c
SC med
+TGFβ
relative viability
IC50 = 13.41
IC50>1600
SN38 (nM)
b
APS
SC med.
no EGF
Organoid Area
Days
P =1.89 x 10-15
d1
d7
d10
SC medium
no EGF
d15
SC medium
d
SC med
no EGF
relative viability
IC50 = 59.98
IC50>1600
SN38 (nM)
e
AKP (SC med. vs +TGFβ)
FUNCTION
Autophagy
TGFβ sig up.
Collagen binding
EMT
KRAS sig.
ECM organization
Cell-matrix adhesion
Ox-Phos
Cholesterol Homeost.
MYC Targets v1
Glycolysis
PI3K/AKT/MTOR sig.
G2M checkpoint
E2F targets
Fatty Ac. metabolism
MTORC1 sig.
- Log10 p-value
IDENTITY
Revival SCs
Fetal prog.
Mex3a signature
Paneth
Enteroendocrine
Mucosecreting
Secretory progenitors
Lgr5 ISC (Muñoz et al.)
LRC
Crypt-Prolif.
- Log10 p-value
f
APS (SC med. vs no EGF)
FUNCTION
ECM organization
TNFα/NFKB sig.
IFNgamma sig.
Wnt-βCatenin sig.
KRAS sig. down
Cell-matrix adhesion
Autophagy
Collagen binding
Ox-Phos
Glycolysis
PI3K/AKT/MTOR sig.
MTORC1 sig.
MYC Targets v1
E2F targets
G2M checkpoint
KRAS sig. Up
- Log10 p-value
IDENTITY
Mex3a
Lgr5
Secretory prog.
Paneth
Mucosecreting
Enteroendocrine
LRC
Fetal prog.
Revival SCs
Crypt Prolif.
- Log10 p-value
g
AKP
Mex3a mRNA
P =8.6 x 10-6
SC med
+TGFβ
h
APS
Mex3a mRNA
P =1.26 x 10-6
SC med
no EGF
i
SC Medium
no EGF + TGFβ
0.81%
Mex3a+
0.68%
Mex3a+
Neg.Cont.
Mex3a+/+
+TGFβ
13.7
Mex3a+
61.9
Mex3a+
AKP
Mex3aTom/+
No EGF
16.1
Mex3a+
84.2
Mex3a+
APS
Mex3aTom/+
SSC-A
Mex3a-tdTomato
j
Ki67 signature
UMAP-2
UMAP-1
k
MEX3A gene
l
LGR5 signature
m
Cell Cycle phase
Fraction
S
G2M
G1
G0
Mex3a
Lgr5

Figure 2

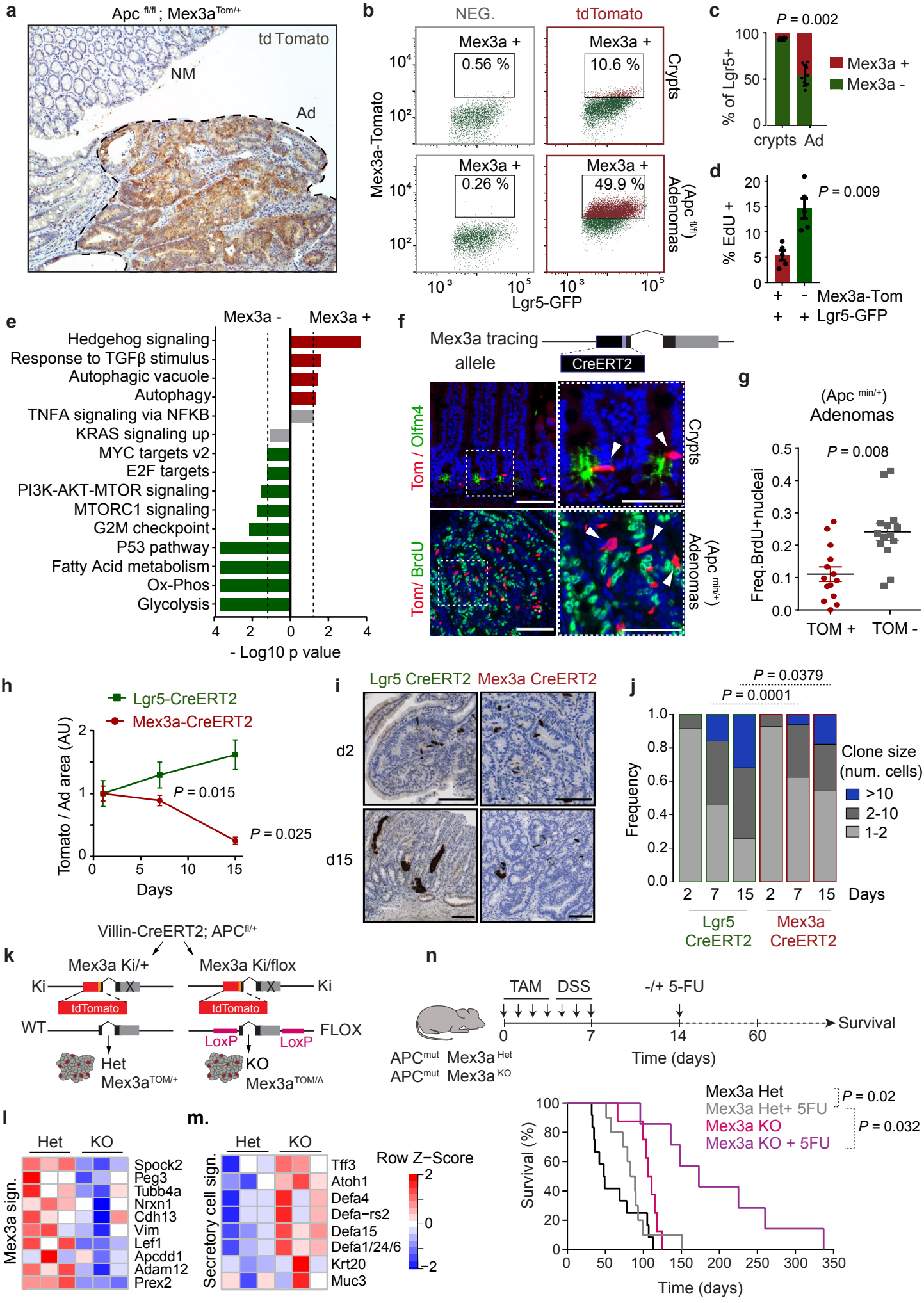
a
Apc fl/fl ; Mex3a Tom/+
td Tomato
NM
Ad
b
NEG.
tdTomato
Mex3a +
0.56 %
10.6 %
0.26 %
49.9 %
Crypts
(Apc fl/fl) Adenomas
Mex3a-Tomato
Lgr5-GFP
c
P = 0.002
% of Lgr5+
Mex3a +
Mex3a -
crypts
Ad
d
P = 0.009
% EdU +
Mex3a-Tom
Lgr5-GFP
e
Mex3a -
Mex3a +
Hedgehog signaling
Response to TGFβ stimulus
Autophagic vacuole
Autophagy
TNFA signaling via NFKB
KRAS signaling up
MYC targets v2
E2F targets
PI3K-AKT-MTOR signaling
MTORC1 signaling
G2M checkpoint
P53 pathway
Fatty Acid metabolism
Ox-Phos
Glycolysis
- Log10 p value
f
Mex3a tracing allele
CreERT2
Tom / Olfm4
Tom/ BrdU
Crypts
(Apc min/+) Adenomas
g
(Apc min/+) Adenomas
P = 0.008
Freq.BrdU+nucleai
TOM +
TOM -
h
Lgr5-CreERT2
Mex3a-CreERT2
Tomato / Ad area (AU)
P = 0.015
P = 0.025
Days
i
Lgr5 CreERT2
Mex3a CreERT2
d2
d15
j
P = 0.0379
P = 0.0001
Frequency
Clone size (num. cells)
>10
2-10
1-2
Days
Lgr5 CreERT2
Mex3a CreERT2
k
Villin-CreERT2; APC fl/+
Mex3a Ki/+
Mex3a Ki/flox
Ki
tdTomato
WT
FLOX
LoxP
Het Mex3a TOM/+
KO Mex3a TOM/Δ
n
TAM
DSS
-/+ 5-FU
Survival
Time (days)
APCmut Mex3a Het
APCmut Mex3a KO
Mex3a Het
Mex3a Het+ 5FU
Mex3a KO
Mex3a KO + 5FU
P = 0.02
P = 0.032
Survival (%)
Time (days)
l
Het
KO
Mex3a sign.
Spock2
Peg3
Tubb4a
Nrxn1
Cdh13
Vim
Lef1
Apcdd1
Adam12
Prex2
m.
Secretory cell sign.
Tff3
Atoh1
Defa4
Defa−rs2
Defa15
Defa1/24/6
Krt20
Muc3
Row Z−Score

Figure 3

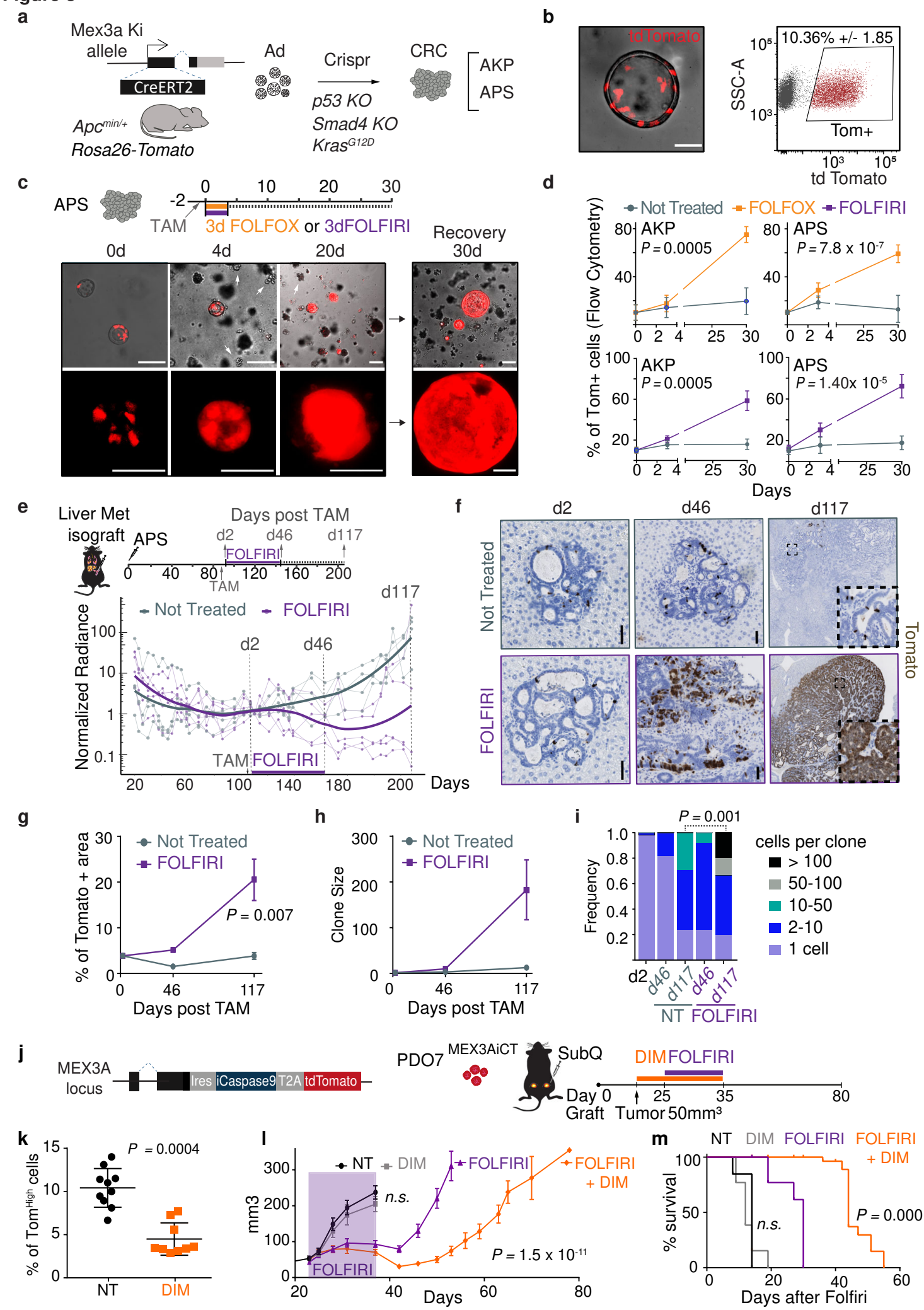
a
Mex3a Ki allele
CreERT2
Apc^min/+
Rosa26-Tomato
Ad
Crispr
p53 KO
Smad4 KO
Kras^G12D
CRC
AKP
APS
b
tdTomato
10.36% +/- 1.85
SSC-A
Tom+
td Tomato
c
APS
TAM
3d FOLFOX or 3dFOLFIRI
Recovery
0d
4d
20d
30d
d
Not Treated
FOLFOX
FOLFIRI
AKP
APS
P = 0.0005
P = 7.8 x 10-7
P = 1.40x 10-5
% of Tom+ cells (Flow Cytometry)
Days
e
Liver Met isograft
APS
Days post TAM
d2
d46
d117
FOLFIRI
TAM
Not Treated
FOLFIRI
Normalized Radiance
Days
f
d2
d46
d117
Not Treated
FOLFIRI
Tomato
g
Not Treated
FOLFIRI
P = 0.007
% of Tomato + area
Days post TAM
h
Not Treated
FOLFIRI
Clone Size
Days post TAM
i
P = 0.001
Frequency
cells per clone
> 100
50-100
10-50
2-10
1 cell
d2
d46
d117
d46
d117
NT
FOLFIRI
j
MEX3A locus
Ires
iCaspase9
T2A
tdTomato
PDO7
MEX3AiCT
SubQ
DIM
FOLFIRI
Day 0
Graft
Tumor 50mm3
k
P = 0.0004
% of Tom^High cells
NT
DIM
l
NT
DIM
FOLFIRI
FOLFIRI + DIM
n.s.
P = 1.5 x 10-11
mm3
Days
m
NT
DIM
FOLFIRI
FOLFIRI + DIM
n.s.
P = 0.0001
% survival
Days after Folfiri

Figure 4

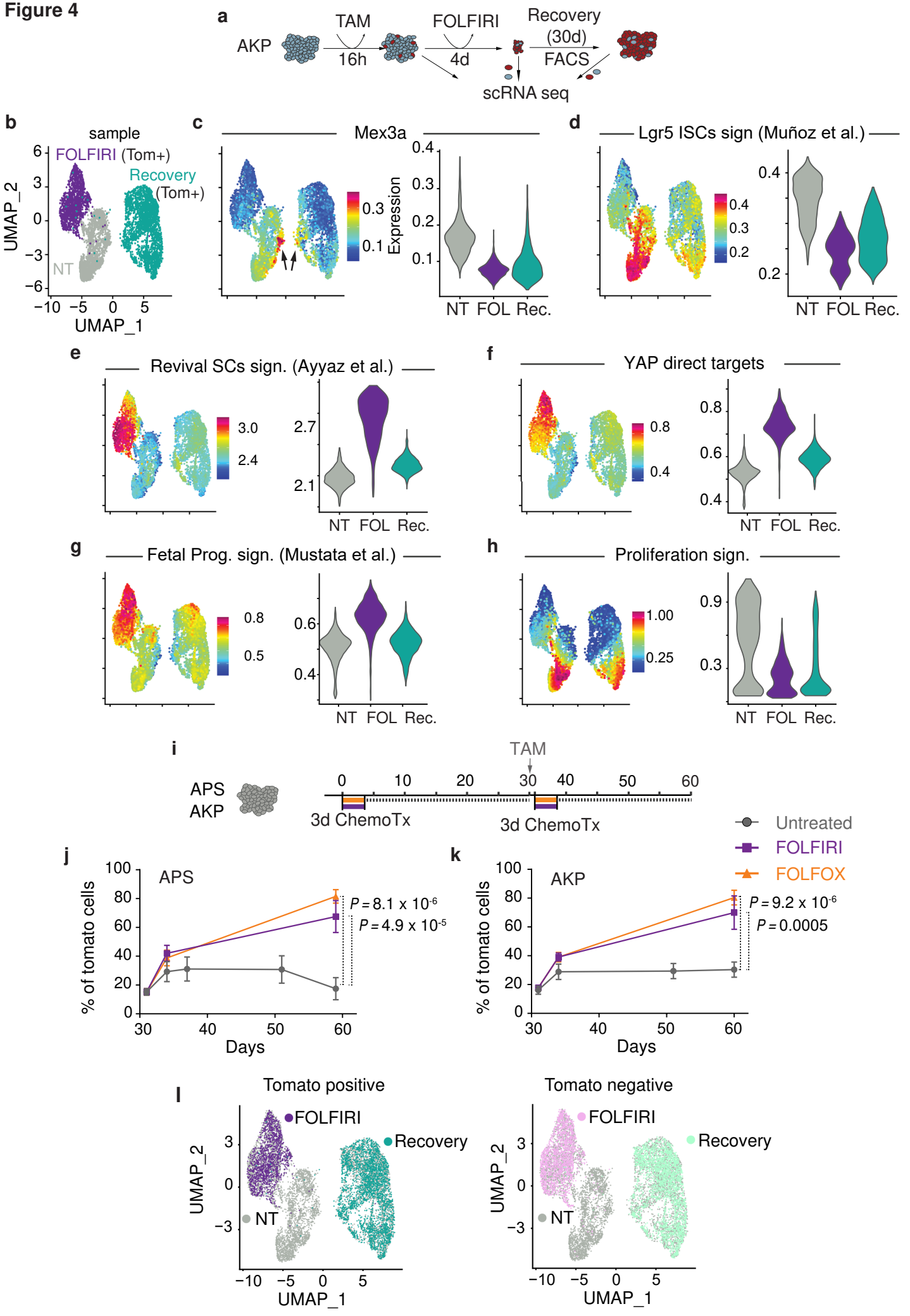
a
AKP
TAM
16h
FOLFIRI
4d
Recovery
(30d)
FACS
scRNA seq
b
sample
FOLFIRI (Tom+)
Recovery
(Tom+)
NT
UMAP_2
UMAP_1
c
Mex3a
Expression
NT FOL Rec.
d
Lgr5 ISCs sign (Muñoz et al.)
NT FOL Rec.
e
Revival SCs sign. (Ayyaz et al.)
NT FOL Rec.
f
YAP direct targets
NT FOL Rec.
g
Fetal Prog. sign. (Mustata et al.)
NT FOL Rec.
h
Proliferation sign.
NT FOL Rec.
i
APS
AKP
TAM
3d ChemoTx
3d ChemoTx
Untreated
FOLFIRI
FOLFOX
j
APS
% of tomato cells
Days
P = 8.1 x 10-6
P = 4.9 x 10-5
k
AKP
% of tomato cells
Days
P = 9.2 x 10-6
P = 0.0005
l
Tomato positive
Tomato negative
FOLFIRI
Recovery
NT
UMAP_2
UMAP_1

Figure 5

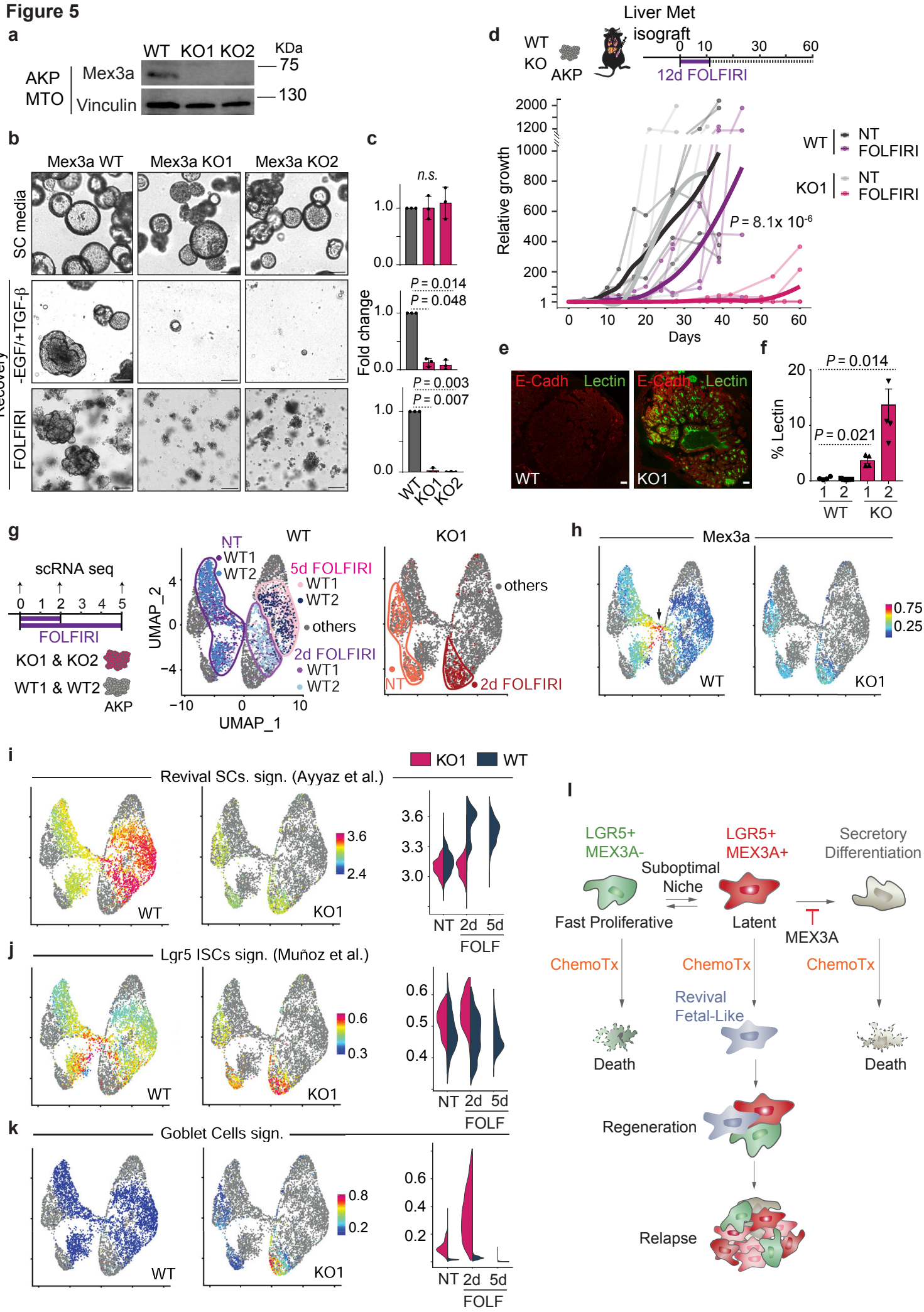
a
WT KO1 KO2 KDa
AKP
MTO
Mex3a
Vinculin
75
130
b
Mex3a WT
Mex3a KO1
Mex3a KO2
SC media
Recovery
-EGF/+TGF-β
FOLFIRI
c
n.s.
P = 0.014
P = 0.048
P = 0.003
P = 0.007
Fold change
WT KO1 KO2
d
Liver Met isograft
WT
KO
AKP
0 10 30 60
12d FOLFIRI
Relative growth
P = 8.1x 10-6
Days
WT NT FOLFIRI
KO1 NT FOLFIRI
e
E-Cadh Lectin
WT
KO1
f
P = 0.014
P = 0.021
% Lectin
WT KO
g
scRNA seq
FOLFIRI
KO1 & KO2
WT1 & WT2
AKP
NT WT1 WT2
5d FOLFIRI WT1 WT2
2d FOLFIRI WT1 WT2
others
UMAP_1
UMAP_2
WT
KO1
NT
2d FOLFIRI
h
Mex3a
i
KO1 WT
Revival SCs. sign. (Ayyaz et al.)
j
Lgr5 ISCs sign. (Muñoz et al.)
k
Goblet Cells sign.
NT 2d 5d
FOLF
l
LGR5+ MEX3A-
Suboptimal Niche
LGR5+ MEX3A+
Secretory Differentiation
Fast Proliferative
Latent
MEX3A
ChemoTx
Revival Fetal-Like
Death
Regeneration
Relapse

Extended Data Figure 1

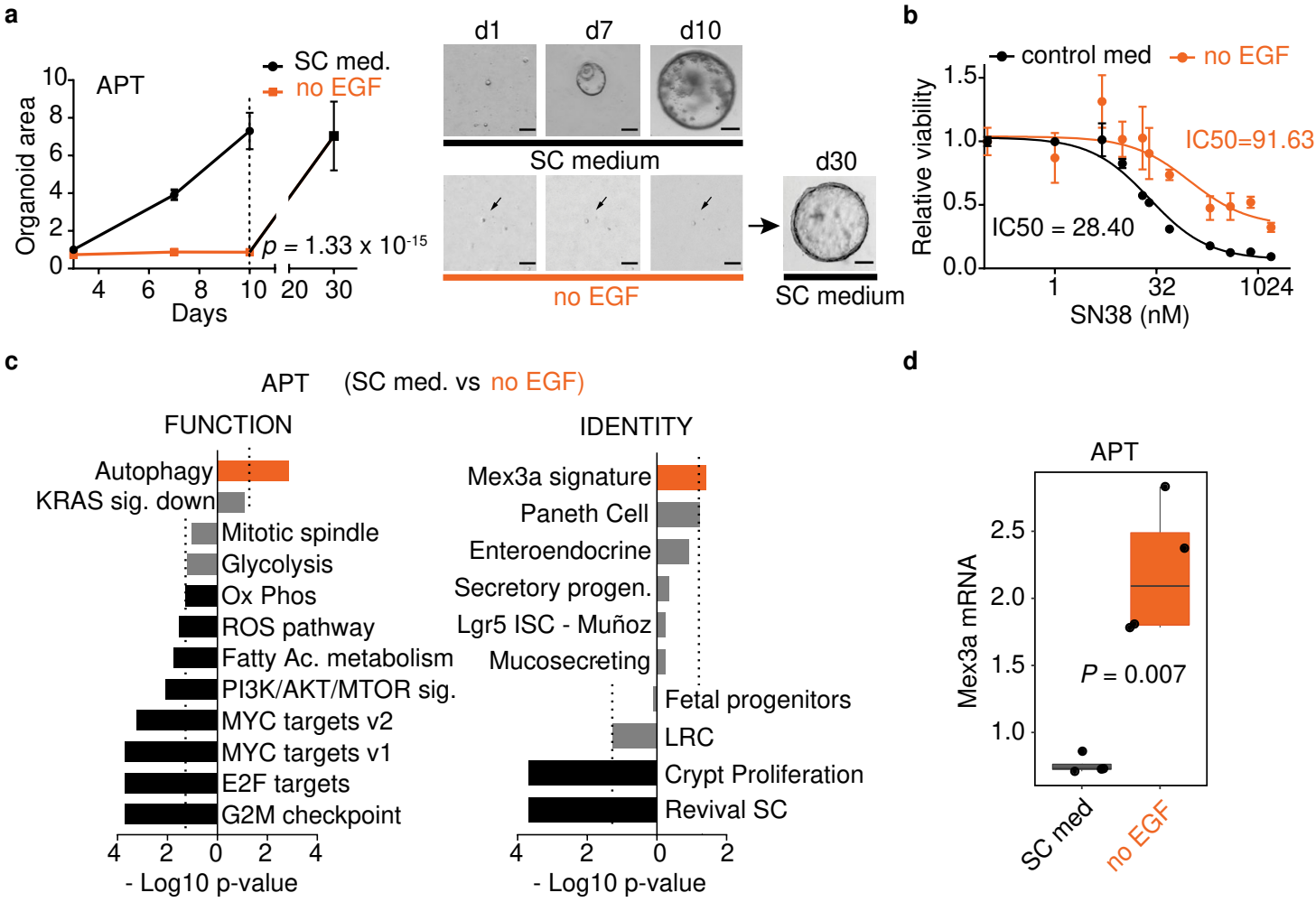

Extended Data Figure 2

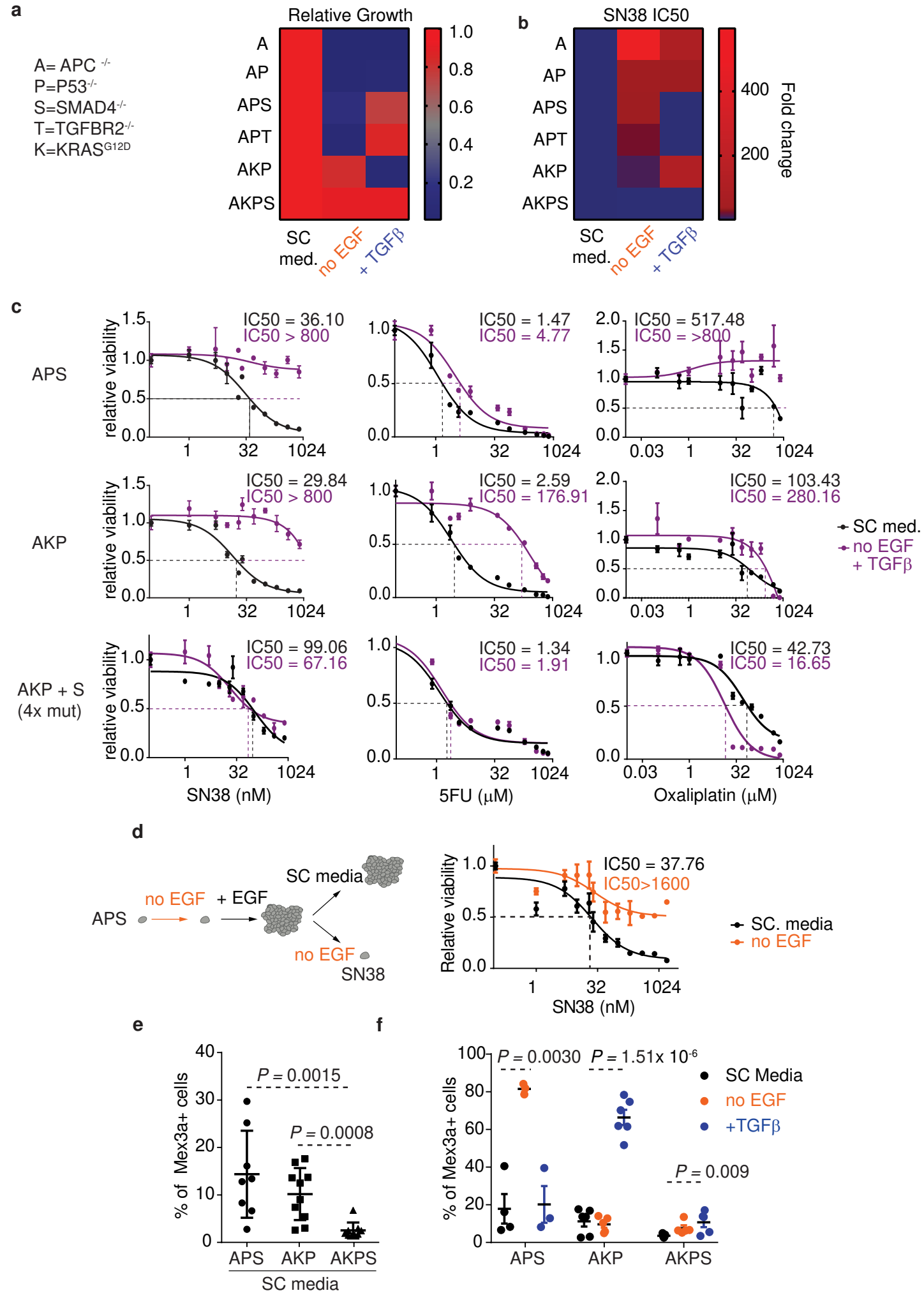

Extended Data Figure 3

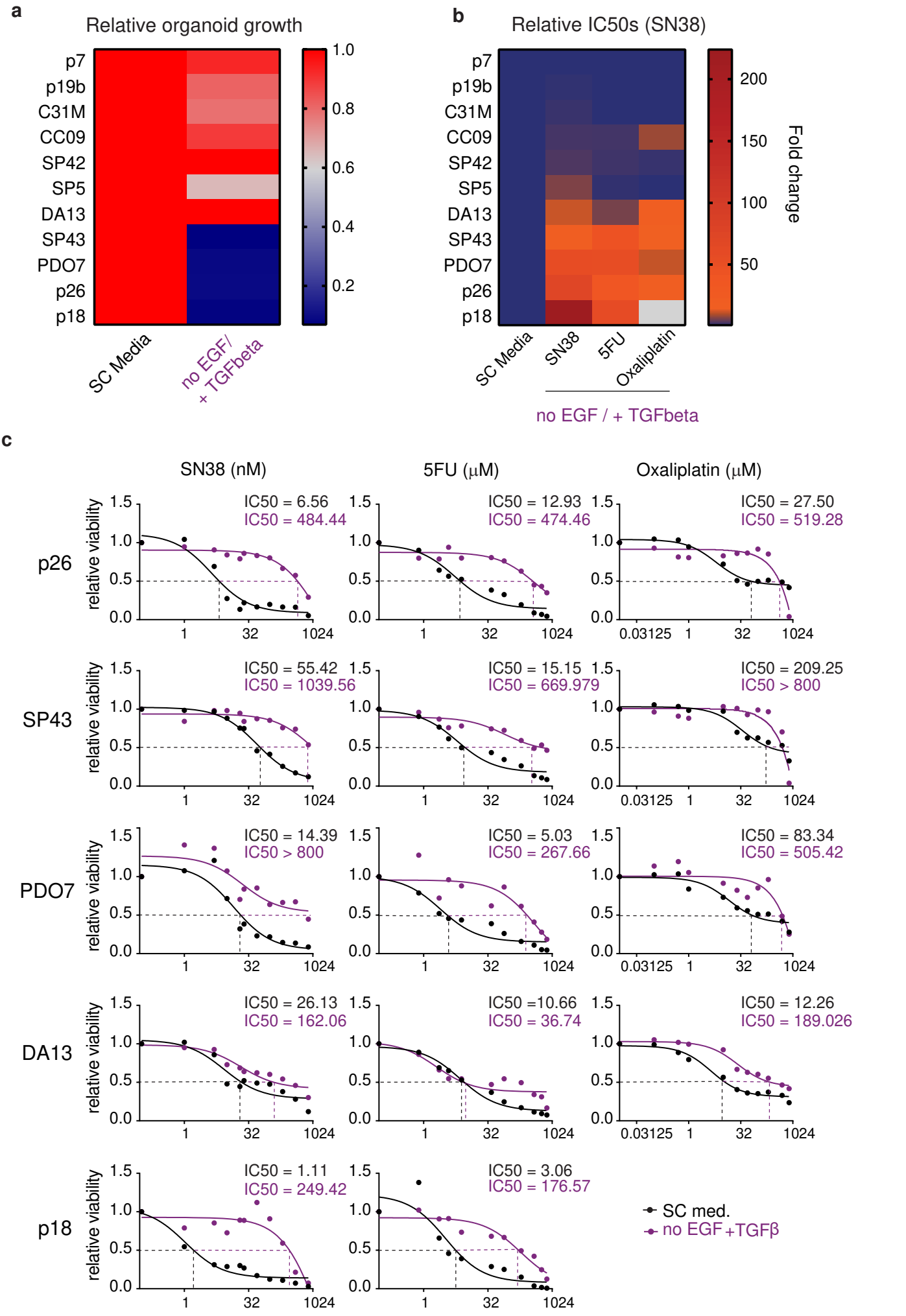

Extended Data Figure 4

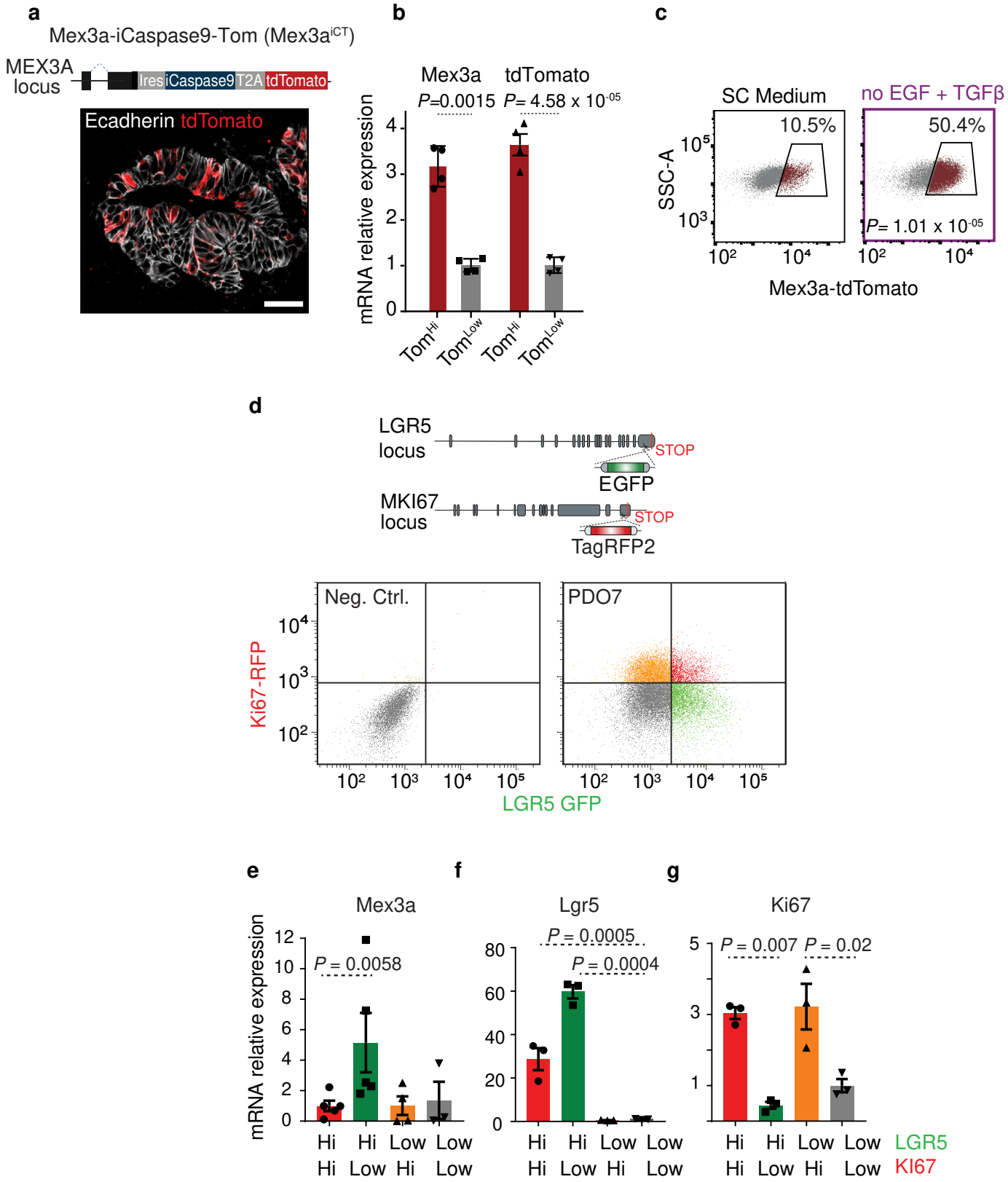

Extended Data Figure 5

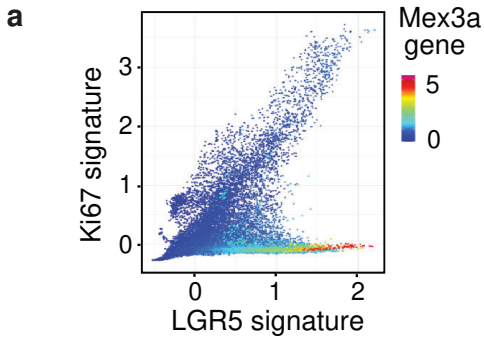

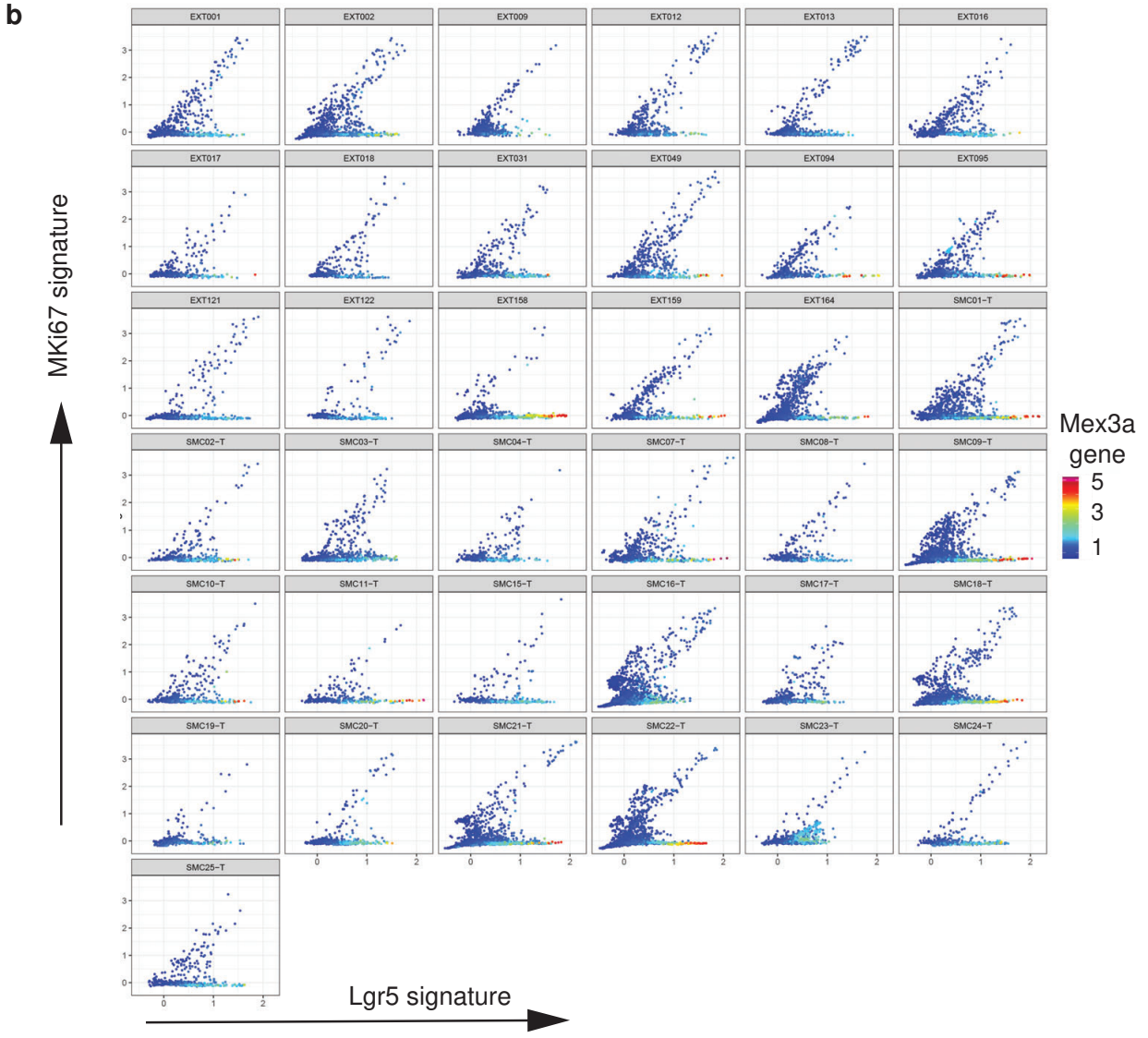

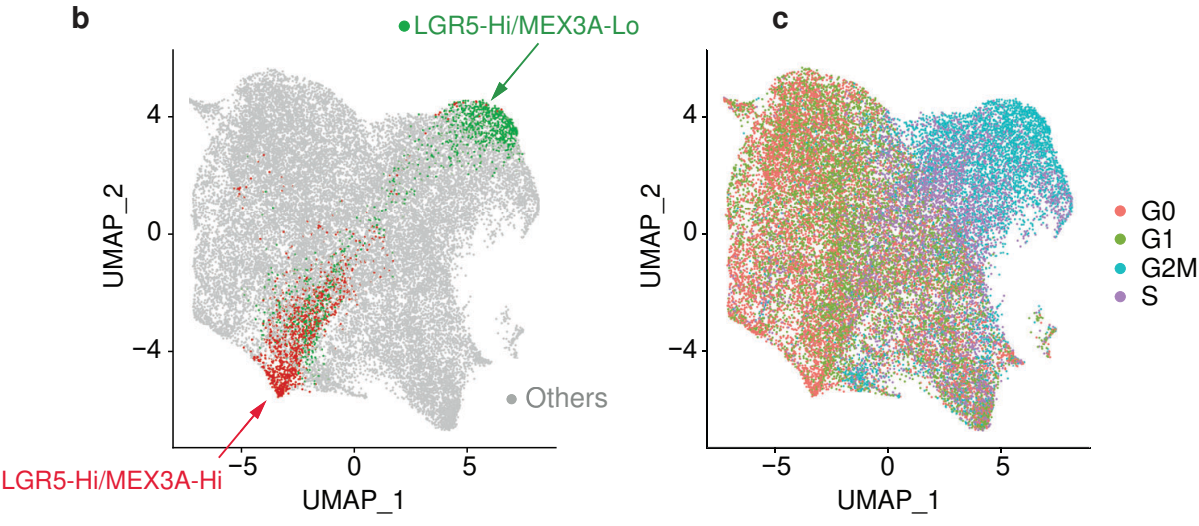

Extended Data Figure 6

a

Patients n= 816

Cohorts	TCGA.COAD.HS	TCGA.COAD.GA	GSE14333	GSE39582
	66	42	224	484
Gender	Male	Female		
	440	376		
Mismatch Repair	Proficient	Deficient		
	666	150		
Stage	Stage I	Stage II	Stage III	
	98	394	324	

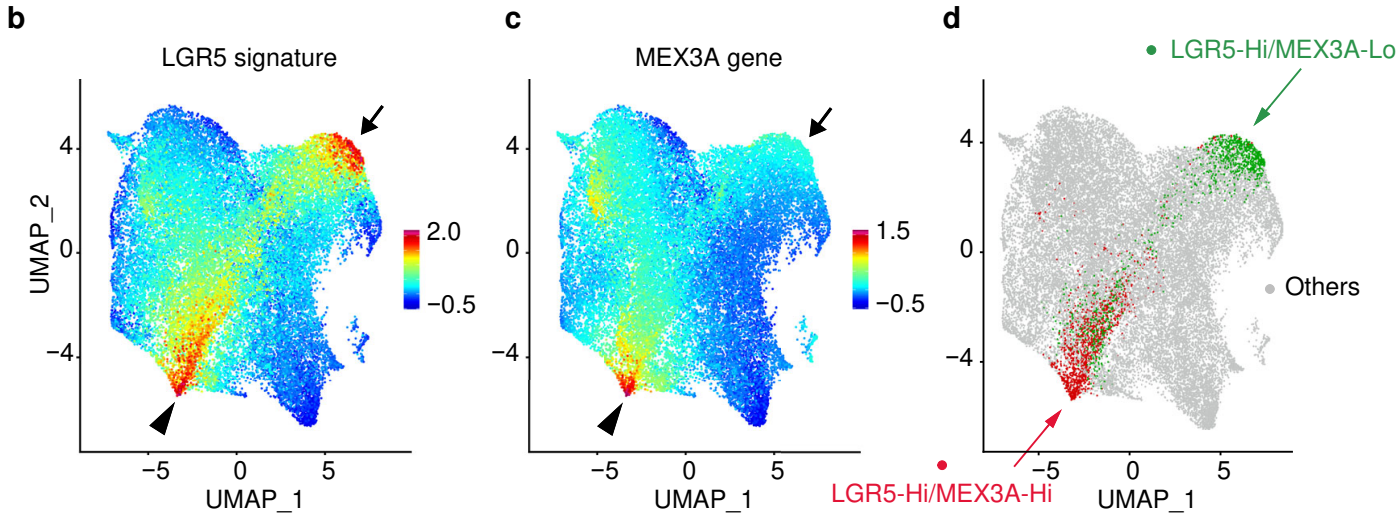

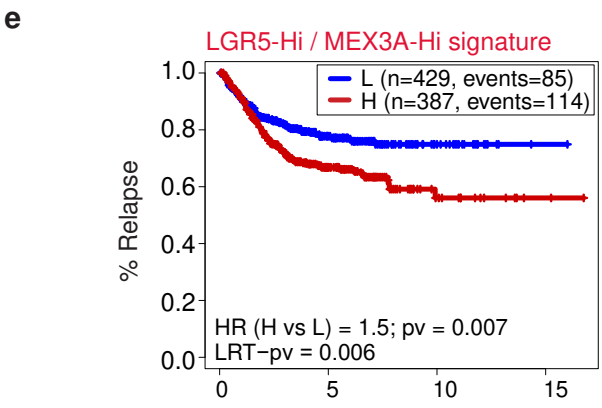

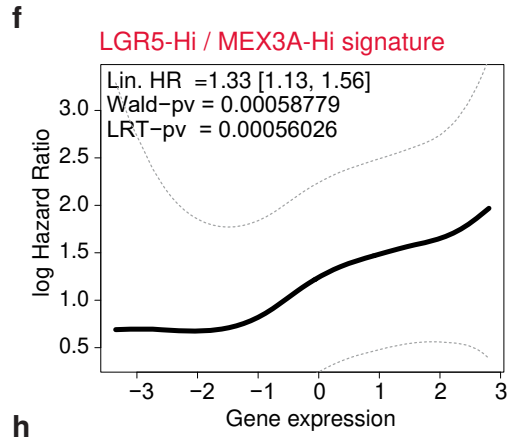

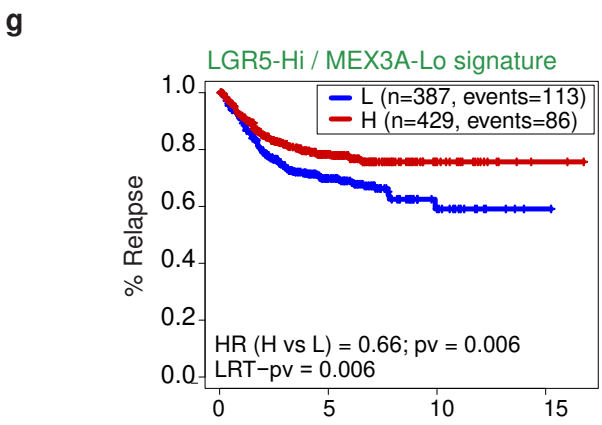

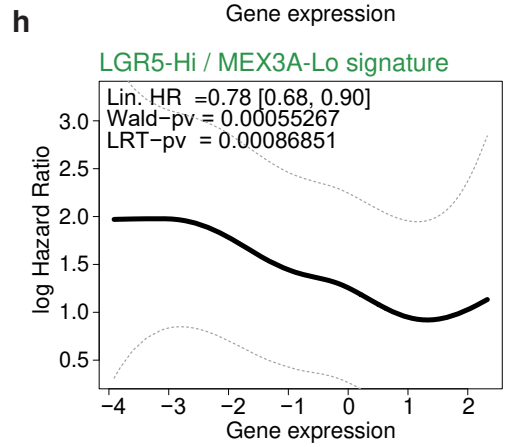

Extended Data Figure 7

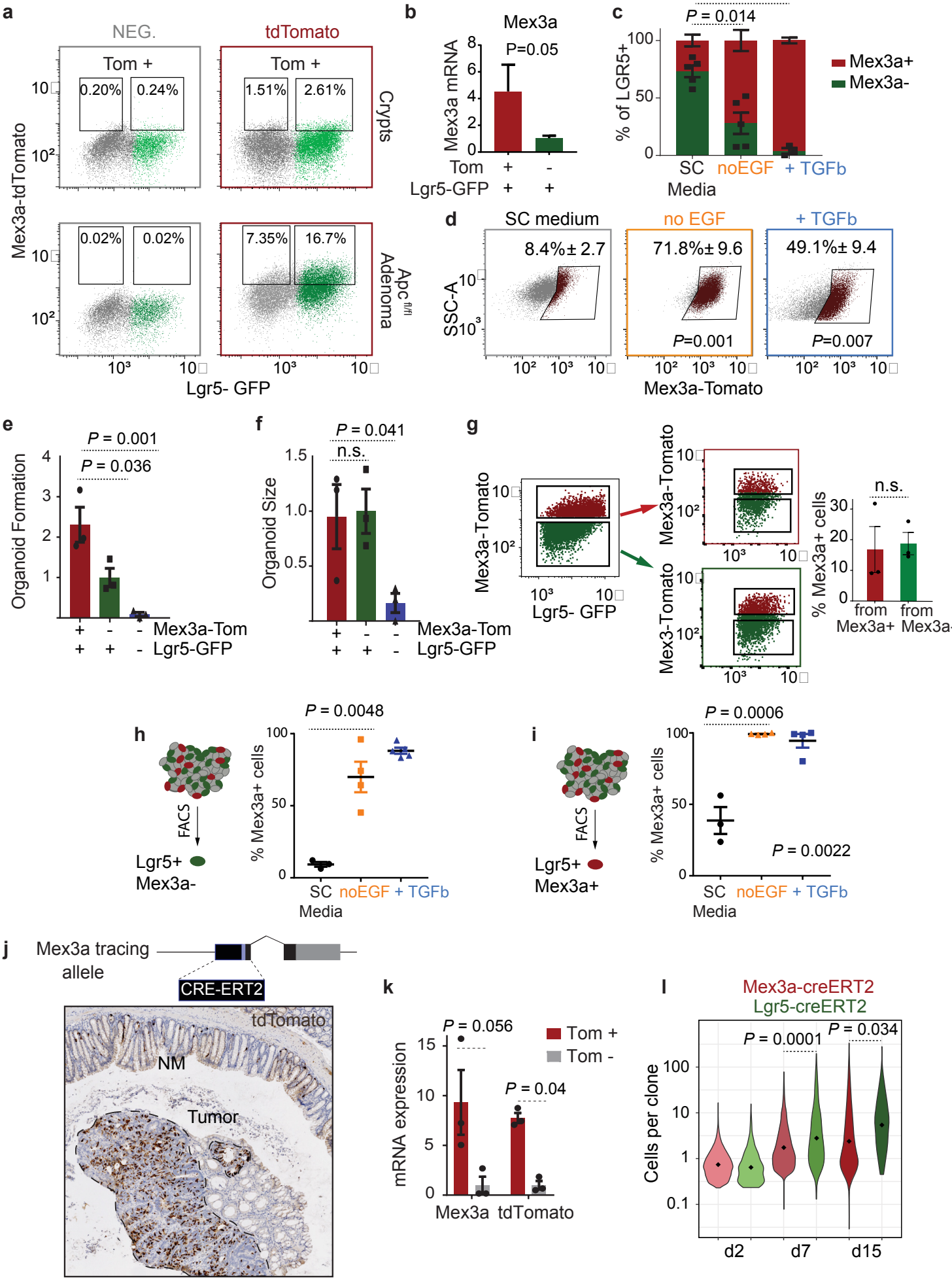

Extended Data Figure 8

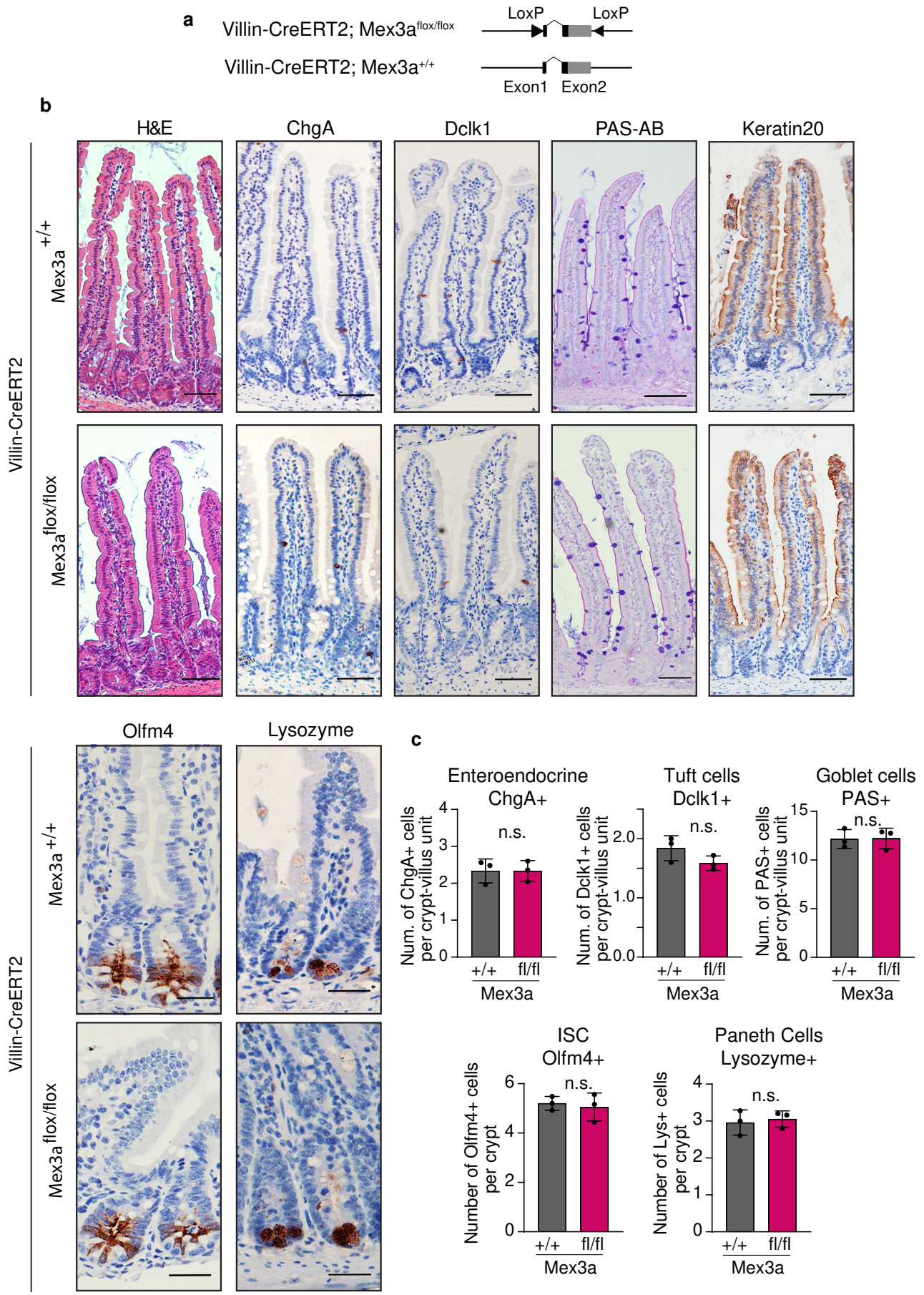

Extended Data Figure 9

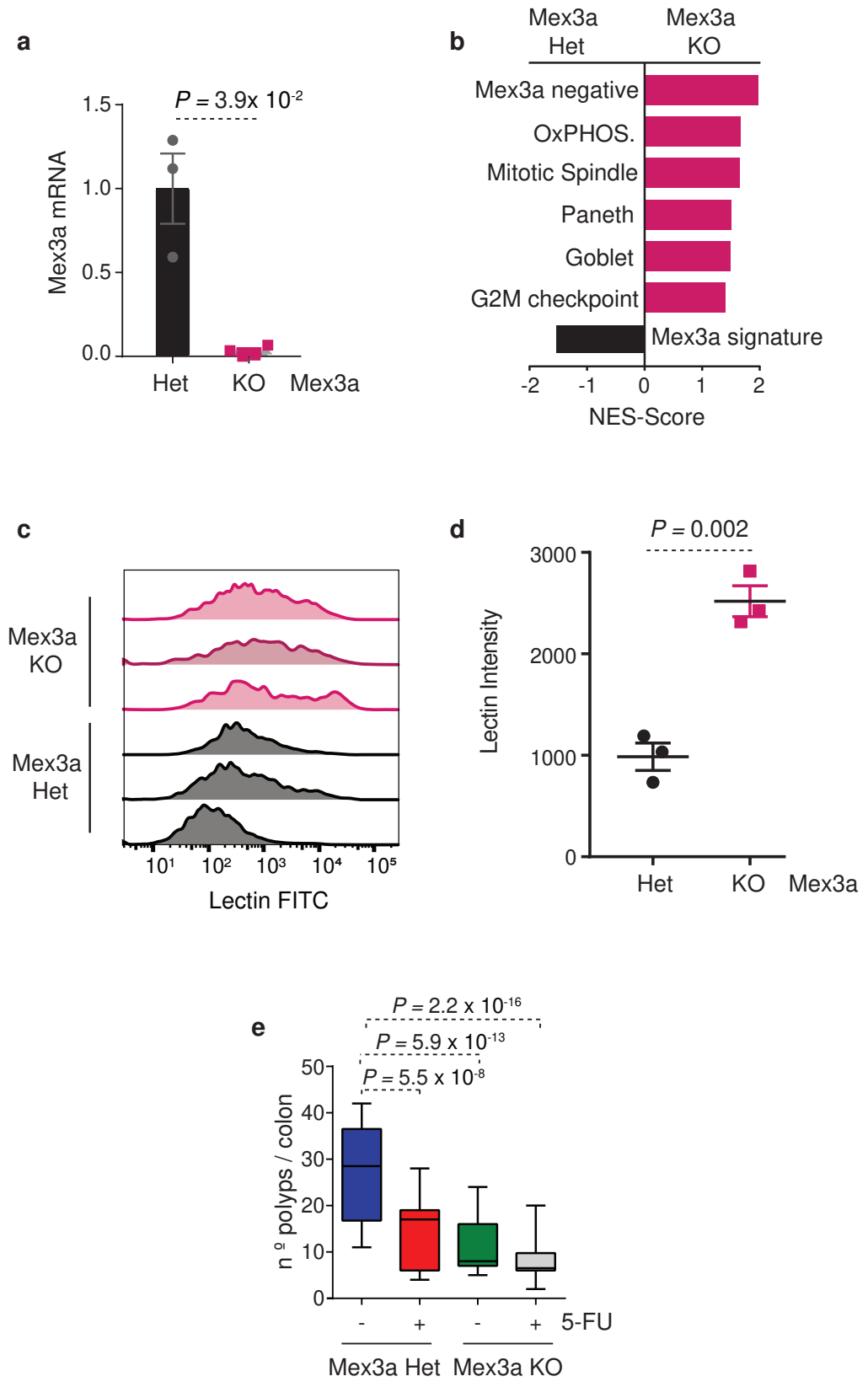

Extended Data Figure 10

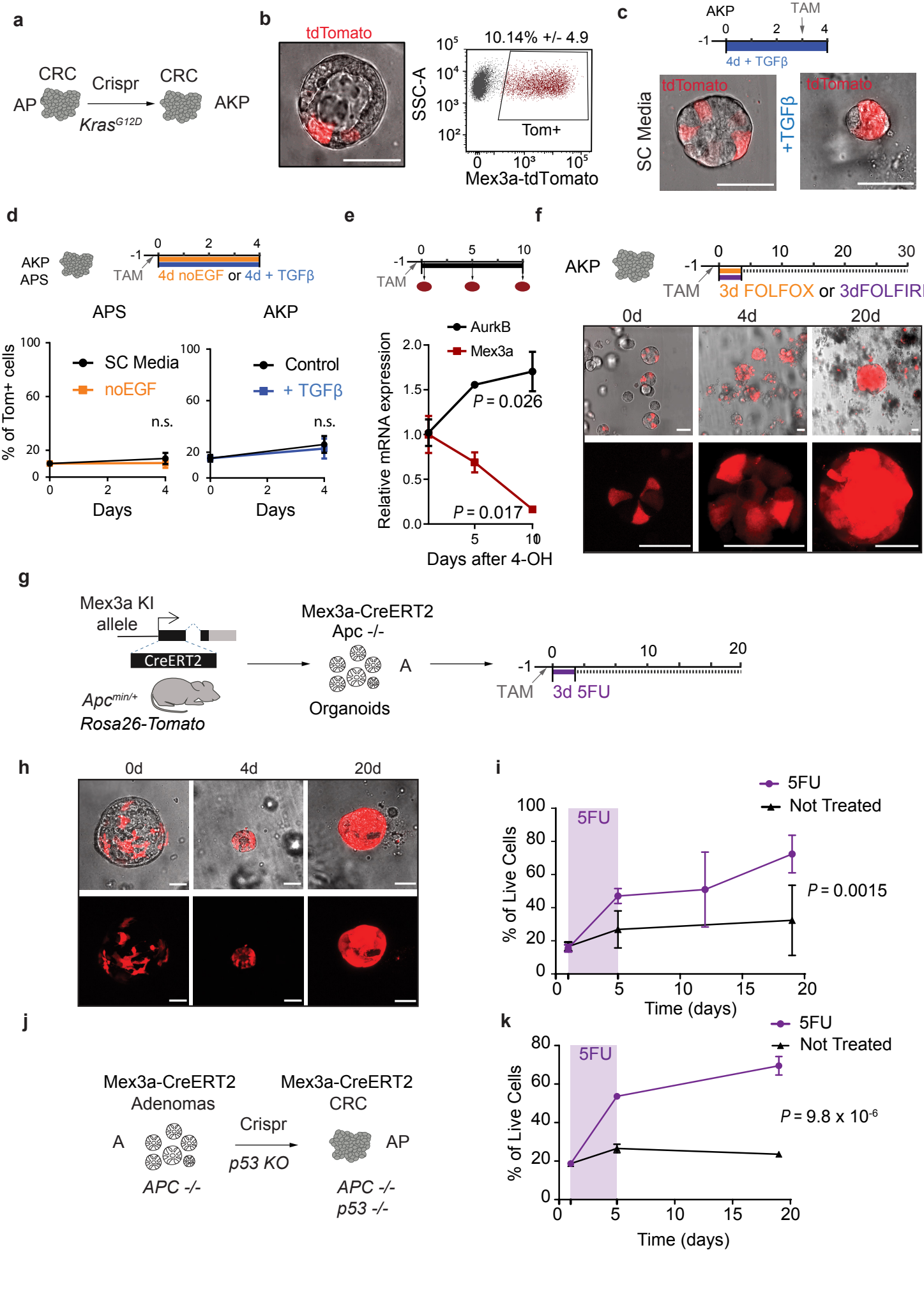

Extended Data Figure 11

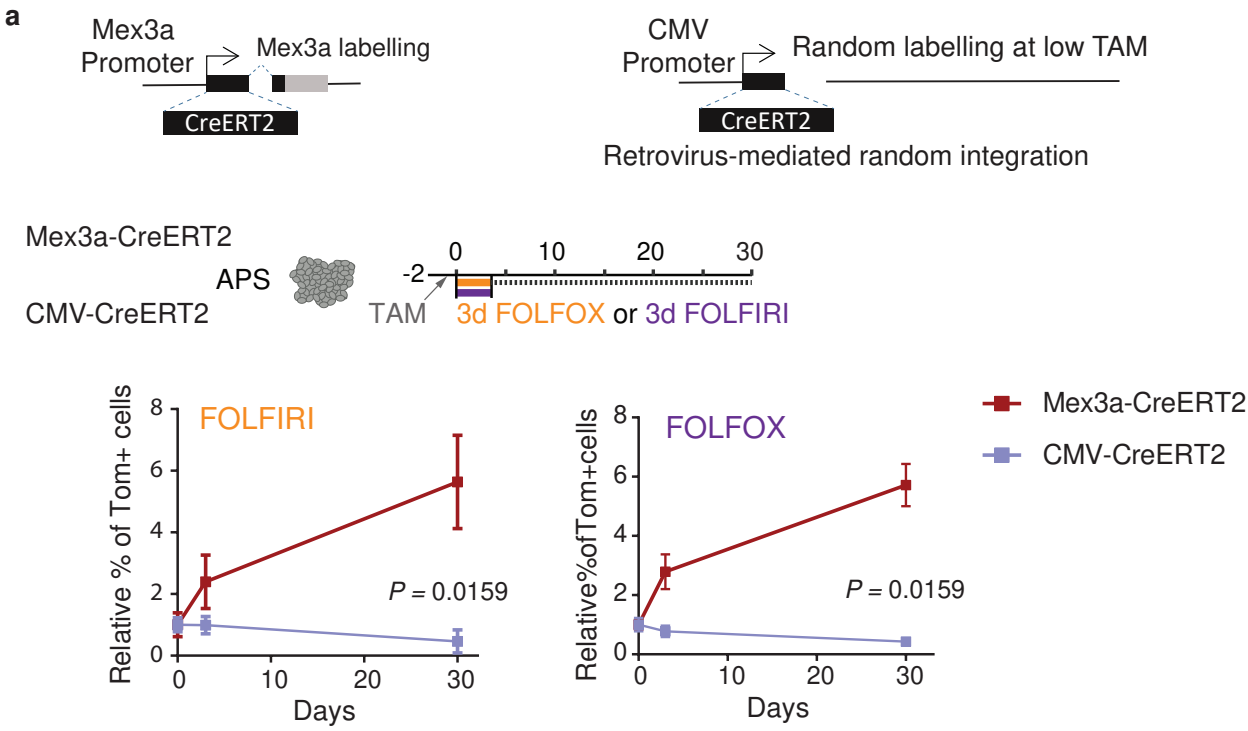

Extended Data Figure 12

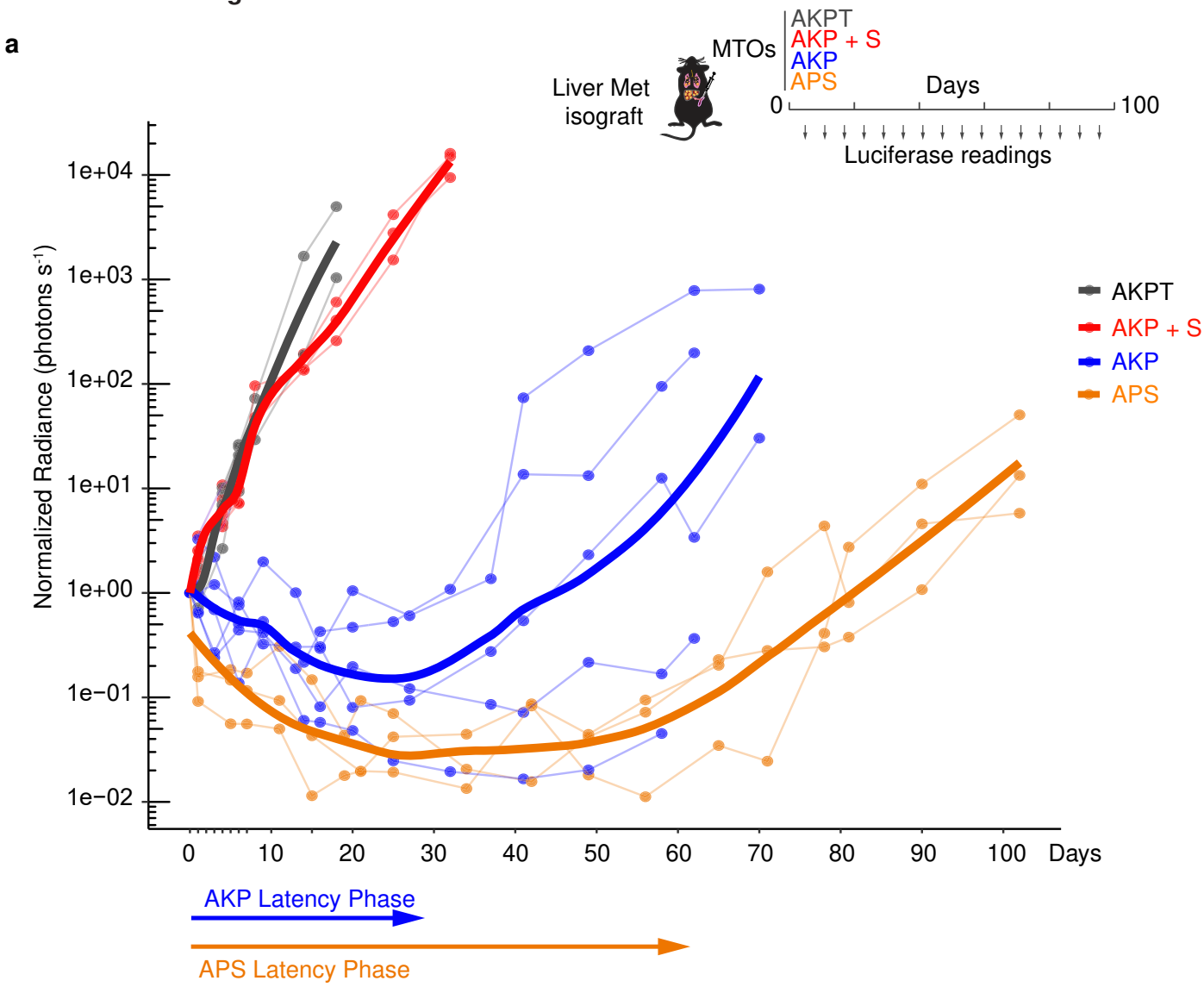

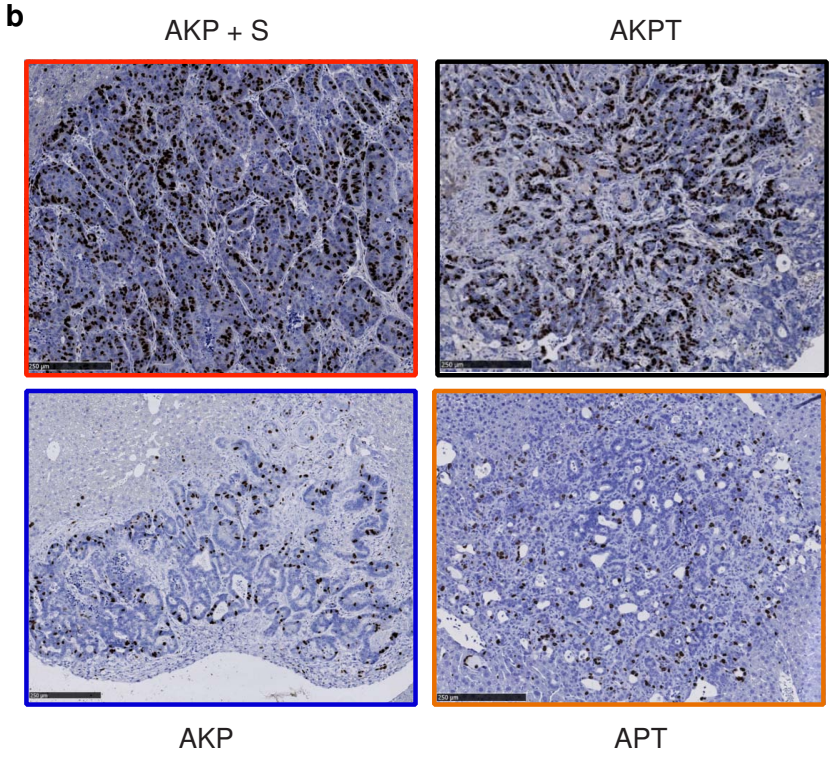

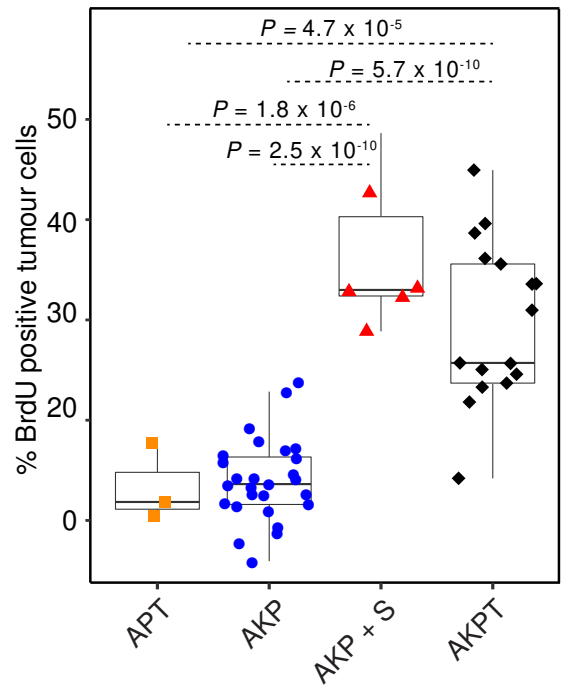

Extended Data Figure 13

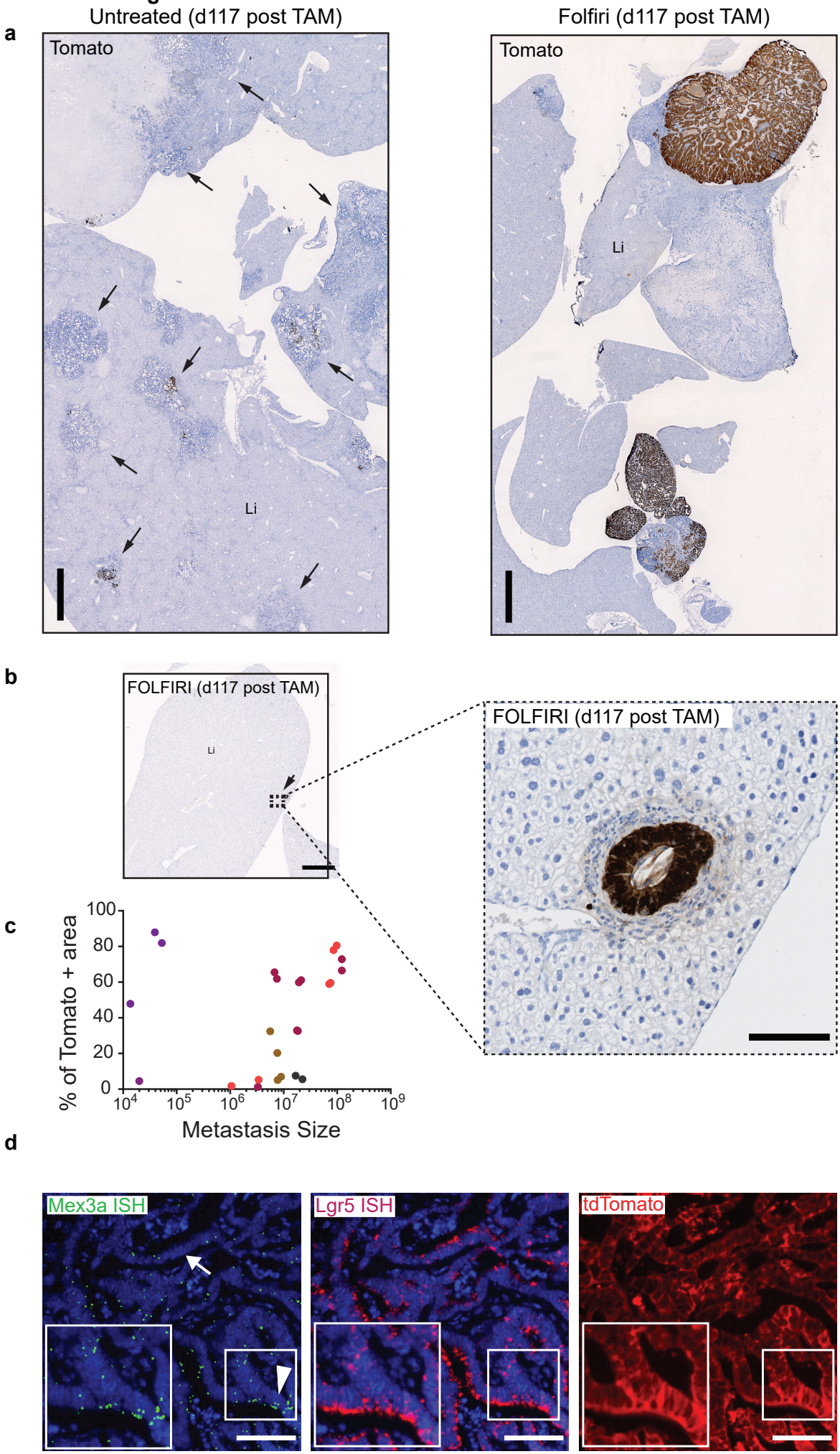

Extended Data Figure 14

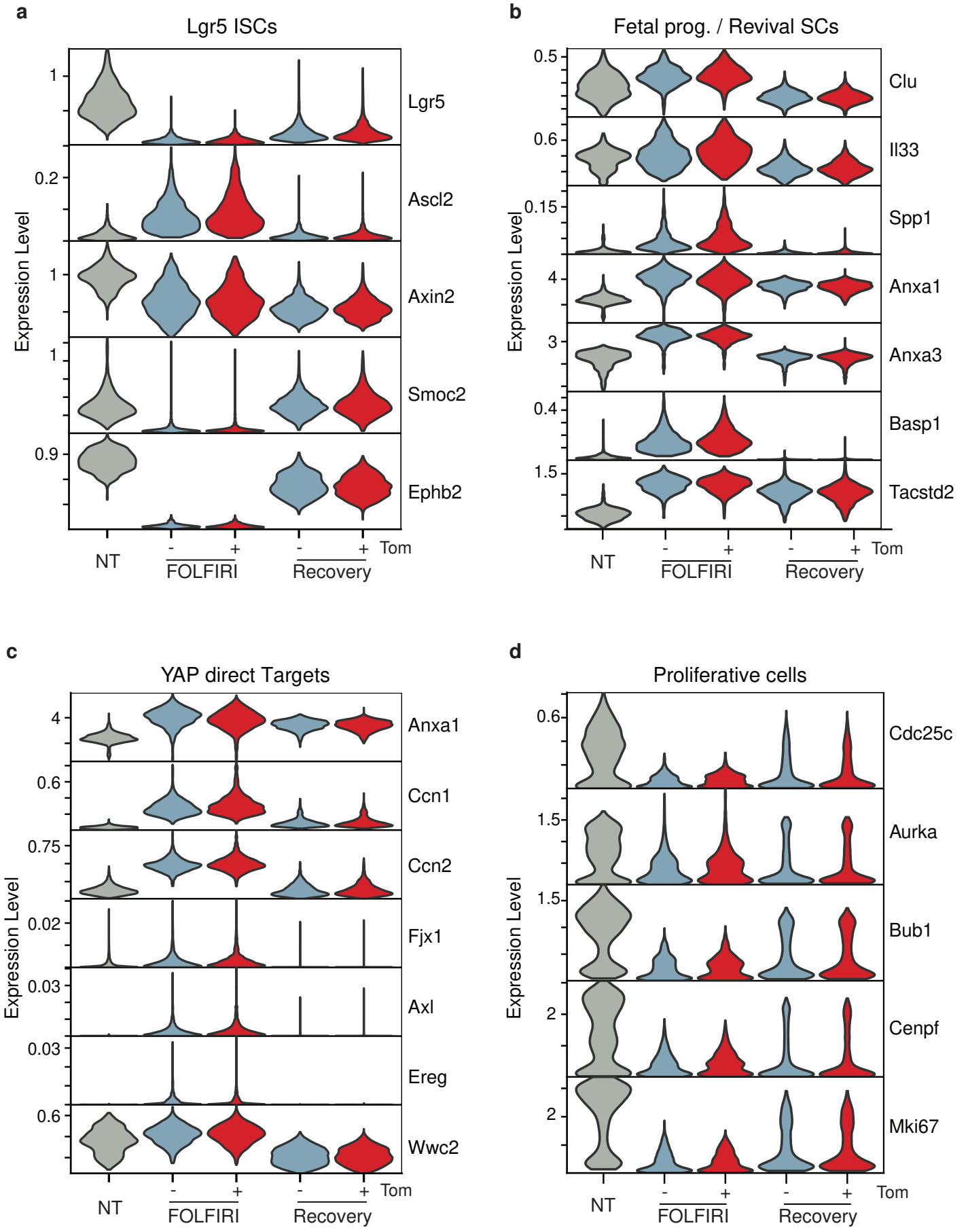

Extended Data Figure 15

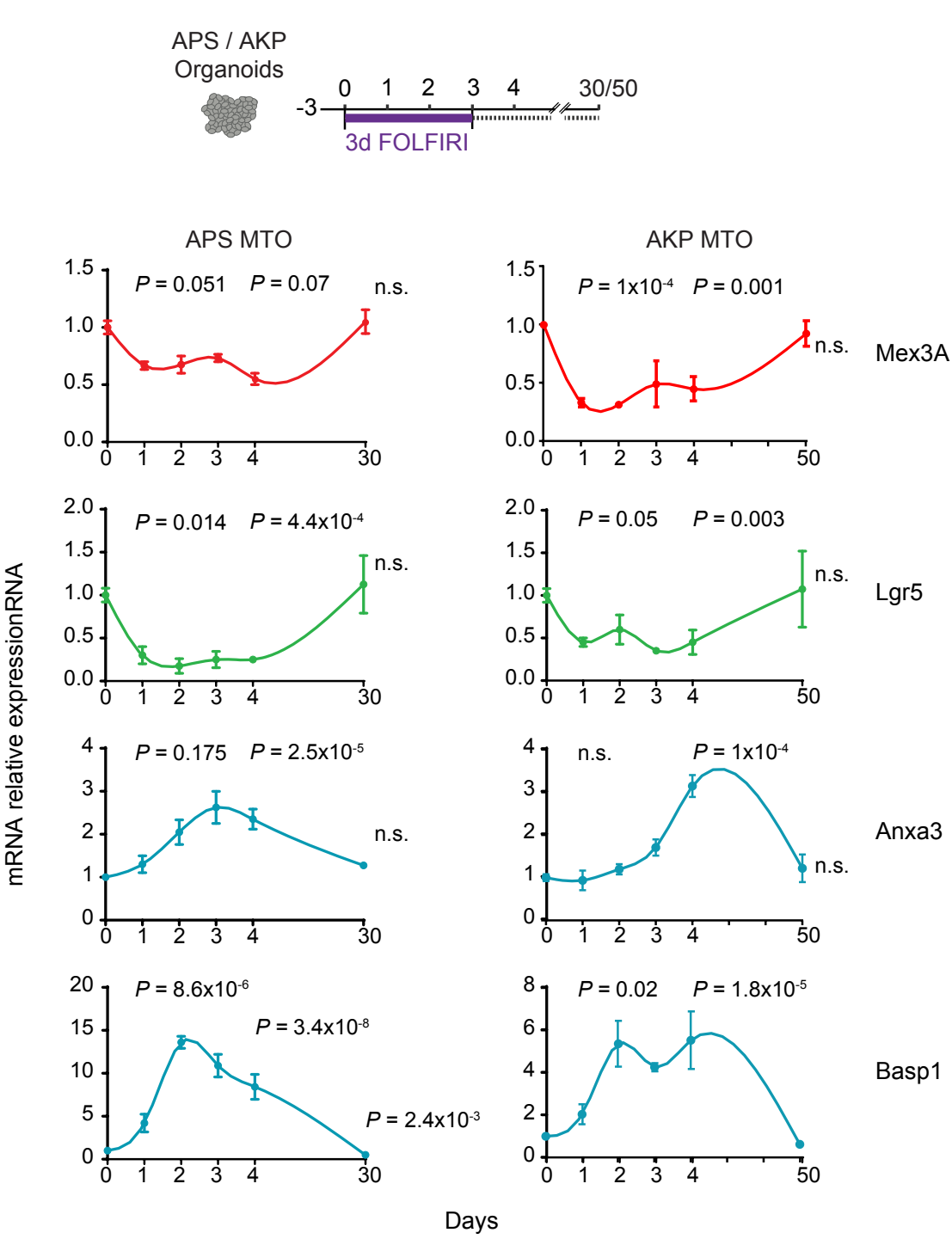

Extended Data Figure 16

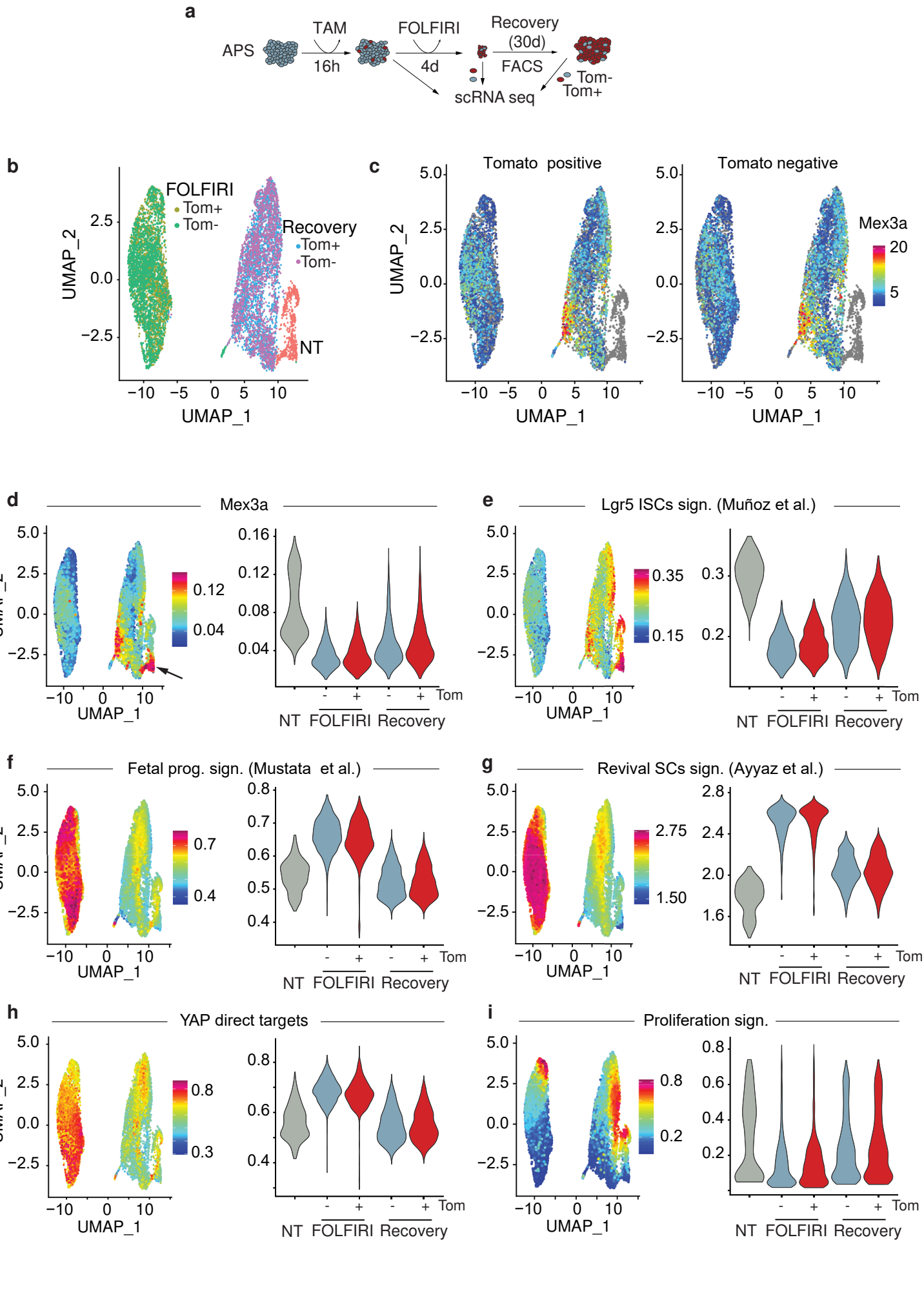

Extended Data Figure 17

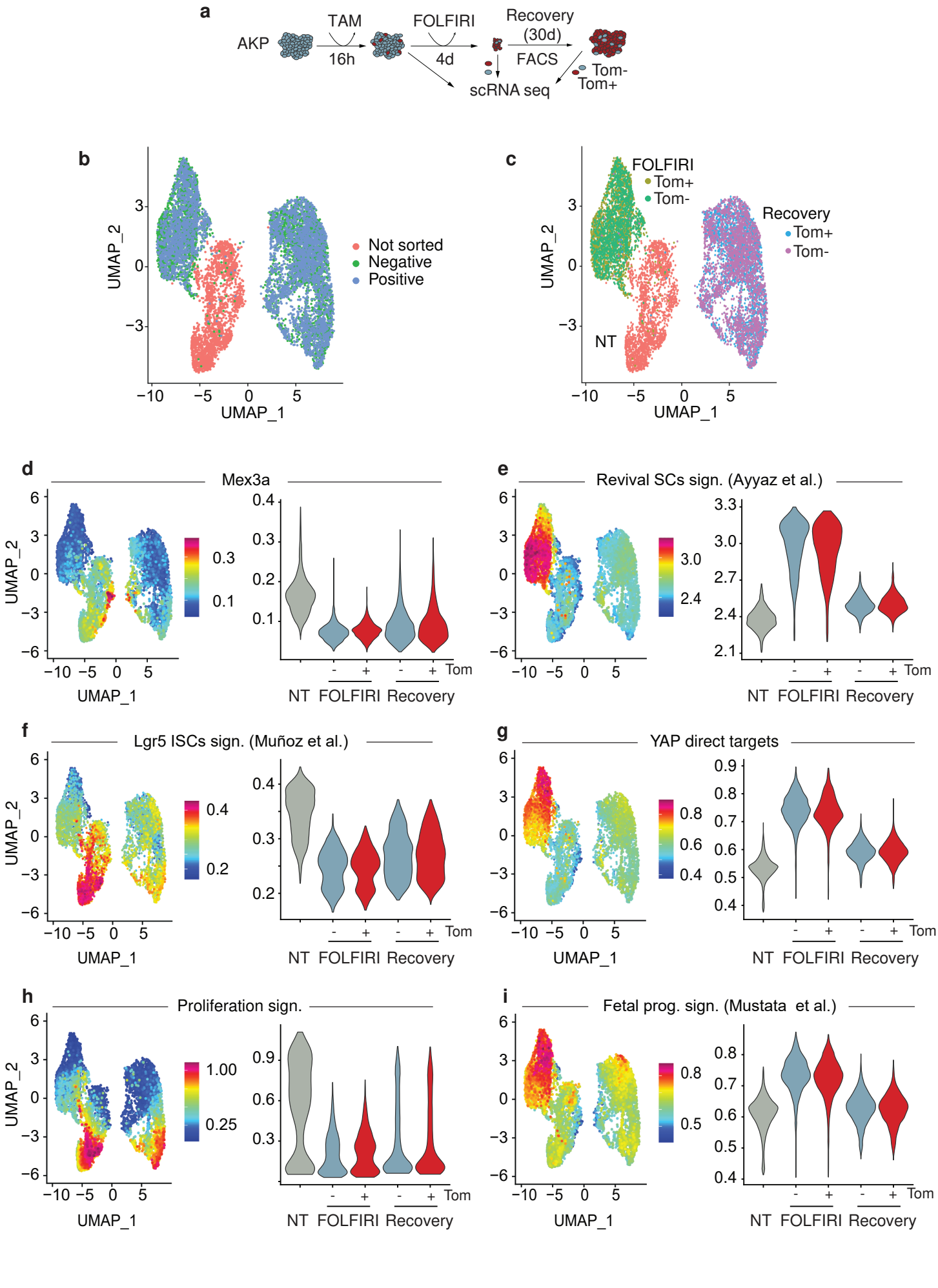

Extended Data Figure 18

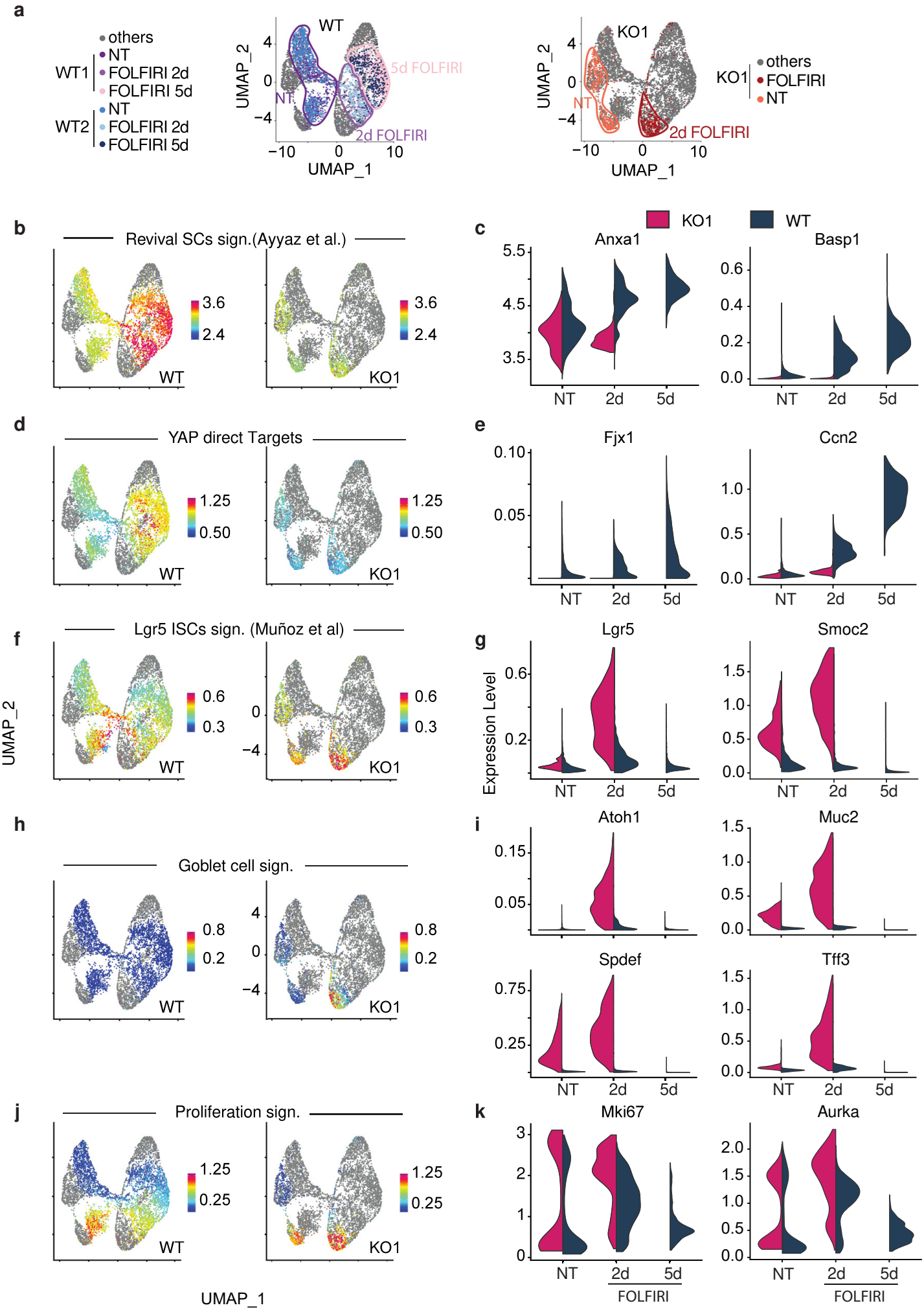

Extended Data Figure 19

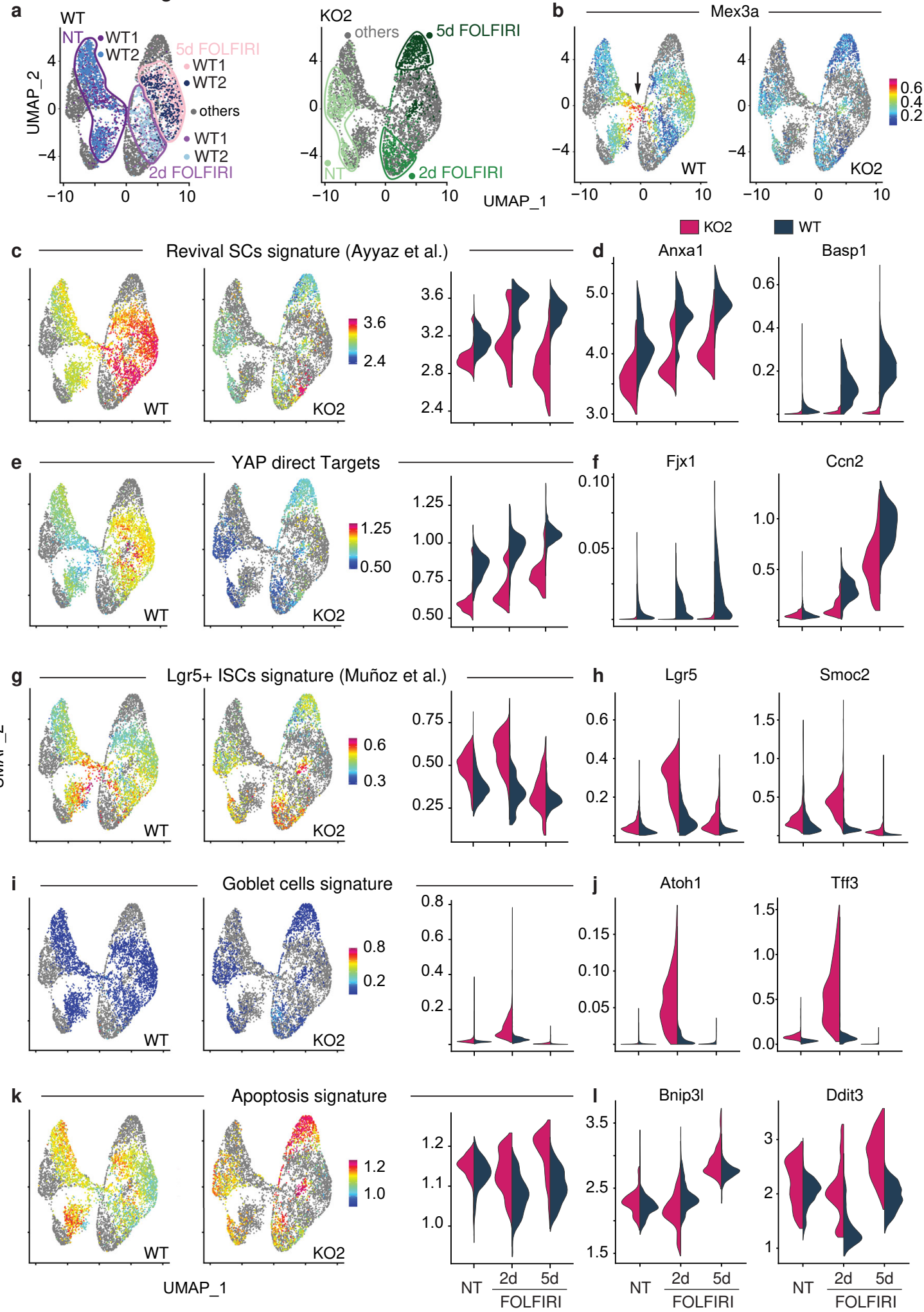

Extended Data Figure 20

Genes mutated in main CRC driver pathways

A=WNT pathway (APC, CTNNB1, ZNRF3, RNF43, etc)
K=RTK/RAS pathway (KRAS, BRAF NRAS, HRAS, etc)
P=p53 pathway (TP53, ATM, MDM2, MDM4, etc)
T=TGFβ pathway (SMAD4, TGFBR2, SMAD2, SMAD3, etc)

a

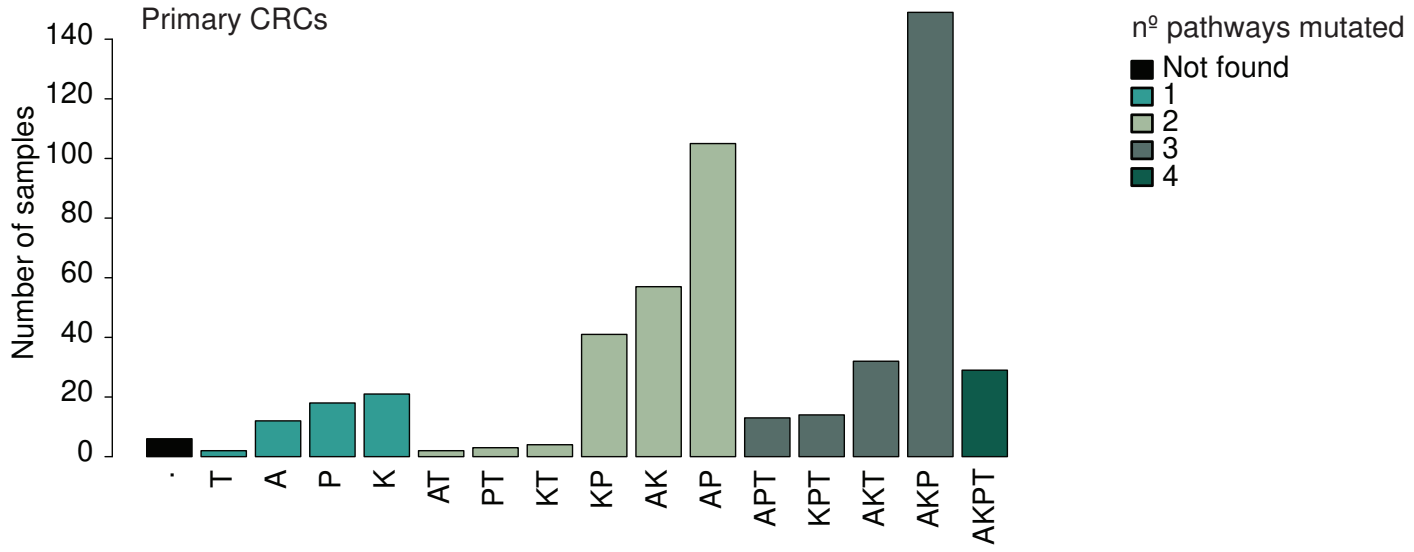

b

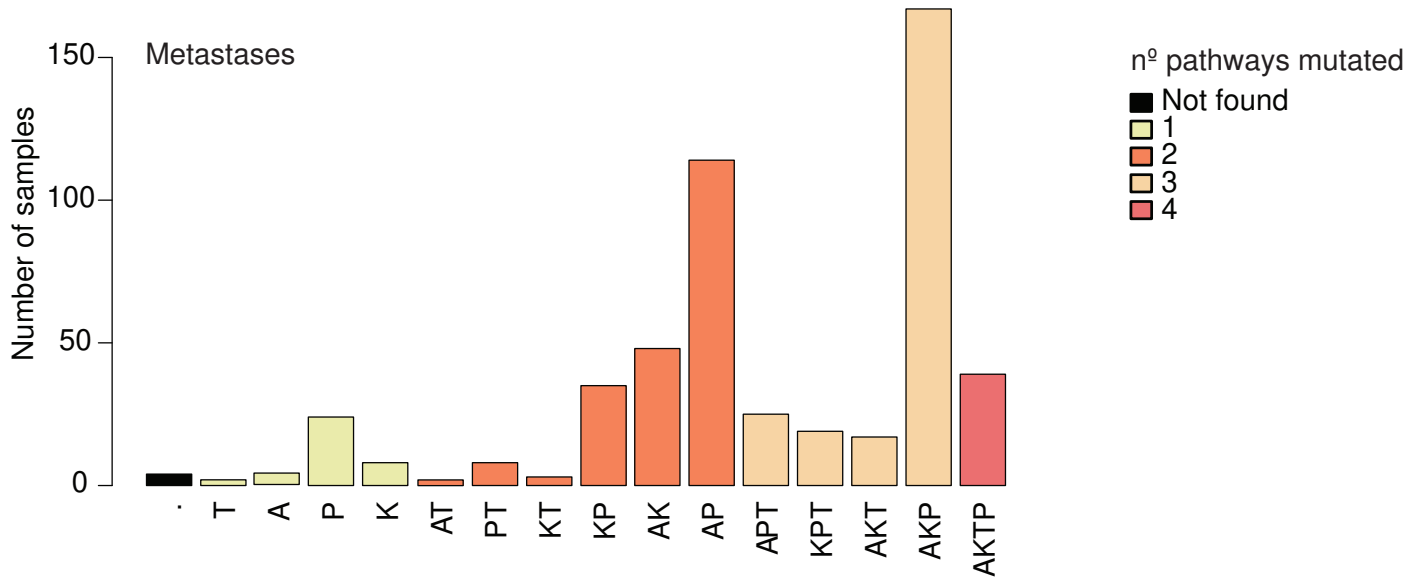

c